The Thesis Committee for Ali Abouie
Certifies that this is the approved version of the following thesis:

Development and Application of a Compositional Wellbore Simulator for Modeling Flow Assurance Issues and Optimization of Field Production

APPROVED BY
SUPERVISING COMMITTEE:

Supervisor:

Kamy Sepehrnoori

Mahdy Shirdel

Development and Application of a Compositional Wellbore Simulator for Modeling Flow Assurance Issues and Optimization of Field Production

by

Ali Abouie, B.S.P.E

Thesis

Presented to the Faculty of the Graduate School of

The University of Texas at Austin

in Partial Fulfillment

of the Requirements

for the Degree of

Master of Science in Engineering

The University of Texas at Austin

May 2015

Dedication

To my lovely parents

Nasrin and **Yahya**

And to my dear sister

Maryam

Acknowledgements

I would like to express my great gratitude to my supervisor, Dr. Kamy Sepehrnoori, for his invaluable guidance, support, and encouragement throughout my study. I am privileged to have had an opportunity to work under his supervision. I have learned a lot from his profound knowledge, keen observation, and vast knowledge.

I am also deeply indebted to my second reader, Dr. Mahdy Shirdel, for his priceless input into my research, reviewing my work, and contributing insightful technical comments. Special thanks go to Dr. Chowdhury Mamun for his review and comments on my thesis.

I am grateful for the financial support provided by Abu Dhabi National Oil Company and Reservoir Simulation JIP at the Center for Petroleum and Geosystems Engineering Department at The University of Texas at Austin.

I would like to acknowledge the staff of the Department of Petroleum and Geosystems Engineering at The University of Texas at Austin, John Cassibry, Frankie Hart, Mary Pettengil, and Glen Baum for their technical and administrative support.

Special thanks to my friends, Aboulghasem Kazemi Nia and Hamed Darabi for their vast knowledge and discussion about IPhreeqc and UTCOMP. I would like to extend my special thanks to my great colleagues and friends, Hamidreza Lashgari, Mohsen Taghavifar, Reza Ganjdanesh, Mahmood Shakiba, Mohsen Rezaveisi, Soheil Ghanbarzadeh, Ali Goudarzi, Mohammad Lotfollahi, Shayan Tavassoli, Alireza Sanaei, and many other friends that I have not mentioned their names for all their technical discussion and moral support.

Finally, I would like to express my sincere appreciation to my beloved parents, Nasrin and Yahya, for their endless love and incredible support through my entire life. This work would not have been possible without their continuous support and unconditional love.

Abstract

Development and Application of a Compositional Wellbore Simulator for Modeling Flow Assurance Issues and Optimization of Field Production

Ali Abouie, M.S.E

The University of Texas at Austin, 2015

Supervisor: Kamy Sepehrnoori

Flow assurance is crucial in the oil industry since it guarantees the success and economic production of hydrocarbon fluid, especially in offshore and deep water oil fields. In fact, the ultimate goal of flow assurance is to maintain flow in the wellbore and pipelines as long as possible. One of the most common challenges in flow assurance is the buildup of solids, such as asphaltene and scale particles. These Solid particles can deposit in the wellbore, flowline, and riser and affect the wellbore performance by reducing the cross section of the pipeline, which eventually results in pipeline blockage. Hence, neglecting the importance of flow assurance problems and failure in thorough understanding of the fluid behavior in the production systems may result in plugged pipeline, production loss, flowline replacement, and early abandonments of the well. As a result, continuous evaluations are needed at the development stage and during the life of reservoirs to predict the potential, the extent, and the severity of the problem to plan for

inhibition and remediation jobs. In fact, it is more preferable to prevent flow assurance problems through the designing and operating procedures rather than remediating the problems, which has higher risks of success and higher loss of revenue due to frequent well shut down.

As a part of this research, we enhanced the capabilities of our in-house compositional wellbore simulator (UTWELL) to model various production and flow assurance scenarios. Initially, we developed and implemented a robust gas lift model into UTWELL to model artificial lift technique for reservoirs with low pressure. The developed model is able to model both steady state and transient flow along with blackoil and Equation-of-State compositional models. The improved version was successfully validated against a commercial simulator.

Then, we applied our dynamic model to track the behavior of asphaltene during gas lift processes and evaluated the risk of asphaltene deposition. Several deposition mechanisms were incorporated to study the transportation, entrainment, and deposition of solid particles in the wellbore. The simulation results illustrated the effect of light gas injection on asphaltene deposition and well performance.

Finally, a step by step algorithm is presented for coupling a geochemical package, IPhreeqc, with UTWELL. The developed model is able to model homogenous and heterogeneous, non-isothermal, non-isobaric aqueous phase reactions assuming local equilibrium or kinetic conditions. This tool was then utilized to model scale deposition in the wellbore for various scenarios. In addition, the results showed that integrating IPhreeqc has promise in terms of CPU time compared to the traditional approach of reading and writing the input and output files.

Table of Contents

List of Tables

List of Figures

Chapter 1: Introduction

In this chapter, we discuss the main objectives and the overall scope of this thesis. In addition, we briefly describe each chapter of the thesis.

1.1 PROBLEM DESCRIPTION

Flow assurance is crucial in the oil industry since it guarantees the success and economic production of hydrocarbon fluid, especially in offshore and deep water oil fields. In fact, the ultimate goal of flow assurance is to maintain flow in the wellbore and pipelines as long as possible.

One of the most common challenges in flow assurance is the buildup of solids such as asphaltene and scale particles. These solid particles can deposit in the wellbore, flowline, and riser and affect the wellbore performance by reducing the cross section of the pipeline which eventually results in pipeline blockage. Hence, neglecting the importance of flow assurance problems and failure in thorough understanding of the fluid behavior in the production systems may result in plugged pipeline, production loss, flowline replacement, and early abandonments of the well. As a result, continuous evaluations are needed at the development stage and during the life of reservoirs to predict the potential, extent, and severity of the problem to plan for inhibition and remediation jobs. In fact, it is more preferable to prevent flow assurance problems through the designing and operating procedures rather than remediating the problems which has higher risks for success and higher loss of revenue due to frequent well shut down. This evaluation (i.e. tracking the fluid phase behavior and flow assurance

problems) become more complicated and challenging as pressure, temperature, fluid composition, and operating condition vary through the life of the reservoir.

Therefore, there is an urgent need for a wellbore simulator with the capability of identifying the potential, magnitude, and location of the deposited solids in the system. These predictions can assist the operators in optimizing the operation conditions in a way to minimize production loss. In more severe cases, operators can optimize the number of work overs (i.e. mechanical and chemical techniques) to reduce the associated expenses. Thus, development of a comprehensive multiphase wellbore simulator with the capability of modeling flow assurance issues is necessary for the purpose of facility design, production optimization, and remediation.

In this work, we enhanced the capabilities of a compositional wellbore simulator to model different production and flow assurance scenarios. For the purpose of production, we implemented a gas lift module to model artificial lift technique in the cases that reservoir pressure and well productivity declined. Then, we applied the developed gas lift model in a reservoir with asphaltic fluid to investigate the effect of injection gas composition and flow rate on phase behavior of asphaltene and consequent deposition rate. Additionally, we improved the capability of the wellbore simulator by coupling it with a geochemistry package to model geochemical reactions during the flow in the pipeline and determine the profile of deposited scale.

To the best of our knowledge, our simulator has additional features compared to the commonly available wellbore simulators. These features include modeling gas lift process during steady-state or transient flow using both black oil and compositional approaches, modeling asphaltene deposition during production and gas lift process, and

modeling scale deposition in the wellbore considering the effect of pressure, temperature, salinity, and pH.

1.2 RESEARCH OBJECTIVES

The main objective of this thesis is developing a gas lift model, predicting asphaltene deposition in the wellbore during gas lift, and modeling scale deposition in the wellbore. All of the developed models in this thesis are embedded in UTWELL, The University of Texas wellbore simulator.

The main objectives of this work can be summarized as below:

- Implementation of steady state/transient gas lift module in UTWELL.
- Characterizing a fluid in way that is in agreement with the experimental data.
- Dynamic modeling of asphaltene deposition during gas-lift in the wellbore.
- Studying the risk of asphaltene deposition when light hydrocarbons are injected as the lift gas.
- Dynamic modeling and implementation of IPhreeqc in UTWELL to model scale deposition in the wellbore.
- Studying the risk of scale deposition in the case of incompatible water injection

1.3 BRIEF DESCRIPTION OF THE CHAPTERS

The following paragraphs give a general overview of the material covered in this thesis.

Chapter 2 presents a brief description of assumptions, governing equations, flow regimes, and numerical models in UTWELL to model multiphase flow in the injection and production wells.

Chapter 3 presents the formulation, implementation, and results of gas lift module in UTWELL for both steady state and transient models.

In Chapter 4, we investigate asphaltene phase behavior during gas lift process. First, we describe characterization of a Middle Eastern oil. Then, we investigate the effect of the injected lift gas on dynamics of asphaltene deposition in the wellbore.

Chapter 5 presents the coupling of USGS geochemical package, IPhreeqc, with UTWELL to model geochemistry reactions in the wellbore to predict carbonate and sulfate deposition profiles in the wellbore. The effects of pressure, temperature, salinity, and pH were also considered in the developed tool.

Finally, Chapter 6 presents the summary and conclusion of this research and a few recommendations are made for future work.

Chapter 2: Overview of UTWELL Wellbore Simulator

In this thesis, the formulation of UTWELL, The University of Texas at Austin in-house wellbore simulator, was extended to enhance its capability for modeling several gas lift scenarios and flow assurance problems. In this chapter, we present an overview of UTWELL and its formulation, assumptions, and features. More details on these topics can be found in Shirdel (2010; 2013), Shirdel et al. (2009; 2012a, b), and UTWELL Technical Manual (2014).

2.1 INTRODUCTION TO UTWELL WELLBORE SIMULATOR

UTWELL is a thermal, one-dimensional, Equation-of-State (EOS) compositional wellbore simulator capable of modeling production and injection wells, steady state and transient states, and flow assurance issues. UTWELL was first developed by Shirdel (Shirdel 2010). He used finite difference approach to compute pressure, temperature, phase velocities, and holdup. The wellbore was also coupled with a compositional reservoir simulator (UTCOMP) to study primary and secondary production as well as well test analysis. The main features of UTWELL are summarized as below:

- One-dimensional EOS compositional and black oil models
- Rigorous and simplified flash calculation (including three-phase flash calculation capability)
- Single phase and multiphase flow capability

- Production and injection wells simulation
- Pipeline modeling
- Steady state and transient Modeling
- Different numerical methods, such as fully-implicit, nearly-implicit, and semi-implicit approaches
- Wellbore heat loss model
- Modeling flow assurance problems, such as asphaltene, wax, and scale

UTWELL allows existence of up to three phases in the wellbore: aqueous phase, oil phase, and gas phase. Phase equilibrium calculation is done using the Peng-Robinson EOS (Peng and Robinson, 1976). The main assumptions for fluid flow in the UTWELL include:

- One-dimensional flow is assumed along the wellbore
- Several flow regimes are used to consider the effect of wall shear force, interface shear force, and spatial geometry
- The liquid and gas phases have identical pressure and temperature in each gridblock
- Physical dispersion is neglected in the axial direction since convection is dominant
- Interphase mass transfer is only considered between oil and gas

- Drift slip is assumed between the oil and water in the liquid
- There is no slip between the solid particles and liquid
- Slip models are calculated based on the basic relations of interphase drag forces and drift-flux models
- Local equilibrium condition is considered in the wellbore

2.2 GOVERNING FORMULATIONS

In this section, the principal mathematical formulations of UTWELL are discussed by the three main equations: mass conservation, momentum conservation, and heat transfer model. There are also constitutive relations to determine the parameters in momentum equations.

2.2.1 Mass Conservation

In UTWELL, the mass conservations for oil, gas, and water are solved to determine the hydrocarbon mole fractions in the oil and gas phases. The following equations describe the mass conservation for oil, gas, and water phases, respectively.

$$\frac{\partial(\rho_o \alpha_o)}{\partial t} + \frac{1}{A}\frac{\partial(A\rho_o \alpha_o u_o)}{\partial x} = \dot{\psi}_o - \Gamma_g, \tag{2.1}$$

$$\frac{\partial(\rho_g \alpha_g)}{\partial t} + \frac{1}{A}\frac{\partial(A\rho_g \alpha_g u_g)}{\partial x} = \dot{\psi}_g + \Gamma_g, \tag{2.2}$$

$$\frac{\partial(\rho_w \alpha_w)}{\partial t} + \frac{1}{A}\frac{\partial(A\rho_w \alpha_w u_w)}{\partial x} = \dot{\psi}_w, \tag{2.3}$$

where

ρ_o, ρ_g, ρ_w = oil/gas/water density

$\dot{\psi}_o, \dot{\psi}_g, \dot{\psi}_w$ = oil/gas/water mass influx

$\alpha_o, \alpha_g, \alpha_w$ = oil/gas/water volume fraction

u_o, u_g, u_w = oil/gas/water velocity

Γ_g = Interphase mass transfer between oil and gas

In the above equations, mass influxes are calculated with the productivity indices of the wellbore and reservoir. In addition, interphase mass transfer is calculated by the following equation:

$$\Gamma_g = -\frac{\rho_{gsc}}{5.615\, B_o}\left[\left(\frac{\partial R_s}{\partial P}\right)\frac{\partial P}{\partial t}\alpha_o + \left(\frac{\partial R_s}{\partial P}\right)\frac{\partial P}{\partial x}(u_o\alpha_o) + \left(\frac{\partial R_s}{\partial T}\right)\frac{\partial T}{\partial t}\alpha_o + (\frac{\partial R_s}{\partial T})\frac{\partial T}{\partial x}(u_o\alpha_o)\right], \quad (2.4)$$

where R_s is solution gas oil ratio and B_o is oil formation volume factor.

2.2.2 Momentum Conservation

To determine the velocity of each phase during multiphase flow, three models were implemented to solve the momentum conservation equation. In the following section, the three different models are discussed.

2.2.2.1 Homogenous Model

In homogenous model, it is assumed that the different phases have identical velocities, therefore, no slippage is considered between the phases. Hence, the momentum equation can be represented as

$$\frac{\partial(\rho_m u_m)}{\partial t} + \frac{\partial(\rho_m {u_m}^2)}{\partial x} + 144 g_c \frac{\partial P}{\partial x} + \rho_m g sin\theta + \frac{\tau_m \Pi D}{A} = 0 \quad (2.5)$$

In the above equation, u_m is the mixture velocity,τ_m is the mixture shear stress, and ρ_m is the mixture density. The mixture density can be calculated by Equation (2.6),

$$\rho_m = \rho_g \alpha_g + \rho_o \alpha_o + \rho_w \alpha_w. \quad (2.6)$$

2.2.2.2 Drift-flux Model

In drift-flux model, gas, oil, and water velocities are determined as a function of bulk volumetric average velocity and the drift velocities as given as

$$U_g = C_0 J + V_d. \quad (2.7)$$

In the above equation, J is the bulk volumetric average velocity, V_d is the drift velocity, and C_0 is the distribution coefficient. Considering the slippage between the phases, the momentum equation can be given as

$$\frac{\partial(\rho_m u_m)}{\partial t} + \frac{\partial(\rho_g \alpha_g {u_g}^2 + \rho_o \alpha_o {u_o}^2 + \rho_w \alpha_w {u_w}^2)}{\partial x} + 144 g_c \frac{\partial P}{\partial x} + \rho_m g sin\theta + \frac{\tau_m \pi D}{A} = 0. \quad (2.8)$$

In addition, Equation (2.9) is applied to calculate the mixture velocity,

$$u_m = \frac{\rho_g \alpha_g u_g + \rho_o \alpha_o u_o + \rho_w \alpha_w u_w}{\rho_m}. \quad (2.9)$$

Equations (2.10) through (2.13) are also integrated to determine the velocity of gas, liquid, oil, and water phases.

$$u_g = C_1^{gl} u_m + v d_1^{gl}, \quad (2.10)$$

$$u_l = C_2^{gl} u_m + v d_2^{gl}, \quad (2.11)$$

$$u_o = C_1^{ow} u_l + v d_1^{ow}, \quad (2.12)$$

$$u_w = C_2^{ow} u_l + v d_2^{ow}, \quad (2.13)$$

where $C_1^{gl}, C_2^{gl}, C_1^{ow}, C_2^{ow}$ are profile parameters and $vd_1^{gl}, vd_2^{gl}, vd_1^{ow}, vd_2^{ow}$ are drift velocities.

2.2.2.3 Two-Fluid Model

In the two-fluid model, momentum equations are solved for liquid and gas phases separately and the interphase forces are considered in the momentum equations of both phases. It should be noted that liquid properties are calculated based on the average properties of the oil and water. Then, the drift velocity is utilized to determine the velocities of oil and water in the liquid phase,

$$\rho_g \alpha_g \frac{\partial u_g}{\partial t} + \rho_g \alpha_g \frac{\partial {u_g}^2}{2\partial x} + (144 g_c)\alpha_g \frac{\partial P}{\partial x} + \rho_g \alpha_g B_x + \rho_g \alpha_g u_g FWG + \Gamma_g \left(u_g - u_{gi}\right) + u_g \dot{\psi}_g + \rho_g \alpha_g \left(u_g - u_l\right) FIG = 0.0, \quad (2.14)$$

$$\rho_l \alpha_l \frac{\partial u_l}{\partial t} + \rho_l \alpha_l \frac{\partial {u_l}^2}{2\partial x} + (144 g_c)\alpha_l \frac{\partial P}{\partial x} + \rho_l \alpha_l B_x + \rho_l \alpha_l u_l FWL - \Gamma_g (u_l - u_{li}) + u_l \dot{\psi}_l + \rho_l \alpha_l \left(u_l - u_g\right) FIL = 0.0, \quad (2.15)$$

where

$\rho_g \alpha_g \frac{\partial u_g}{\partial t}$ = Momentum accumulation term

$\rho_g \alpha_g \frac{\partial {u_g}^2}{2\partial x}$ = Momentum convection term

$(144 g_c)\alpha_g \frac{\partial P}{\partial x}$ = Pressure gradient

$\rho_g \alpha_g B_x$ = Body forces

$\rho_g \alpha_g u_g FWG$ = Phasic wall friction

$\Gamma_g(u_g - u_{gi})$ = Momentum of the interphase mass transfer

$\rho_g \alpha_g (u_g - u_l) FIG$ = Interphase drag friction

2.2.3 Energy Conservation

Energy equation is used for calculating the heat transfer between the wellbore and the surrounding formulation to determine the temperature of the fluid in the wellbore. The energy equation solved in UTWELL is described as below:

$$\frac{\partial\left[\rho_o \alpha_o\left(\bar{h}_o+\frac{u_o{}^2}{2g_cJ_c}\right)\right]}{\partial t}+\frac{\partial\left[\rho_g \alpha_g\left(\bar{h}_g+\frac{u_g{}^2}{2g_cJ_c}\right)\right]}{\partial t}+\frac{\partial\left[\rho_w \alpha_w\left(\bar{h}_w+\frac{u_w{}^2}{2g_cJ_c}\right)\right]}{\partial t}+\frac{1}{A}\frac{\partial\left[A\rho_o \alpha_o u_o(\bar{h}_o+\frac{u_o{}^2}{2g_cJ_c}\right]}{\partial x}+$$
$$\frac{1}{A}\frac{\partial\left[A\rho_g \alpha_g u_g(\bar{h}_g+\frac{u_g{}^2}{2g_cJ_c})\right]}{\partial x}+\frac{1}{A}\frac{\partial\left[A\rho_w \alpha_w u_w(\bar{h}_w+\frac{u_w{}^2}{2g_cJ_c})\right]}{\partial x}+\dot{H}_o+\dot{H}_g+\dot{H}_w+\rho_o \alpha_o \frac{u_o}{g_cJ_c} g sin\theta+$$
$$\rho_g \alpha_g \frac{u_g}{g_cJ_c} g sin\theta+\rho_w \alpha_w \frac{u_w}{g_cJ_c} g sin\theta+\frac{\dot{Q}_{loss}}{A}=0, \quad (2.16)$$

where

$\bar{h}_o, \bar{h}_g, \bar{h}_w$ = Oil, gas, and water enthalpies per unit mass

$\dot{H}_o, \dot{H}_g, \dot{H}_w$ = Oil, gas, and water influx enthalpies per gridblock volume

$\dot{Q}_{loss}$ = Heat transfer between the wellbore and surrounding formation per unit length

The heat exchange between the fluid and the surrounding formation is also estimated by Equation (2.17).

$$\dot{Q}_{loss} = 2\pi r_{to} U_{to} (T_f - T_{wb}), \tag{2.17}$$

where r_{to} is the tubing outer radius, U_{to} is the overall heat transfer coefficient, T_f is the fluid temperature, and T_{wb} is the surrounding formation temperature.

Equation (2.18) is also used to determine the overall heat transfer coefficient,

$$\frac{1}{U_{to}} = \frac{r_{to}}{r_{ti} h_{to}} + \frac{r_{to} \ln(\frac{r_{to}}{r_{ti}})}{k_t} + \frac{r_{to} \ln(\frac{r_{ins}}{r_{to}})}{k_{ins}} + \frac{r_{to}}{r_{ins}(h_c + h_r)} + \frac{r_{to} \ln(\frac{r_{co}}{r_{ci}})}{k_{casing}} + \frac{r_{to} \ln(\frac{r_{wb}}{r_{co}})}{k_{cement}}, \tag{2.18}$$

where k_t, k_{ins}, k_{casing}, k_{cement} are the heat transfer coefficient of tubing, insulator, casing, and cement, respectively, and defined by the user.

2.3 TIME STEP

In UTWELL, two methods were implemented to control the time-step for semi-implicit and fully-implicit models.

In semi-implicit approach, the time-step sizes are determined based on total mass error in the wellbore gridblocks. Equations (2.19) and (2.20) give the total mass error in each gridblock,

$$\varepsilon_m = \frac{\max(|(\rho_{ms})_L^{n+1} - (\rho_{mt})_L^{n+1}|)}{(\rho_{ms})_L^{n+1}}, \tag{2.19}$$

$$\varepsilon_{rms} = \frac{2 \sum_{L=1}^{N} [V_{b,L}((\rho_{ms})_L^{n+1} - (\rho_{mt})_L^{n+1})]^2}{\sum_{L=1}^{N} (V_{b,L}(\rho_{ms})_L^{n+1})^2}. \tag{2.20}$$

In the above equations, ρ_{ms} and ρ_{mt} are the total mass calculated from conservation equation and state relations, respectively, and can be determined by

$$(\rho_{mt})_L^{n+1} = (\rho_g \alpha_g)_L^{n+1} + (\rho_o \alpha_o)_L^{n+1} + (\rho_w \alpha_w)_L^{n+1}, \tag{2.21}$$

$$(\rho_{ms})_L^{n+1} = \left(\rho_{g,L}^{n+1} \alpha_{g,L}^{n+1}\right) + \left(\rho_{o,L}^{n+1} \alpha_{o,L}^{n+1}\right) + \left(\rho_{w,L}^{n+1} \alpha_{w,L}^{n+1}\right). \tag{2.22}$$

Then, the time step size is calculated based on the magnitude of the relative error as shown below:

$$\Delta t^{new} = \frac{1}{2}\,\Delta t^{old} \quad \text{if} \quad URME < \varepsilon_m, \varepsilon_{rms} \tag{2.23}$$

$$\Delta t^{new} = \Delta t^{old} \quad \text{if} \quad \text{LRME} < \varepsilon_m, \varepsilon_{rms} < URME \tag{2.24}$$

$$\Delta t^{new} = 2\Delta t^{old} \quad \text{if} \quad \varepsilon_m, \varepsilon_{rms} < LRME \tag{2.25}$$

In the above equations, URME and LRME are the upper and the lower residual mass errors and defined by the user. In addition, it is necessary to incorporate the phasic CFL number for stability condition. Therefore, by consideration of the CFL number, the time step size is estimated by

$$(\Delta t_c)_j = \Delta x_j \times \frac{\max(\alpha_{o,j},\alpha_{g,j},\alpha_{w,j})}{\max(|\alpha_{o,j}u_{o,j}|,|\alpha_{g,j}u_{g,j}|,|\alpha_{w,j}u_{w,j}|)}\,. \tag{2.26}$$

Finally, the time step is selected based on the following criterion:

$$\Delta t = \min(\Delta t^{new}, (\Delta t_c)_j). \tag{2.27}$$

For fully-implicit approach, the time step size is calculated based on the total mass error index as indicated below:

$$\Delta t^{new} = \frac{RME}{\left(\frac{(\rho_{ms})_L^{n+1}-(\rho_{ms})_L^{n}}{(\rho_{ms})_L^{n}}\right)}\,\Delta t^{old}, \tag{2.28}$$

In the above equation, RME is residual mass error.

2.4 FLOW REGIME

In UTWELL, the dominant flow regime is determined based on several parameters, such as liquid velocity, gas velocity, fluid density, viscosity, and inclination of the wellbore. For deviated and vertical wells, Kaya's model (Kaya et al., 1999) was

used for determining the flow pattern. Five flow regimes can exist based on this model: bubbly, dispersed bubbly, slug, churn, and annular flow (Figure 2.1). For horizontal wells, four flow patterns were incorporated based on Shoham's model (Shoham, 2006). He considered stratified, bubbly, intermittent, and annular flow as the four categories of flow regimes in horizontal flow (Figure 2.2). More details of flow regime detection can be found in Shirdel (2013). It should be emphasized that to improve the stability criteria during transient flow and avoid discontinuities in flow pattern transition, a transition criterion was improved based on the RELAP5-3D (2012).

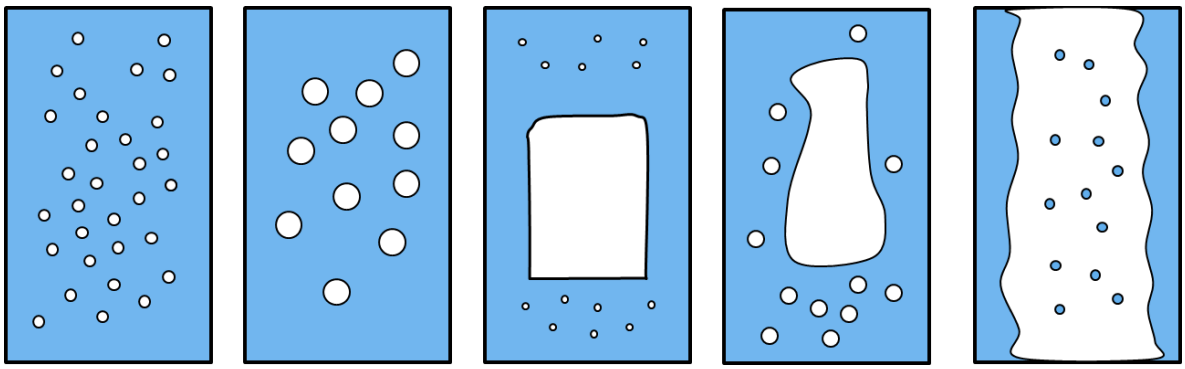

Figure 2.1: Schematic views of vertical flow regimes, (a) Dispersed bubbly flow (b) Bubbly flow (c) Slug flow (d) Churn flow (e) Annular flow

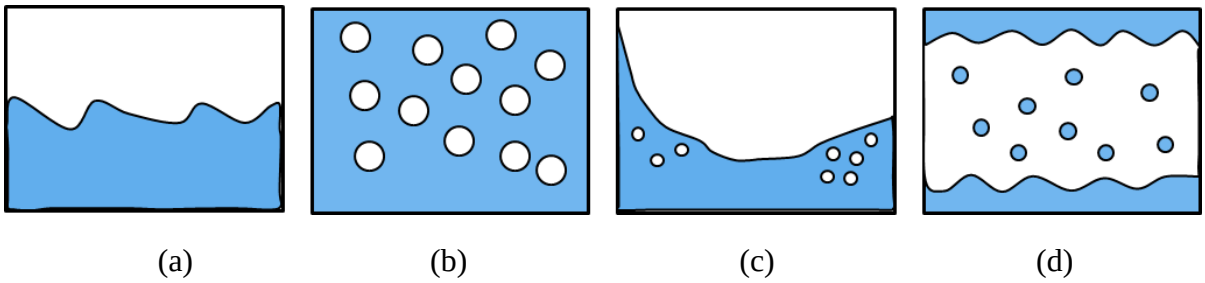

Figure 2.2: Schematic views of horizontal flow regimes, (a) Stratified flow, (b) Bubbly flow, (c) Intermittent flow, (d) Annular flow

Chapter 3: Gas Lift

Gas lift is one of the common artificial lift techniques usually used in wells when high water production, low gas oil ratio, and low pressure are observed in the oil field. During this process, gas is injected from the annular space into the tubing through a gas lift valve. Reduction in the liquid holdup and hydrostatic pressure in the wellbore results in a greater drawdown pressure and more liquid production.

This chapter presents a comprehensive thermal compositional wellbore model with the capability of modeling gas lift process. Both steady state and transient models were implemented into the developed model. In addition, the thermodynamic equilibrium condition can be calculated using both black oil approach and an equation of state (i.e. Peng-Robinson).

3.1 BACKGROUND

Nowadays, one of the highest operation costs in the oil fields is related to the artificial lift systems. Artificial lift systems are required when the reservoir pressure declines and the pressure of the well is not high enough to maintain the oil production rate with reasonable economic return. Therefore, selecting the proper artificial lift technique becomes crucial to maintain oil production and minimizes the operation costs. Clegg et al. (1993) presented an extensive comparison of the available artificial lift techniques and described the applicability condition of each method. It is obvious that each method has its pros and cons, and each mechanism should be evaluated over the entire life of the production. Ramirez et al. (2000) compared the most appropriate artificial lift methods for eight reservoirs based on the possible production rate, power

consumption, and efficiency. They defined a parameter named Specific Power which is defined as the number of watts that is required to produce one barrel of oil at the surface condition. By calculating specific power, it was possible for them to compare efficiency of several artificial lift methods.

Among the several artificial lift techniques, gas lift is the most widely used method. Gas lift is inexpensive, easy to implement, very effective in a wide range of operating conditions, and requires less maintenance in comparison to the other methods. This technique is usually incorporated in mature oil fields having low reservoir pressure, high water cut, low GOR, and low production rates. Clegg et al. (1993) reported that about 10% of the oil wells in the United States operate under gas lift mechanism. Therefore, important decisions should be made during designing the gas lift operation such as the source of lift gas, required insulating, operating envelope, flow assurance occurrence due to low temperature, and corrosion analysis to increase the oil production rate.

In the gas lift method, high pressure gas is injected through the annulus into the production well to modify the mixture density and provide sufficient energy to produce the fluid (Figure 3.1). The pressure gradient in the liquid is reduced by injecting the gas. Hence, the resulting mixture becomes lighter than the original fluid and causes the oil to flow. Although natural gas is the most common type of gas used in the production systems, it is also possible to use other types of gas, such as nitrogen. Lifting by using the reservoir gas is the other practical alternative for oil production which leads to cost reduction in the oil field infrastructure (Betancourt et al., 2002).

In addition to production enhancement, gas lift has several other applications in the oil field. Gas lift might be used to control severe slugging by changing the flow into

smaller and more frequent liquid slugs. Moreover, gas lift might be used during the flow line depressurization to prevent hydrate formation during the shut-ins. In fact, gas injection helps to remove the liquid by lowering the flow line pressure and increasing the gas velocity in the flow stream (Jayawardena et al., 2007).

Gas lift operation can be categorized mainly into two major mechanisms. The first mechanism is continuous gas injection, where compressed gas is injected continuously from the annulus space to the tubing during the production. Most of the wells operate under continuous gas injection mechanism. The second type is intermittent gas injection, where the compressed gas is periodically injected into the flow stream near the perforation zones. Intermittent gas injection becomes an alternative to continuous gas injection in the fields with limited amount of gas supply. In addition, low reservoir pressure and wells with small tubing are the other candidates for using intermittent gas lift process. It should be noted that intermittent gas injection is not an efficient way and in the near future, other artificial lift methods should be used. Santos et al. (2001) provided an empirical table as guidance for selecting continuous or intermittent gas lift injections (Table 3.1).

In recent years, several models have been developed to model production scenarios under gas lift mechanism.

Mach et al. (1979) applied a nodal analysis approach to evaluate the production systems including the reservoir boundary, perforations, tubing, surface choke, flow line, and separator.

Liao et al. (1995) presented a mechanistic model for intermittent gas lift system based on the physical principles by solving a system of ordinary and partial differential equation. This model included several parameters, such as reservoir inflow performance,

fluid properties, and the performance of gas lift valves. The results were in relatively good agreement with the experimental data. They concluded that the amount of injection gas during each cycle is the most important parameter in the gas lift efficiency. In addition, controlling each cycle period can be calculated by determining the optimum tubing load.

Vazquez and Hernandez (2005) also developed a continuous gas lift model based on differential algebraic equations to predict the wellhead pressure and optimum amount of lift gas. First, the model solved mass, momentum, and energy balance equations in the wellbore. Then, thermodynamic properties were calculated by assuming homogenous mixture of the reservoir fluid and lift gas.

It is important to emphasize that the gas lift efficiency depends on several parameters, such as reservoir performance, fluid properties, and flow line characteristics. In addition, parameters such as amount of gas injection and depth of injection should be assigned in a way that yields the maximum oil production with low operating cost over the entire life of the reservoir. Therefore, it is necessary to determine the optimal operability of the gas lift mechanism at the early life of the project.

As mentioned before, gas lift optimization plays a major role in obtaining the maximum oil production rate during gas lift. Most of the time, the amount of the lift gas, depth of injection, and injection pressure at the surface choke are considered as the common variables for optimizing the gas lift process. Hence, several attempts have been done to optimize the efficiency of a gas lift system.

Blann and Williams (1984) emphasized the importance of gas injection pressure on the lift efficiency since high injection pressure requires a useless compression and low injection pressure causes low efficiency. They concluded that several factors, such as

reservoir fluid properties, well productivity, water cut, well head pressure, properties of the injected gas, etc. affect the optimum injection pressure. Higher production rate, less amount of injection gas, and lower compression power are few of the advantages of high pressure gas injection for cases having the gas lift valve at maximum depth of injection.

Chia and Hussain (1999) reported that 35% of the Esso Production Malaysia Inc. (EPMI) oil production is through gas lift process. As a result, gas lift optimization became the most important priority for enhancing the production rate as the reservoir pressure declines. Therefore, several optimization tools, such as GOAL, GLMS, Gas Lift Surveillance Database, and Training were developed to assist in optimization process and overcome the common challenges during the production.

Santos et al. (2001) developed a transient simulation model to investigate the effect of the operation parameters, such as the time period of each gas injection cycle on different types of intermittent gas lift efficiency.

Wang et al. (2002) proposed a formulation to optimize the well rates and lift gas rates for a short term production period in a black oil model and the suggested formulation was solved by using sequential quadratic programming algorithm. The results showed that the incorporated algorithm performs well for the optimization of well rates and lift gas rates.

Guet et al. (2003) investigated the effect of bubble gas injection on gas lift efficiency. The findings showed that injection of small size bubbles increases the oil production rate at constant flow rate of gas injection. In fact, since small size bubbles have a lower rising velocity and more uniform distributed gas concentration along the flow area, the gas lift efficiency becomes greater. Moreover, small size bubbles prevent the transition of flow regime from bubbly flow to slug flow which significantly affects

the oil production rate. Hence, they presented a drift-flux model to predict the bubble size effect on gas lift efficiency.

3.2 MODEL DEVELOPMENT

There are several approaches to model gas lifts mechanism. One of the approaches is to use look up tables for a range of wellhead pressure, GLR, WOR, and flow rate. Based on this approach, by specifying the GLR, amount of the injection gas, and wellhead pressure, the bottom-hole pressure of the well is determined.

In this section, we present a dynamic multi-segment wellbore model. This model is able to apply a multi-point gas injection option with specified gas flow rate and wellhead pressure. In addition, several other options such as fluid properties calculation, thermal calculation, mechanistic or correlation based estimates, can be used in the gas lift model. Although the mechanistic, thermal, compositional wellbore model is more challenging in terms of robustness and more expensive in terms of computational time, it provides the most accurate results for simulation purposes.

3.2.1 Steady State Single Well Gas Lift Model

The main design of a continuous steady-state gas lift includes two main parameters: The amount of injection gas and the operating valve depth. Therefore, in this process, the gas lift process is simulated by specifying these two parameters. Both black oil and compositional approaches were included in this model to consider the miscibility of gas in the tubing fluid.

In the developed annulus model, *Nc+2* transport equations are solved including *Nc* hydrocarbon components mass conservations, gas momentum conservation, and gas energy conservation to determine gas phase velocity, pressure, and temperature. Equations (3.1) and (3.2) are the governing mass conservation equations for component *k* in the gas phase:

$$(Mass_{in} - Mass_{out}) \pm (Source/Sink) = 0, \tag{3.1}$$

$$\frac{1}{A}\frac{\partial(A\hat{\rho}_{gk}u_g)}{\partial x} = -\sum_{k=1}^{Nc}\hat{\psi}_{gk}, \tag{3.2}$$

where $\hat{\rho}_{gk}$ is the molar density of the component *k*, u_g is the gas phase velocity, and $\hat{\psi}_{gk}$ is the outflow of the component *k* into the tubing. This parameter is determined by gas lift valve performance which will be described later in this chapter.

By summing up Equation (3.2) over all components, we obtain

$$\frac{1}{A}\frac{\partial(A\rho_g u_g)}{\partial x} = -\dot{\psi}_g. \tag{3.3}$$

In UTWELL, a staggered gridding is incorporated for the purpose of discretization in tubing and annulus as shown in Figure 3.2. Two main control volumes are considered in the developed model: mass control volume and momentum control volume. The pressure and the temperature are calculated at the center of mass control volume and velocity is calculated at the center of momentum control volume. Therefore, Equation (3.3) can be discretized as below:

$$\rho_{g,L}u_{g,j} - \rho_{g,k}u_{g,j-1} = -\frac{V_b}{A_j}(\dot{\psi}_{g,L}), \tag{3.4}$$

where ρ_g is the molar density of the gas phase and ψ_g is the total outflow into the tubing. Equations (3.5) and (3.6) present momentum balance for the gas flow in the annulus.

$$(Momentum_{in} - Momentum_{out}) + (Forces) = 0, \tag{3.5}$$

$$\frac{\partial(\rho_g {u_g}^2)}{\partial x} + (144 g_c)\frac{\partial P}{\partial x} - \rho_g g sin\Theta + \frac{\tau_g \Pi D}{A} = 0. \quad (3.6)$$

The momentum equation can be discretized as

$$P_L = P_K + \Delta x_j \frac{\rho_j g sin\theta}{144.0 g_c} - \Delta x_j \frac{\pi D \tau_j}{(144.0 g_c) A_j^n} + \frac{\rho_L({u_L}^2) - \rho_k({u_k}^2)}{(144.0 g_c)}. \quad (3.7)$$

In the above equation, P is the pressure, D is the pipe diameter, and τ is the wall shear stress. By solving the momentum balance in the annulus, gas velocity is determined. Finally, the energy equations can be described and discretized as

$$\left(Energy_{in} - Energy_{out}\right) + \left(W_{force}\right) \pm (Source/Sink) = 0, \quad (3.8)$$

$$\frac{1}{A}\frac{\partial\left[A\rho_g u_g\left(\bar{h}_g + \frac{u_g^2}{2g_C J_C}\right)\right]}{\partial x} = \dot{H}_g + \rho_g \frac{u_g}{g_C J_C} g sin\theta - \frac{\dot{Q}loss}{A}, \quad (3.9)$$

$$\left[A_j \rho_{g,L} u_{g,j}\left(\bar{h}_{g,L} + \frac{({u_g}^2)_j}{2g_c J_c}\right) - A_{j-1}\rho_{g,K} u_{g,j-1}\left(\bar{h}_{g,K} + \frac{({u_g}^2)_{j-1}}{2g_c J_c}\right)\right] = V_b\left[\dot{H}_{g,L}\right] + V_b\left[\rho_{g,L}\frac{u_{g,L}}{g_c J_c} g sin\theta\right] - V_b\left[\frac{\dot{Q}_{loss,L}}{A_j}\right]. \quad (3.10)$$

In Equation (3.10), $\dot{Q}_{loss,L}$ is the heat exchange between the formation and the wellbore and V_b is the volume of the gridblock. The above equation is applied for determining the gas temperature.

It is important to emphasize that lift gas is usually injected in a way to stay in the gas phase region during flow in the annulus. Therefore, it is recommended to use black oil approach for flow in the annulus. Although compositional model is more accurate, this approach leads to higher CPU time.

3.2.2 Transient Single Well Gas Lift Model

Transient model is employed to more accurately monitor the gas lift process. In addition, due to the transient nature of the intermittent gas lift process, transient gas lift model should be applied.

It should be noted that this method is expensive in terms of computational memory. In addition, the transient models need more limiting conditions to overcome the numerical problems in the calculations. Hence, this approach is not usually used in multiphase simulation for the flowing wells producing under gas lift process.

This section presents the development of a transient gas lift model in the wellbore to obtain five primary variables in the tubing: pressure, temperature, liquid velocity, gas velocity, and holdup. In addition, pressure, temperature, and gas velocity are calculated in the annulus. The outcome of this model leads to a more accurate and reliable simulation of the multiphase flow in the wellbore producing under gas lift mechanism.

Similar to the steady-state model presented in the previous section, the simulator is developed as a coupled annulus/tubing model. One dimensional, single phase flow with Eulerian coordinates is used for the flow simulation in the annulus. Fully implicit model is used for simulation of the gas flow in the annulus to build a robust, accurate, and flexible tool. The gas velocity is calculated at the junctions of each gridblock while pressure and temperature are calculated in the center of the gridblocks. The primary equations for flow in the annulus can be expressed as

Gas Mass Conservation

$$\frac{\partial\left(\rho_g \alpha_g\right)}{\partial t}+\frac{1}{A}\frac{\partial A\left(\rho_g \alpha_g u_g\right)}{\partial x}=-\dot{\psi}_g, \tag{3.11}$$

Gas Momentum Conservation

$$\frac{\partial\left(\rho_g u_g\right)}{\partial t}+\frac{\partial\left(\rho_g \alpha_g u_g^2\right)}{\partial x}=-\left(144.0 g_C\right)\frac{\partial P}{\partial x}+\rho_g g sin\theta-\frac{\tau_g \pi D}{A}, \tag{3.12}$$

Gas Energy Conservation

$$\frac{\partial\left[\alpha_g \rho_g\left(\bar{h}_g+\frac{u_g^2}{2g_C J_C}\right)\right]}{\partial t}+\frac{1}{A}\frac{\partial\left[A\alpha_g \rho_g u_g\left(\bar{h}_g+\frac{u_g^2}{2g_C J_C}\right)\right]}{\partial x}=\dot{H}_g+\alpha_g \rho_g \frac{u_g}{g_C J_C} g sin\theta-\frac{\dot{Q}_{loss}}{A} \tag{3.13}$$

where

ρ_g = Gas density $(^{lb_m}/_{ft^3})$

α_g = Gas volume fraction (equal to one since only gas exists in the annulus)

$\dot{\psi}_g$ = Outflux mass into the tubing per gridblock bulk volume $(^{lb_m}/_{ft^3.sec})$

U_g = Gas velocity $(^{ft}/_{s})$

τ_g = Gas shear stress $(^{lb_m}/_{sec^2.ft})$

P = Pressure (psi)

$\dot{Q}_{loss}$ = Heat loss with the surrounding formation $(^{Btu}/_{sec.ft})$

$\bar{h}_g$ = Gas enthalpy outflux into the tubing per gridblock bulk volume $(^{\mathrm{BTU}}/_{\mathrm{ft^3.sec}})$

Using a first-order upwind scheme, the discretized form of the Equations (3.11) through (3.13) becomes

Gas Mass Conservation

$$V_b\left[\rho_{g,L}^{n+1}-\rho_{g,L}^{n}\right]+$$
$$\Delta t\left[\rho_{g,j}^{n+1}A_j^n u_{g,j}^{n+1}-\rho_{g,j-1}^{n+1}A_{j-1}^n u_{g,j-1}^{n+1}\right]=-V_b\Delta t\dot{\psi}_{g,L}^{n+1}, \tag{3.14}$$

Gas Momentum Conservation

$$\Delta x_j\left[\rho_{g,j}^{n+1}u_{g,j}^{n+1}-\rho_{g,j}^{n}u_{g,j}^{n}\right]+$$
$$\Delta t\left[\rho_{g,L}^{n+1}(u_g^2)_L^{n+1}-\rho_{g,K}^{n+1}(u_g^2)_K^{n+1}\right]=$$
$$-\Delta t\left(144.0g_c\right)\left(P_L^{n+1}-P_K^{n+1}\right)+\Delta t\Delta x_j\rho_{g,j}^{n+1}gsin\theta-\Delta t\Delta x_j\tau_{g,j}^{n+1}\frac{\pi D}{A_j^n}, \tag{3.15}$$

Gas Energy Conservation

$$V_b\left[\rho_{g,L}^{n+1}\left(\bar{h}_{g,L}^{n+1}+\frac{(u_g^2)_L^{n+1}}{2g_cJ_c}\right)-\rho_{g,L}^{n}\left(\bar{h}_{g,L}^{n}+\frac{(u_g^2)_L^{n}}{2g_cJ_c}\right)\right]+$$
$$\Delta t\left[A_j^{n+1}\rho_{g,L}^{n+1}u_{g,j}^{n+1}\left(\bar{h}_{g,L}^{n+1}+\frac{(u_g^2)_j^{n+1}}{2g_cJ_c}\right)-A_{j-1}^{n+1}\rho_{g,K}^{n+1}u_{g,j-1}^{n+1}\left(\bar{h}_{g,K}^{n+1}+\frac{(u_g^2)_{j-1}^{n+1}}{2g_cJ_c}\right)\right]=$$
$$V_b\Delta t\left[\dot{H}_{g,L}^{n+1}\right]+V_b\Delta t\left[\rho_{g,L}^{n+1}\frac{u_{g,L}^{n+1}}{g_cJ_c}gsin\theta\right]-V_b\Delta t\left[\frac{\dot{Q}_{loss,L}^{n+1}}{A_j^n}\right]. \tag{3.16}$$

As described before, fully implicit approach is used to solve the gas flow in the annulus. Newton method was used to linearize the equations and solve for the primary variables of pressure, velocity, and temperature. In the developed model, mass and momentum conservations are solved first and then, we solve the energy equation to update the temperature. Mass and momentum conservations are solved by constructing Jacobian matrix, J, and a residual vector, R, that are constructed using pressure and velocity parameters. The equations are solved for f_1 as gas momentum balance and f_2 as gas mass balance.

$$J = \begin{bmatrix} \frac{\partial f_{1,1}}{\partial u_{g,1}} & \frac{\partial f_{1,1}}{\partial P_1} & \frac{\partial f_{1,1}}{\partial u_{g,2}} & \frac{\partial f_{1,1}}{\partial P_2} & \cdots & \frac{\partial f_{1,1}}{\partial u_{g,N-1}} & \frac{\partial f_{1,1}}{\partial P_{N-1}} & \frac{\partial f_{1,1}}{\partial u_{g,N}} & \frac{\partial f_{1,1}}{\partial P_N} \\ \frac{\partial f_{2,1}}{\partial u_{g,1}} & \frac{\partial f_{2,1}}{\partial P_1} & \frac{\partial f_{2,1}}{\partial u_{g,2}} & \frac{\partial f_{2,1}}{\partial P_2} & \cdots & \frac{\partial f_{2,1}}{\partial u_{g,N-1}} & \frac{\partial f_{2,1}}{\partial P_{N-1}} & \frac{\partial f_{2,1}}{\partial u_{g,N}} & \frac{\partial f_{2,1}}{\partial P_N} \\ \frac{\partial f_{1,2}}{\partial u_{g,1}} & \frac{\partial f_{1,2}}{\partial P_1} & \frac{\partial f_{1,2}}{\partial u_{g,2}} & \frac{\partial f_{1,2}}{\partial P_2} & \cdots & \frac{\partial f_{1,2}}{\partial u_{g,N-1}} & \frac{\partial f_{1,2}}{\partial P_{N-1}} & \frac{\partial f_{1,2}}{\partial u_{g,N}} & \frac{\partial f_{1,2}}{\partial P_N} \\ \frac{\partial f_{2,2}}{\partial u_{g,1}} & \frac{\partial f_{2,2}}{\partial P_1} & \frac{\partial f_{2,2}}{\partial u_{g,2}} & \frac{\partial f_{2,2}}{\partial P_2} & \cdots & \frac{\partial f_{2,2}}{\partial u_{g,N-1}} & \frac{\partial f_{2,2}}{\partial P_{N-1}} & \frac{\partial f_{2,2}}{\partial u_{g,N}} & \frac{\partial f_{2,2}}{\partial P_N} \\ \cdots & \cdots & \cdots & \cdots & \cdots & \cdots & \cdots & \cdots & \cdots \\ \frac{\partial f_{1,N-1}}{\partial u_{g,1}} & \frac{\partial f_{1,N-1}}{\partial P_1} & \frac{\partial f_{1,N-1}}{\partial u_{g,2}} & \frac{\partial f_{1,N-1}}{\partial P_2} & \cdots & \frac{\partial f_{1,N-1}}{\partial u_{g,N-1}} & \frac{\partial f_{1,N-1}}{\partial P_{N-1}} & \frac{\partial f_{1,N-1}}{\partial u_{g,N}} & \frac{\partial f_{1,N-1}}{\partial P_N} \\ \frac{\partial f_{2,N-1}}{\partial u_{g,1}} & \frac{\partial f_{2,N-1}}{\partial P_1} & \frac{\partial f_{2,N-1}}{\partial u_{g,2}} & \frac{\partial f_{2,N-1}}{\partial P_2} & \cdots & \frac{\partial f_{2,N-1}}{\partial u_{g,N-1}} & \frac{\partial f_{2,N-1}}{\partial P_{N-1}} & \frac{\partial f_{2,N-1}}{\partial u_{g,N}} & \frac{\partial f_{2,N-1}}{\partial P_N} \\ \frac{\partial f_{1,N}}{\partial u_{g,1}} & \frac{\partial f_{1,N}}{\partial P_1} & \frac{\partial f_{1,N}}{\partial u_{g,2}} & \frac{\partial f_{1,N}}{\partial P_2} & \cdots & \frac{\partial f_{1,N}}{\partial u_{g,N-1}} & \frac{\partial f_{1,N}}{\partial P_{N-1}} & \frac{\partial f_{1,N}}{\partial u_{g,N}} & \frac{\partial f_{1,N}}{\partial P_N} \\ \frac{\partial f_{2,N}}{\partial u_{g,1}} & \frac{\partial f_{2,N}}{\partial P_1} & \frac{\partial f_{2,N}}{\partial u_{g,2}} & \frac{\partial f_{2,N}}{\partial P_2} & \cdots & \frac{\partial f_{2,N}}{\partial u_{g,N-1}} & \frac{\partial f_{2,N}}{\partial P_{N-1}} & \frac{\partial f_{2,N}}{\partial u_{g,N}} & \frac{\partial f_{2,N}}{\partial P_N} \end{bmatrix}, \tag{3.17}$$

$$R = \begin{bmatrix} f_{1,1} \\ f_{2,1} \\ f_{1,2} \\ f_{2,2} \\ \dots \\ f_{1,N-1} \\ f_{2,N-1} \\ f_{1,N} \\ f_{2,N} \end{bmatrix}. \tag{3.18}$$

Then, the primary variables are calculated by using

$$\overrightarrow{\Delta X} = J^{-1}R. \tag{3.19}$$

After solving the equations for pressure and velocity, the energy equation is solved to obtain the gas temperature in the annulus.

3.2.3 Gas Lift Valve

Gas lift valves play an important role in the gas lift mechanism by determining the amount of gas passing into the tubing based on the tubing and annulus conditions. Several types of gas lift valves are designed and used for flow control.

Actual flow testing of the gas lift valves under subsurface condition is a way to determine the performance of these valves. However, this method is expensive and time consuming. Therefore, several models were proposed to accurately model the valves performance.

Decker (1986) developed a model to predict the spring operated gas lift valve flow performance. Several parameters such as spring rate, flow coefficient, and internal dimension were included in this model to calculate gas passage. In addition, they

modeled the performance of the nitrogen valves considering the wellbore temperature influence.

Hepguler et al. (1993) also developed a model to predict the performance of both orifice and throttling flow. The model incorporated the effect of pressure, temperature, and valve parameters on its performance. The results were in relatively good agreement with the experimental data.

Hernandez et al. (1999) performed field-scale tests on intermittent gas lift in Lake Maracaibo to improve the current mechanistic models used for designing and modeling the intermittent lift. They showed that spring-loaded gas lift pilot valves pass less gas than the expected amount, while the nitrogen charged valve pass more gas.

Faustinelli and Doty (2001) also developed a model to predict the volumetric flow rate of nitrogen charged gas lift valve under orifice, throttling and transition flows. They included the effect of pressure recovery associated with the sudden gas expansion beyond the minimum area of flow by modifying the compressible flow theory. A good agreement was observed between the experimental data and the predicted values by this model using the suggested empirical coefficients.

Although several models were proposed to model the gas lift valve performance, Thornhill-Craver is still the most used equation for gas lift valves. Therefore, for the sake of simplicity, Thornhill-Craver model is used, which is a simplified version of the flow meter performance as follows:

$$Q_{sc} = 1241 A_p C_d \gamma_g \sqrt{\frac{P_a(P_a - P_t)}{TZ\gamma_g}}, \tag{3.20}$$

where A_p is the port diameter, C_d is the discharge coefficient, γ_g is the gas specific gravity, P_a is the annulus pressure, and P_t is the tubing pressure.

It should be emphasized that two models are integrated to determine the amount of lift gas that flows into the tubing in the commercial wellbore and pipeline simulators. In the first approach, it is assumed that sufficient injection pressure is available and the valve size is suitable to fully inject a constant amount and composition of the gas into the tubing. Thus, the amount of gas that is assigned for each valve will fully pass through the gas lift valves into the tubing (PIPESIM 2013). In the second approach, the valves become dominant and determine the amount of gas passage into the tubing based on several parameters such as annulus/tubing pressure and temperature.

Afterward, the value of the gas flow rate from the annulus into the tubing is transferred as an influx term into the mass, momentum, and energy conservation equations in the tubing. This influx term can be applied to the several numerical approaches that were developed for the multiphase flow in the wellbore, such as fully implicit homogenous model (FIMPHM), fully implicit drift-flux model (FIMPDF), semi-implicit two-fluid model (SIMPTF), nearly-implicit two-fluid model (NIMPTF), semi-implicit homogenous model (SIMPH), and steady state (SS) models.

3.3 VERIFICATION AND RESULTS

In this section, the developed numerical models are implemented to investigate the accuracy and efficiency of the developed model compared to a commercial simulator (i.e. PIPESIM).

3.3.1 Case 1: Steady State Black Oil Model

Table 3.2 presents the main input parameters for simulation of a gas lift model using the black oil steady state approach. As shown, there is a 15,000ft wellbore with constant bottom-hole pressure of 4,071 psi. The lift gas is injected at the depth of 14,800ft to assist in more liquid production. At the initial state, the wellbore cannot produce any fluid due to the high hydrostatic pressure. Initiating the gas injection reduced the fluid density and liquid started to flow. Figure 3.3 presents the pressure profile along the wellbore for the gas injection rate of 3.5 MMSCF/D. As can be seen, the result of UTWELL is in good agreement with PIPESIM. In fact, gas injection reduced the fluid density and hydrostatic pressure that results in more draw down pressure and more liquid production. As shown, the pressure changes linearly from the bottom to the top of the wellbore where the wellhead pressure of 384 psi is observed. Since the gas is injected nearly at the bottom of the wellbore, no sharp changes are observed in the pressure profile. Figure 3.4 shows the temperature profile in the tubing. As we move toward the wellhead, the temperature is decreasing and reaches 185°F at the surface. Figures 3.5 and 3.6 represent the velocity profile for the gas and oil phases, respectively. As we can see, the gas velocity increases as we go toward the wellhead due to the gas compressibility factor and volume expansion. In addition, some of the dissolved gas comes out of the solution at the depth of 6,000ft where the fluid reaches the bubble point and a sharp increase in the gas velocity profile is observed. On the other hand, the oil velocity decreases since some of the dissolved gas comes out of the oil and increases the oil density and viscosity. Additionally, a sensitivity analysis was performed on the amount of injection gas to determine its effect on the oil production rate. We expect that the hydrostatic term is initially the dominant term in calculating the pressure loss. Therefore,

increasing the injection gas flow rate reduces the pressure drop by reducing the liquid density. Thus, considering a constant wellhead pressure, the bottom-hole pressure decreases and higher liquid production is obtained. However, after reaching an optimum value, the friction term becomes the dominant term for the pressure loss. Therefore, increasing the injection gas flow rate above the optimum value has a negative consequence by causing more pressure drop which eventually results in greater bottom-hole pressure and less liquid production.

This trend is observed in Figure 3.7. As shown, increasing the injection gas flow rate from 5 to 20 MMSCF results in 8,000STB more oil production per day. The oil production rate reaches a maximum value of 16,000 STB/day at the 20 MMSCF/D gas injection rate. Beyond this value, the production rate decreases due to higher pressure drop in the wellbore and reduction in wellbore deliverability.

3.3.2 Case 2: Steady State Compositional Model

This case studies compositional model commissioned to simulate the gas injection process. In the compositional approach, the overall composition of the reservoir fluid and injection gas is specified by the user. Then, a vapor-liquid equilibrium flash calculation is performed using Peng-Robinson equation of state to determine mole fractions of each component in the oil and gas phase and fluid properties. The overall composition of the reservoir fluid and injection gas is presented in Table 3.3. The reservoir fluid consists of Methane, Ethane, Octane, and Decane with mole fractions of 0.05, 0.05, 0.1, and 0.8, respectively. In addition, Methane and Ethane are injected with the ratio of 4:1 as the components of the lift gas. The simulation input parameters are also presented in Table 3.4. The initial pressure of the reservoir is 1,500 psi, and the production well with a

length of 7,000ft is not able to produce any liquid in the beginning. After initiating the gas injection at the depth of 4,800ft, the well starts to flow. Figure 3.8 compares the pressure profile along the wellbore operating at a constant wellhead pressure of 100 psi simulated with UTWELL and PIPESIM. As can be observed, there is a good agreement between the results of PIPESIM and UTWELL. As shown, the slope of the pressure profile changes at the depth of 4,800ft which shows that the reservoir fluid density has been reduced. Figure 3.9 indicates the temperature variation along the wellbore. It can be seen that introducing the lift gas with lower temperature at the point of injection valve reduced the mixture temperature by about 7°F and the temperature of the produced fluid is 145°F. Figure 3.10 illustrates that no free gas exists in the reservoir fluid between the bottom-hole and 4,800ft. Injection of lift gas causes gas flow in the wellbore between 4,800ft and the surface. Figure 3.11 also indicates that introducing the lift gas increased the oil velocity from the gas injection point to the wellhead. At the vicinity of the injection valve, a sudden increase in oil velocity is observed due to gas influx from the annulus. Furthermore, Figure 3.12 depicts oil production rate versus different gas injection rate. As we expect, the oil flow rate reaches the maximum value at a specific gas injection rate (5 MMSCF/Day) and beyond this point, the oil production decreases as a result of increase in friction loss. At the optimum rate of gas injection, 8,000STB of oil production per day can be achieved.

3.3.3 Case 3: Transient Model

In this section, we simulate the performance of gas lift in a transient state. Table 3.5 shows the main input parameters of the transient case. A vertical well with 1,600ft length was designed to study the developed transient model. This well is in a reservoir

with initial pressure of 900 psi and initial temperature of 180°F. Due to high hydrostatic pressure, the production has ceased. Therefore, production under gas lift mechanism is considered for this wellbore. The lift gas is injected with injection pressure of 350 psi and surface temperature of 110 °F at the depth of 1,350ft. We performed a transient simulation study in a way that we reach the steady state condition at the end of simulation.

Figures 3.13 through 3.15 show the simulation results calculated by UTWELL at three simulation time-steps (i.e. 1min, 6 min, and 60min) until we reached the steady state condition. Since the case was constructed for a shallow well, we expect to reach the steady state condition not too long after initiating the production. The lift gas is also injected into the annulus with the flow rate of 0.5 MMSCF/D. As we start gas injection and producing from the wellbore, oscillations in gas and oil velocities are observed. Figure 3.13 illustrates that the pressure profile along the wellbore changes smoothly through time and reaches the steady state condition about 6 minutes after initiating production and the trend of pressure remains constant nearly after 6 minutes. Figure 3.14 depicts the gas velocity at three time steps. As shown, the velocity significantly changes along the wellbore through time and especially at the early time of the production. As time progresses, these oscillation in velocity decreases and the results converge to a fixed trend. It can be seen that after 6 minutes, a small wave of oscillation still remains at the middle of the wellbore that shows that the steady state solution is not obtained yet. However, after 1 hour of production, the system reaches the steady state condition and a steady state profile can be observed. Figure 3.15 also shows the existence of oscillations in oil velocity at the early time of the simulation, especially at the point of gas injection (i.e. 1,350ft) where lift gas is injected into the tubing with variable rates due to a transient

state of gas flow in the annulus. As time proceeds, gas flow in the annulus and tubing converges to steady solutions. It is obvious from Figure 3.15 that the oil velocity attains higher value at the point of gas injection and as we go toward the wellhead, the velocity decreases.

3.3.4 Case 4: Multiple Point Gas Injection

This case investigates a more complicated wellbore model in which two types of tubing, casing, and liner with different diameter and specification are designed. In addition, we designed two point gas injections in the tubing since there are many applications of several unloading valves or multiple injection points in many gas lifted wells. All of the simulation parameters are presented in Table 3.6. In addition, a schematic profile of the designed wellbore is presented in Figure 3.16 where the locations and sizes of the casing, tubing, and liner are specified. This wellbore consists of a casing with internal diameter of 0.28645ft from the surface to the depth of 6,500ft. Then a liner with the diameter of 0.236458ft was constructed from 6,500ft to the bottom of the wellbore. Moreover, Tubing 1 with internal diameter of 0.13579ft is placed from the surface to 6,500ft. Tubing 2 with internal diameter of 0.11458 is also constructed from 6,500ft to the bottom-hole.

To study this case thoroughly, we plotted various variables, such as pressure, temperature, and velocity of the gas flow in the annulus as well. Figure 3.17 illustrates the pressure profile in the annulus. As can be seen, the gas is initially injected into the annulus with the pressure of 1,000 psi. Then, the pressure increases linearly from the surface to the bottom-hole where it reaches 1,250 psi. Temperature profile is also shown in Figure 3.18. The injection gas temperature at the surface is 120°F. As we go

downward in the annulus, the temperature initially decreases and then, increases again due to heat transfer with the surrounding formation. Moreover, due to the gas outflow into the tubing and Joule-Thomson effect, two sharp changes in temperature are observed at the location of injection valves. Since two thirds of the gas flow in the tubing from the first injection valve (8,500ft), the change in temperature is more obvious at this location. The gas velocity in the annulus is also presented in Figure 3.19. Initially the gas is injected with the surface velocity of 2.2ft/s and then the velocity smoothly declines as we move downward. There are three sharp changes in the velocity profile corresponding to the depth of 5,000, 6,500, and 8,500ft, respectively. At the depth of 5,000ft, due to the outflow of gas from the annulus into the tubing, the gas mass flow rate decreases causing a reduction in gas velocity. At 6,500ft, the velocity decreases by about 0.2ft/s due to an increase in annulus cross section. Finally, due to the outflow of the gas in the first injection gas, most of the gas goes into the tubing and a negligible amount of gas remains at the lower section of the annulus.

Figure 3.20 shows the pressure profile corresponding to the above case. At depth of 8,500ft, a sharp change in the pressure profile is observed, since almost two thirds of the lift gas is injected at this point into the wellbore. Thus, the liquid density is reduced more significantly. However, the effect of the second gas lift valve at the location of 5,000ft is less pronounced. As shown, a good agreement is observed between the results of UTWELL and PIPESIM.

Figure 3.21 demonstrates temperature variations along the wellbore from 185°F at the bottom-hole to the 76.5°F at the surface. At the location of first gas injection valve (8,500ft), nearly 7°F decrease in the temperature is observed due to the introduction of gas with lower temperature compared to the initial temperature of the reservoir fluid. On

the other hand, at the point of the second gas injection valve, the temperature increases by about 2°F since the lift gas temperature is greater than the mixture temperature in the tubing.

Figures 3.22 and 3.23 present oil and gas velocities in the tubing. A sharp reduction of oil and gas velocities at the depth of 6,500 is attributed to the increase in the tubing cross section area. It is also clear that the gas velocity increases at the location of gas injection valves and as we move toward the wellhead, higher gas velocity is observed. Finally, Figure 3.24 compares the mixture velocity in the tubing calculated by UTWELL and PIPESIM. As can be observed, there is good agreement between the mixture velocity results of PIPESIM and UTWELL.

Table 3.1: Rule of thumb criteria of continuous and intermittent gas lift (Santos et al., 2001)

Static head (h_s/H_w)	Productivity index (PI, m^3/day.MPa)		
	High (> 20)	**Medium (5 to 20)**	**Low (< 5)**
High (>0.7)	Continous Gas Lift	Continous /Intermittent Gas Lift	Intermittent Gas Lift
Medium (0.4 to 0.7)	Continous /Intermittent Gas Lift	Continous /Intermittent Gas Lift	Intermittent Gas Lift
Low (<0.4)	Intermittent Gas Lift	Intermittent Gas Lift	Intermittent Gas Lift

Table 3.2: Input parameters for black oil steady state gas lift model (Case 1)

Parameter	**Value**
Wellbore MD	15000 ft
Wellbore TVD	15000 ft
Gas Lift Valve Depth	14800
Maximum Grid Size	100 ft
Tubing Inner Radius	0.23 ft
Tubing Outer Radius	0.28 ft
Surface Temperature	59.5 °F
Bottom-hole Temperature	250 °F
Injection Temperature	150 °F
Reservoir Pressure	5000 psi
Injection Pressure	3400 psi
Lift Gas Flow Rate	3.5 MMScf/Day
Lift Gas Specific Gravity	0.6
Annulus Heat Transfer	4 Btu/Hr.°F.ft^2
Tubing Heat Transfer	10 Btu/Hr.°F.ft^2
Oil Productivity Index	0.1 STB/psi-day-ft

Table 3.3: Fluid compositions of the steady state compositional gas lift model (Case 2)

	Reservoir Fluid	Gas Lift
Component	**Mole Fraction**	**Mole Fraction**
C1	0.05	0.8
C2	0.05	0.2
NC8	0.1	0
NC10	0.8	0

Table 3.4: Input parameters for compositional steady state gas lift model (Case 2)

Parameter	**Value**
Wellbore MD	7000 ft
Wellbore TVD	7000 ft
Gas Lift Valve Depth	4800 ft
Maximum Grid Size	300 ft
Tubing Inner Radius	0.23 ft
Tubing Outer Radius	0.28 ft
Surface Temperature	60 °F
Bottom-hole Temperature	180 °F
Injection Temperature	120 °F
Reservoir Pressure	1500 psi
Injection Pressure	800 psi
Lift Gas Flow Rate	1.0 MMScf/Day
U_{total}	0.2 Btu/Hr.°F.ft^2
Oil Productivity Index	1 STB/psi-day-ft

Table 3.5: Input parameters for a transient gas lift model (Case 3)

Parameter	**Value**
Wellbore MD	1600 ft
Wellbore TVD	1600 ft
Gas Lift Valve Depth	1350 ft
Maximum Grid Size	50 ft
Tubing Inner Radius	0.1145 ft
Tubing Outer Radius	0.14583 ft
Surface Temperature	60 °F
Bottom-hole Temperature	180 °F
Injection Temperature	110 °F
Reservoir Pressure	900 psi
Injection Pressure	350 psi
Lift Gas Flow Rate	0.5 MMSCF/D
Total Heat Transfer	0.2 Btu/Hr.°F.ft^2
Oil Productivity Index	0.1 STB/psi-day-ft

Table 3.6: Input parameters for multiple point gas injection model (Case 4)

Parameter	Value
Wellbore MD	10200 ft
Wellbore TVD	10200 ft
Gas Lift Valve Depth	8500 ft 5000 ft
Maximum Grid Size	100 ft
Tubing Inner Radius	0.13579 ft @ 0-6500 ft 0.11458 ft @ 6500-10200 ft
Tubing Outer Radius	0.13839 ft @ 0-6500 ft 0.117878 ft @ 6500-10200 ft
Casing Inner Radius	0.28645 ft @ 0-6500 ft
Liner Inner Radius	0.236458 ft @ 6500-10200 ft
Casing Outer Radius	0.3177 ft @ 0-6500 ft
Liner Outer Radius	0.276038 ft @ 6500-10200 ft
Surface Temperature	50 °F
Bottom-hole Temperature	185 °F
Injection Temperature	120 °F
Reservoir Pressure	1500 psi
Injection Pressure	1000 psi
Lift Gas Flow Rate	1.5 MMScf/Day
Lift Gas Specific Gravity	0.8
Total Heat Transfer	2 Btu/Hr.°F.ft^2
Oil Productivity Index	1 STB/psi-day-ft
API	25
Gas Specific Gravity	0.88
Gas Thermal Conductivity	0.02 Btu/Hr.°F.ft
Oil Thermal Conductivity	0.08 Btu/Hr.°F.ft
Water Thermal Conductivity	0.35 Btu/Hr.°F.ft
Gas Specific Heat Capacity	0.55 Btu/lbm.°F
Oil Specific Heat Capacity	0.45 Btu/lbm.°F
Water Specific Heat Capacity	1 Btu/lbm.°F

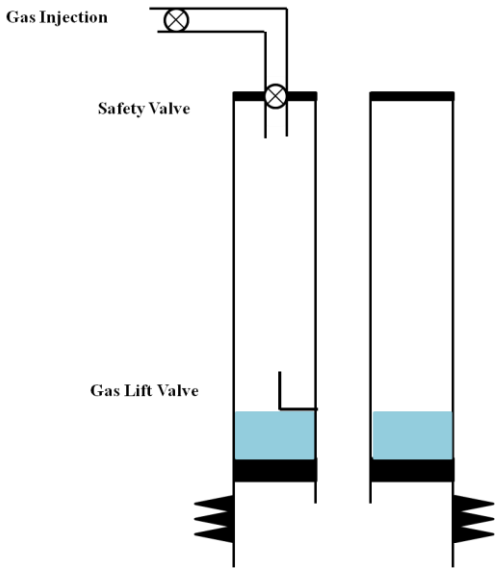

Figure 3.1: Schematic view of the gas lift operation.

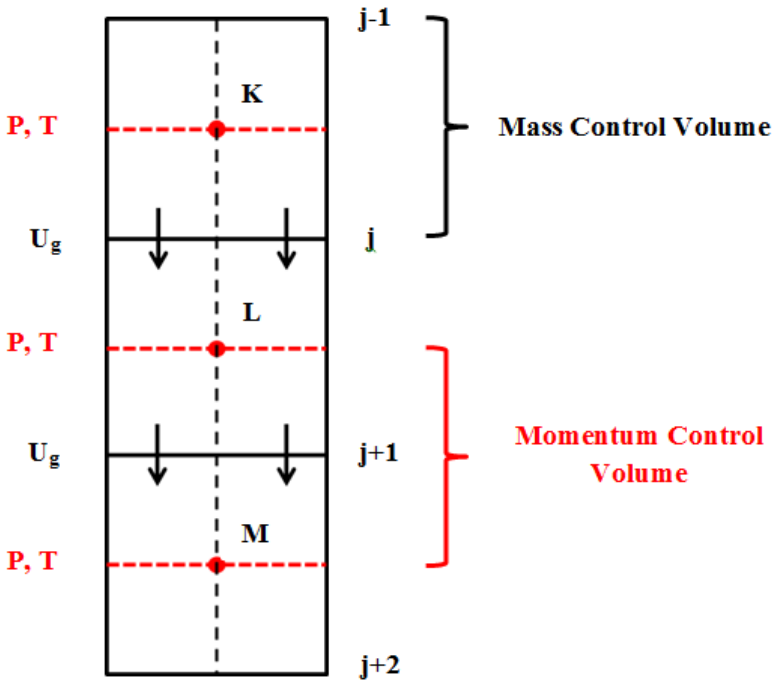

Figure 3.2: Schematic view of annulus gridblocks.

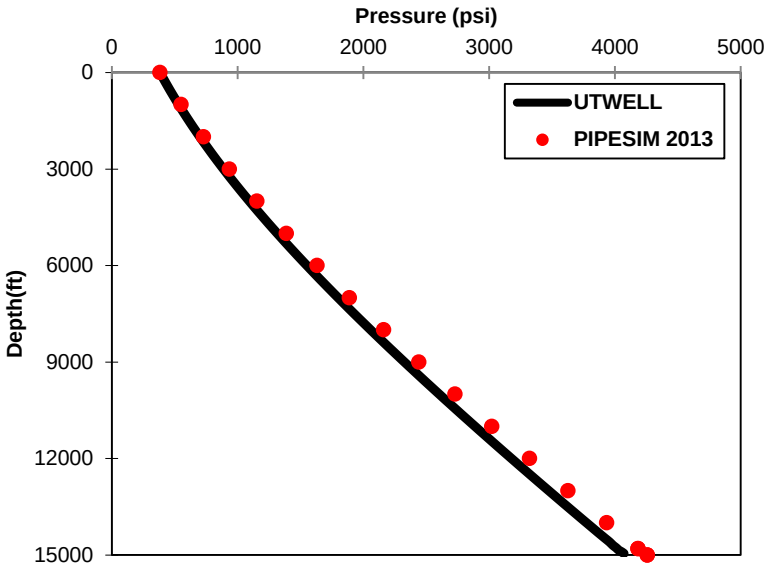

Figure 3.3: Pressure profile in the wellbore after 3.5 MMSCF/D gas injection at depth of 14800ft (Case1). Comparison of the results between PIPESIM and UTWELL.

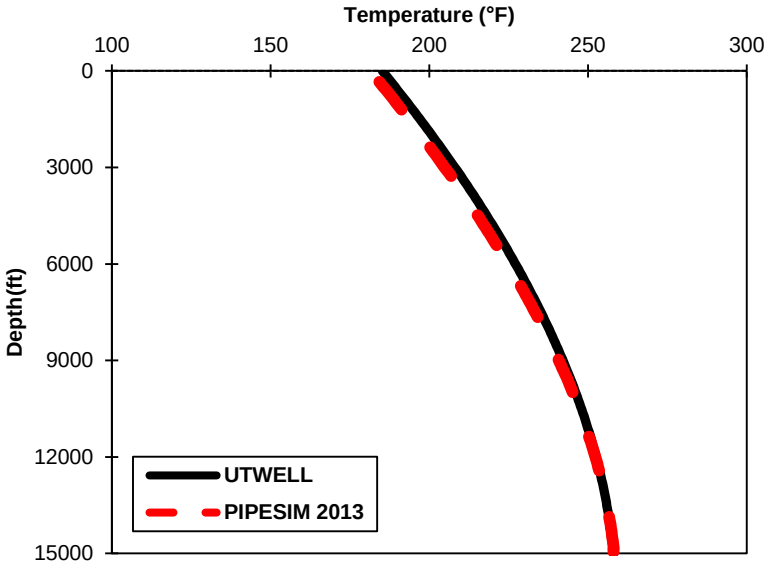

Figure 3.4: Temperature profile in the wellbore after 3.5 MMSCF/D gas injection at depth 14800ft (Case1). Comparison of the results between PIPESIM and UTWELL.

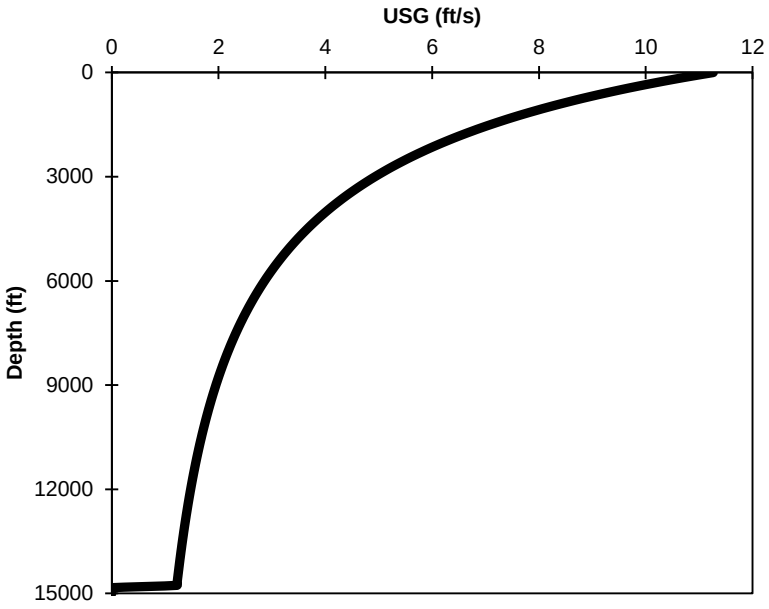

Figure 3.5: Gas velocity profile in the wellbore after 3.5 MMSCF/D gas injection at depth 14800ft (Case1)

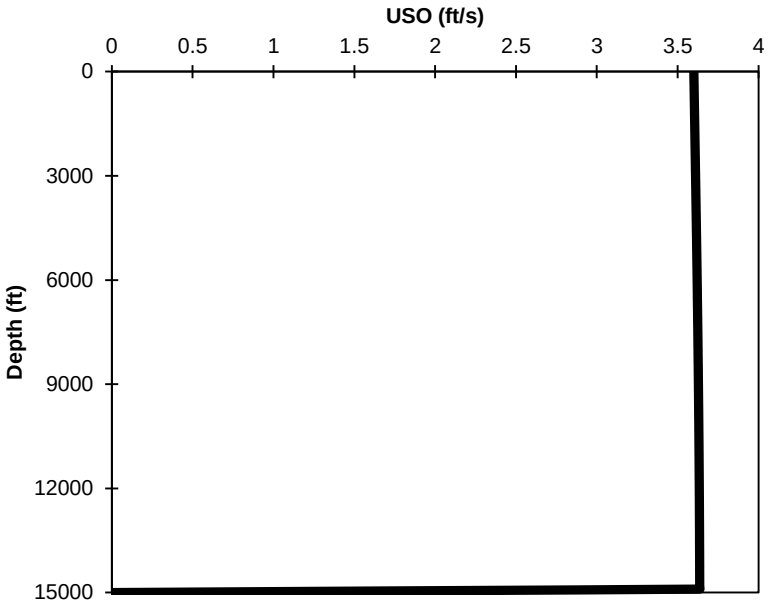

Figure 3.6: Oil velocity profile in the wellbore after 3.5 MMSCF/D gas injection at depth 14800ft (Case1).

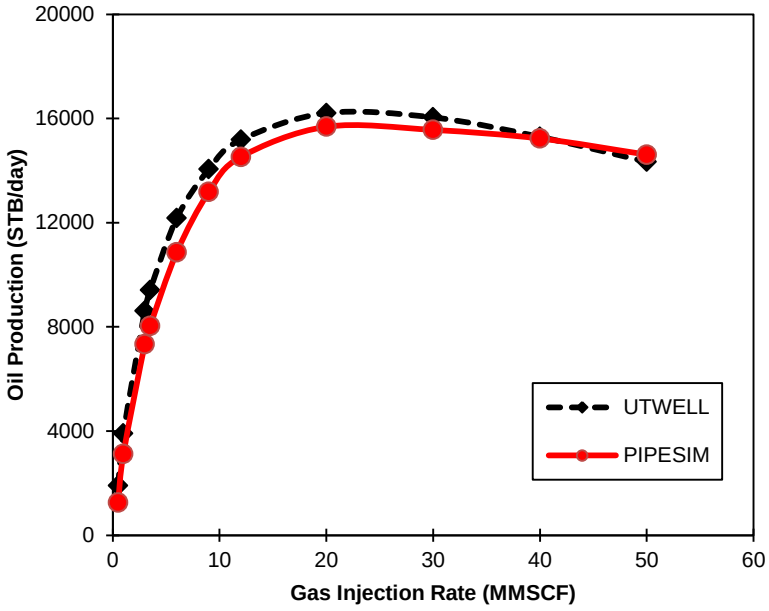

Figure 3.7: Oil flow rate versus gas injection rate for gas lift optimization (Case1). Comparison of the results between PIPESIM and UTWELL.

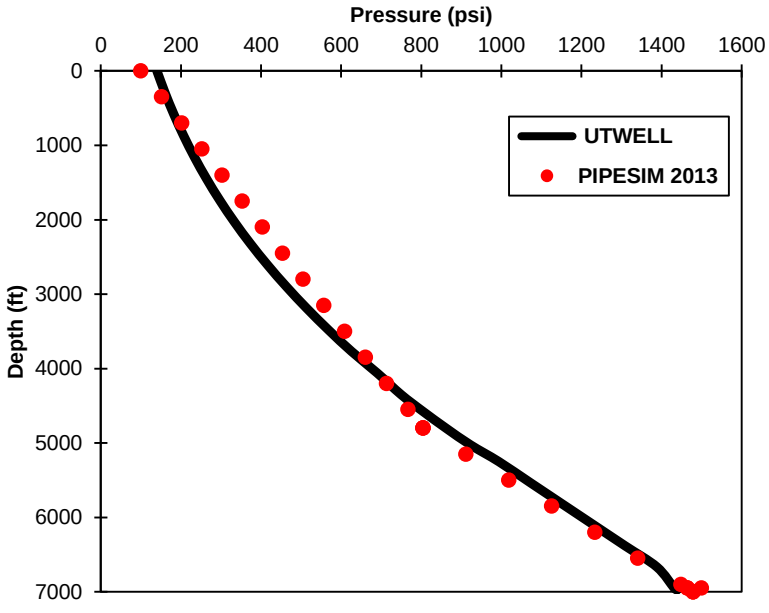

Figure 3.8: Pressure profile in the wellbore after 1 MMSCF/D gas injection at depth 4800ft (Case2). Comparison of the results between PIPESIM and UTWELL.

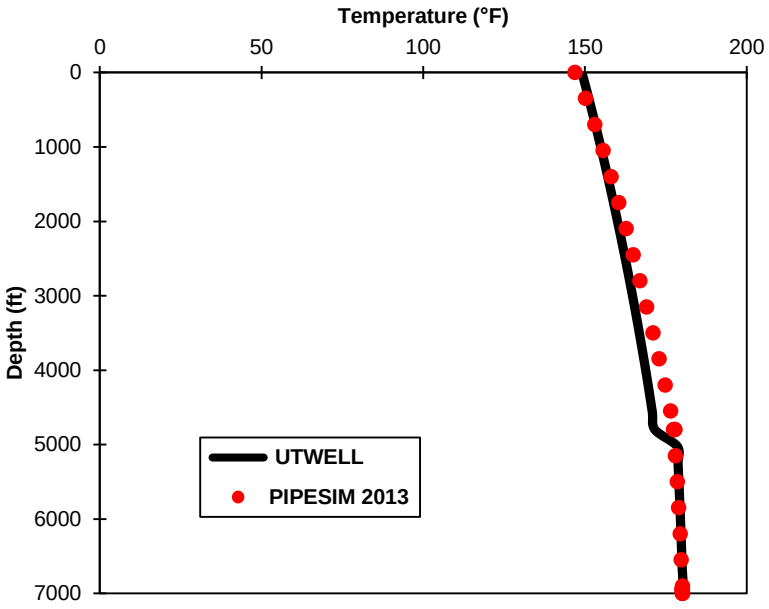

Figure 3.9: Temperature profile in the wellbore after 1 MMSCF/D gas injection at depth 4800ft (Case2). Comparison of the results between PIPESIM and UTWELL.

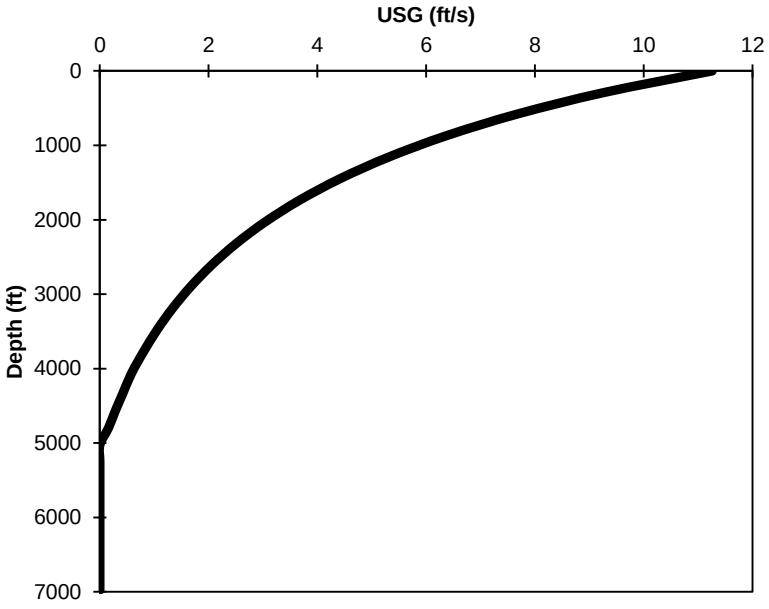

Figure 3.10: Gas velocity profile in the wellbore after 1 MMSCF/D gas injection at depth 4800ft (Case2).

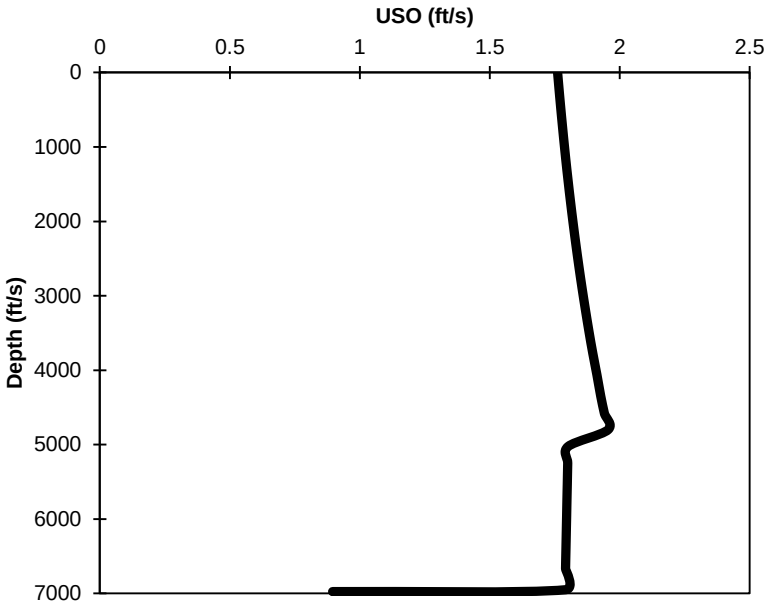

Figure 3.11: Oil velocity profile in the wellbore after 1 MMSCF/D gas injection at depth 4800ft (Case2).

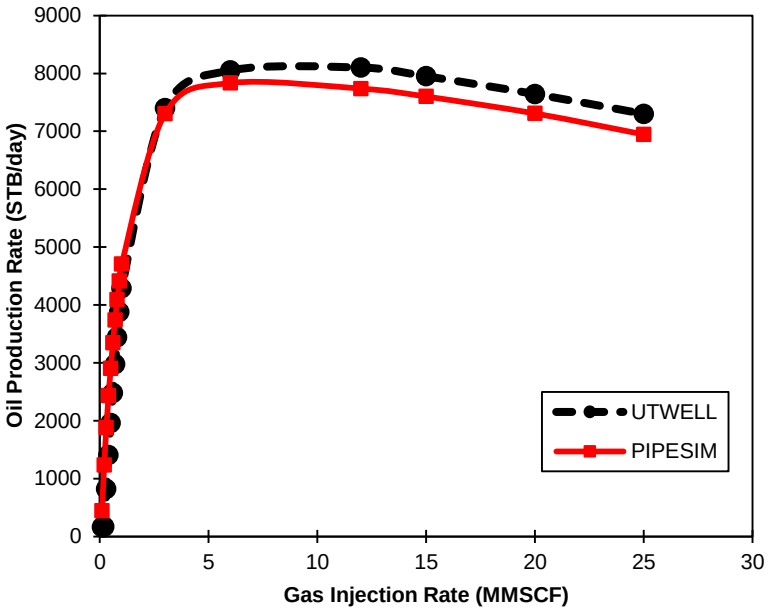

Figure 3.12: Oil flow rate versus gas injection rate for gas lift optimization (Case2). Comparison of the results between PIPESIM and UTWELL.

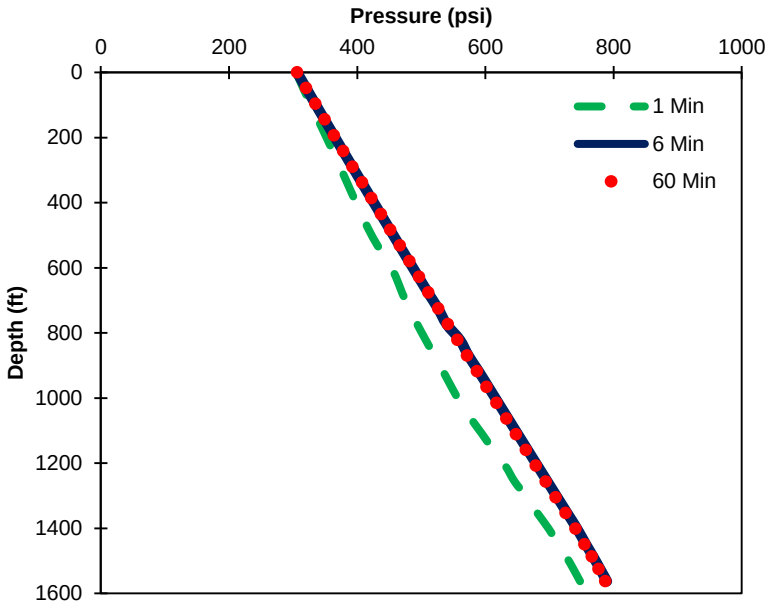

Figure 3.13: Pressure profile in the wellbore after 0.5 MMSCF/D gas injection at depth 1350ft (Case3).

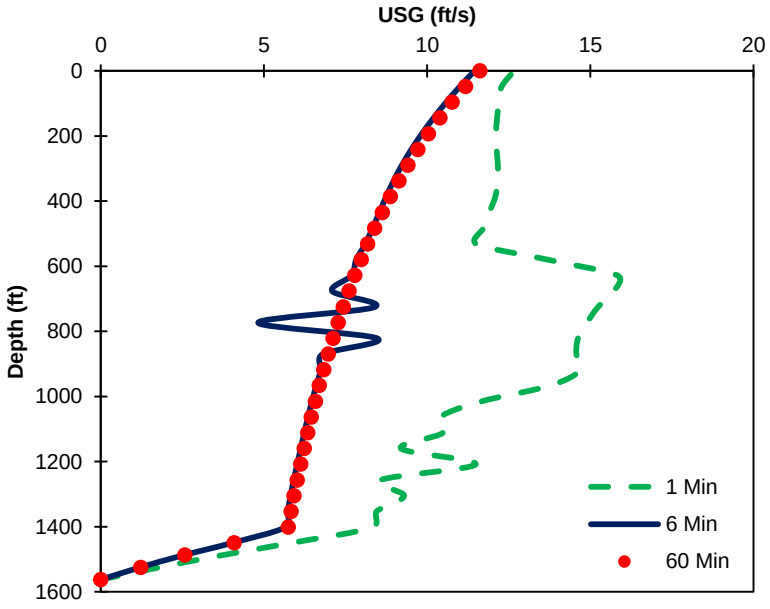

Figure 3.14: Gas velocity profile in the wellbore after 0.5 MMSCF/D gas injection at depth 1350ft (Case3).

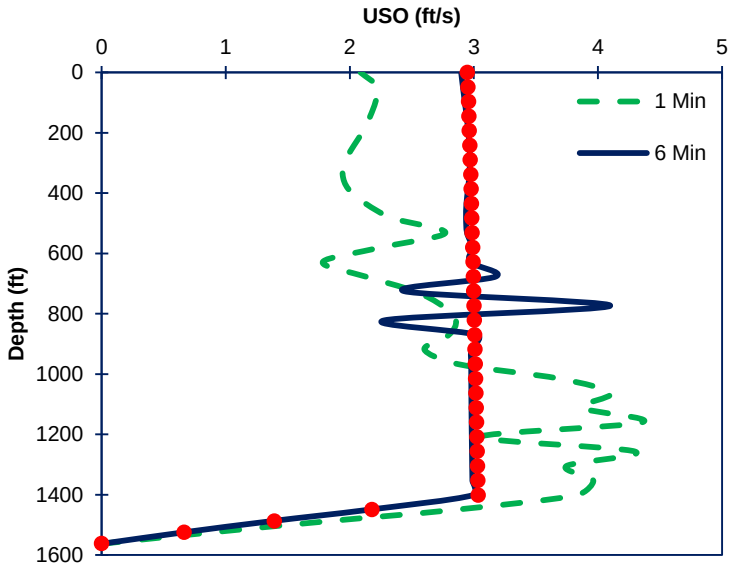

Figure 3.15: Gas velocity profile in the wellbore after 0.5 MMSCF/D gas injection (Case3).

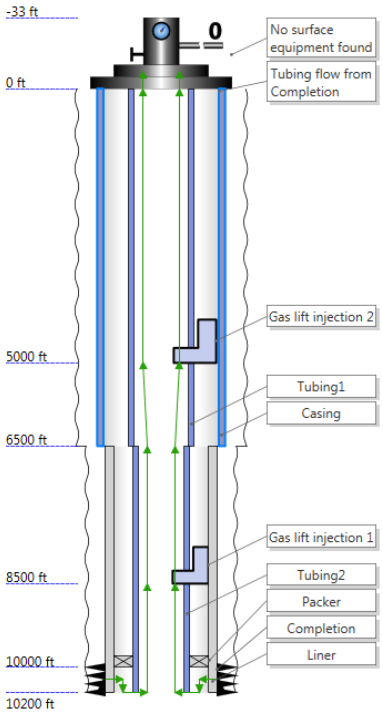

Figure 3.16: Schematic design of the wellbore for Case 4 (PIPESIM 2013).

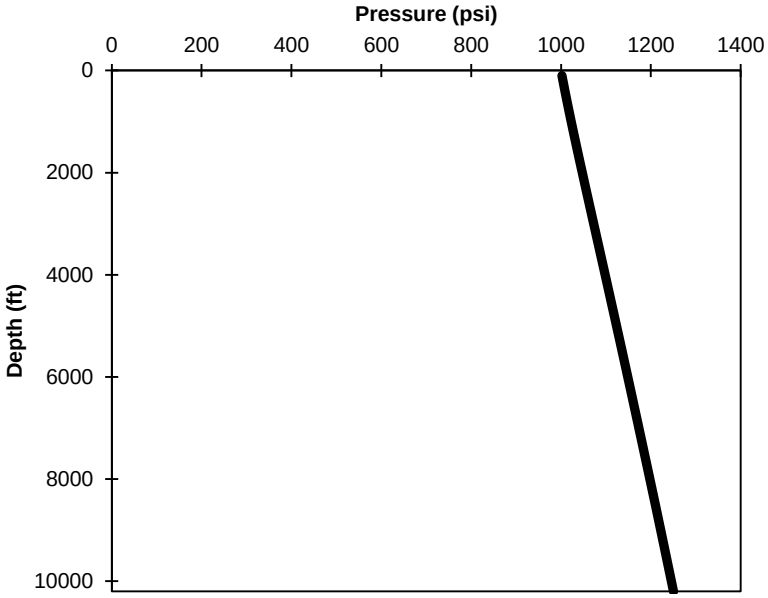

Figure 3.17: Pressure profile in the annulus after 1.5 MMSCF/D gas injection at two points: 5000ft, 8500ft (Case 4).

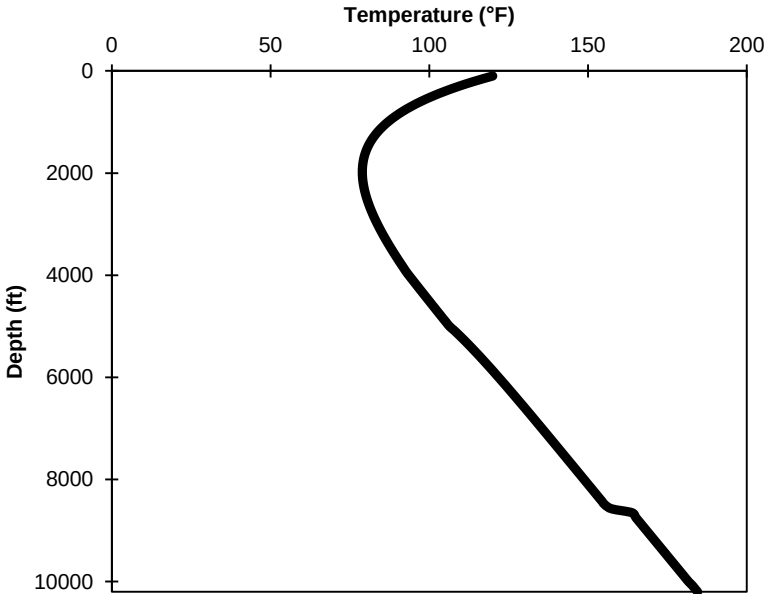

Figure 3.18: Temperature profile in the annulus after 1.5 MMSCF/D gas injection at two points: 5000ft, 8500ft (Case 4).

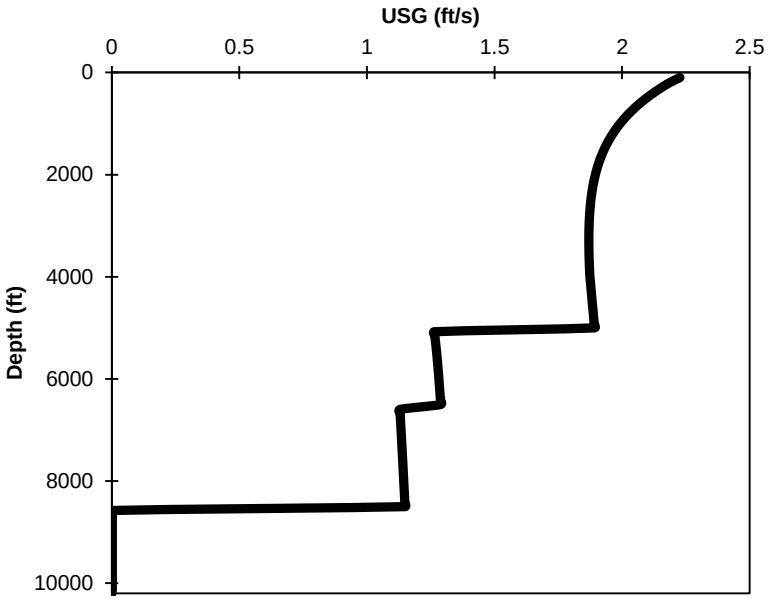

Figure 3.19: Gas velocity profile in the annulus after 1.5 MMSCF/D gas injection at two points: 5000ft, 8500ft (Case 4).

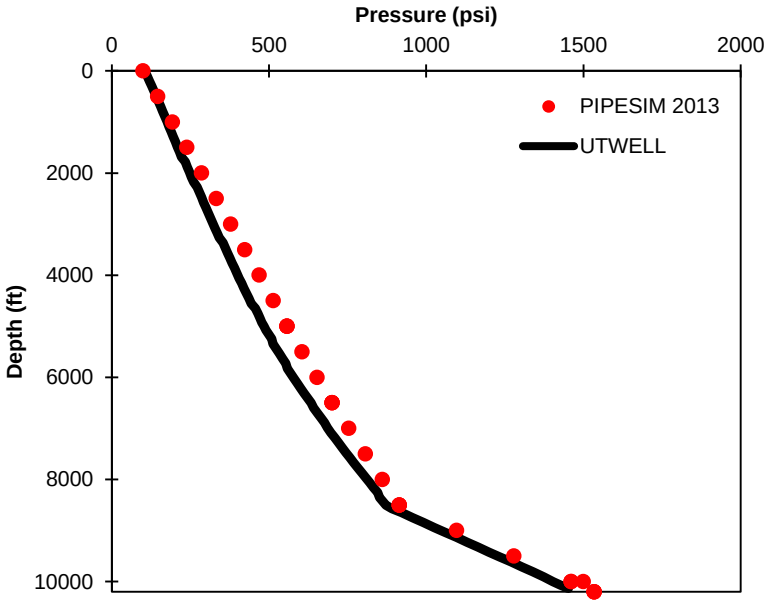

Figure 3.20: Pressure profile in the wellbore after 1.5 MMSCF/D gas injection at two points: 5000ft, 8500ft (Case 4).

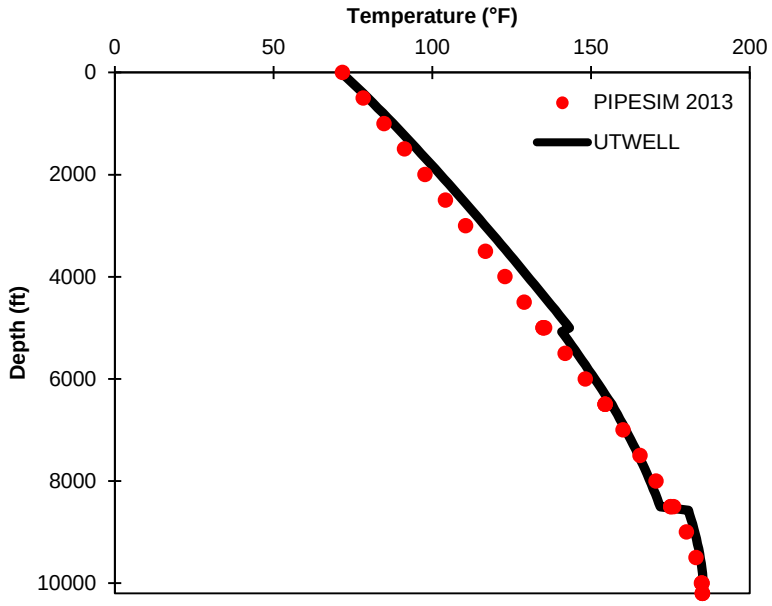

Figure 3.21: Temperature profile in the wellbore after 1.5 MMSCF/D gas injection at two points: 5000ft, 8500ft (Case 4).

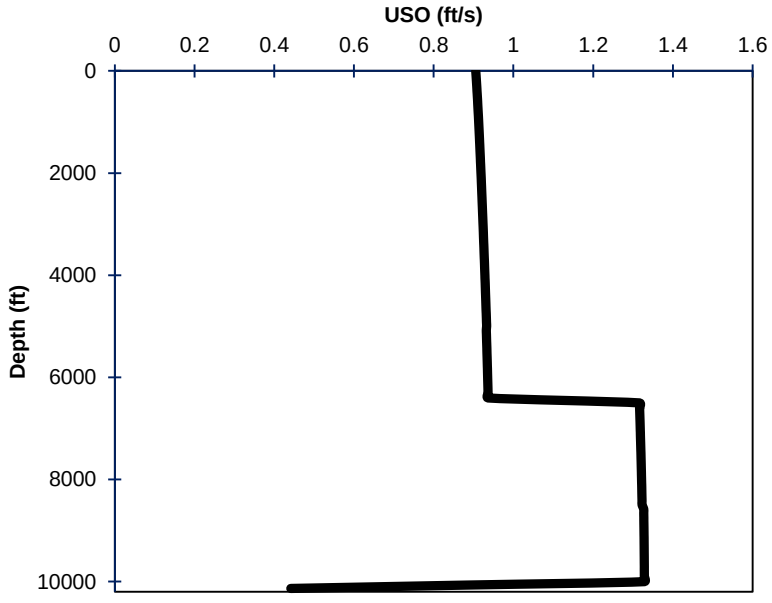

Figure 3.22: Oil velocity in the wellbore after 1.5 MMSCF/D gas injection at two points: 5000ft, 8500ft (Case 4).

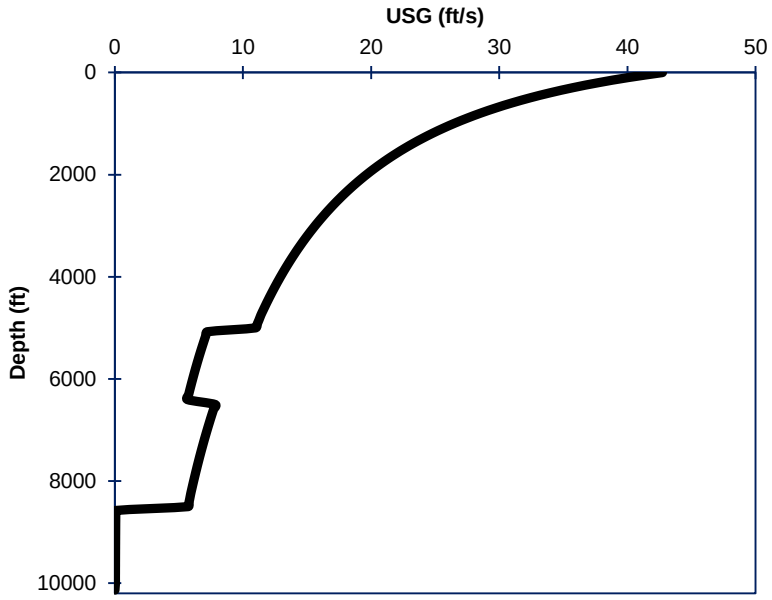

Figure 3.23: Gas velocity in the wellbore after 1.5 MMSCF/D gas injection at two points: 5000ft, 8500ft (Case 4).

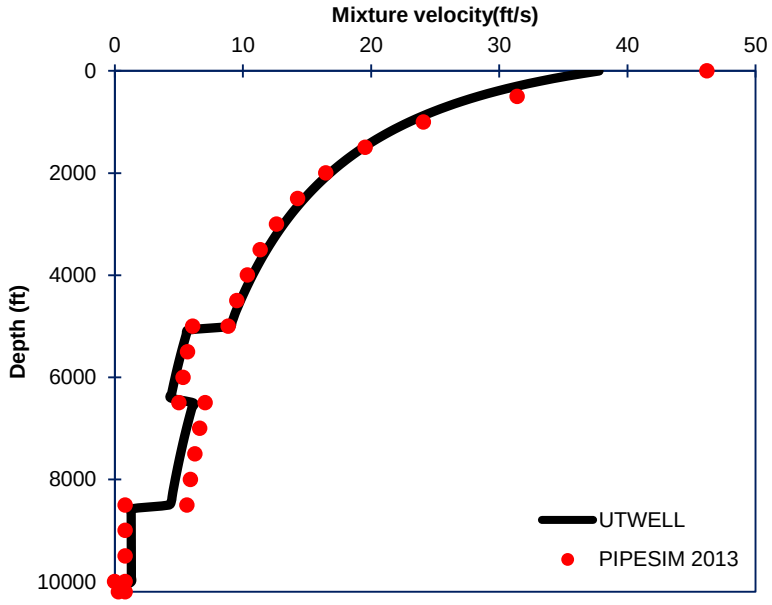

Figure 3.24: Mixture velocity in the wellbore after 1.5 MMSCF/D gas injection at two points: 5000ft, 8500ft (Case 4).

Chapter 4: Modeling Asphaltene Deposition in the Wellbore During Gas Lift Process[1]

Asphaltene deposition during oil production may partially or totally plug the wellbore and result in significant reduction in well production and frequent asphaltene remediation jobs. It is well known that injection of lighter hydrocarbons into an asphaltic oil (e.g. during gas lift) may decrease the stability of asphaltene particles in the solution and increase the risk of asphaltene precipitation and deposition. Although a great deal of research has investigated the effect of gas injection on the phase behavior and the mechanism of asphaltene deposition in the wellbore, there is a lack of comprehensive dynamic model that can track the behavior of asphaltene during gas lift processes. Therefore, a comprehensive model is required for evaluating the risk of gas lift on asphaltene deposition in production wells.

This chapter presents a comprehensive thermal compositional wellbore model with the capability to model asphaltene phase behavior during gas lift and determine the effect of the injected gas on asphaltene deposition in the wellbore. In the developed model, various numerical approaches were used to model multiphase flow in the wellbore. An equation of state was used to calculate the thermodynamic equilibrium conditions of the phases. In addition, several deposition mechanisms were incorporated to study the transportation, entrainment, and deposition of solid particles in the wellbore.

[1] Some parts of Chapter 3 and 4 are published in the following citation:
Abouie, A., Shirdel, M., Darabi, H., and Sepehrnoori, K. 2015. Modeling Asphaltene Deposition in the Wellbore During Gas Lift Process. Presented in SPE Western Regional Meeting, Garden Grove, California, USA. (SPE-174067-MS).

In this work, various case studies investigated the effect of gas lift on asphaltene deposition. To predict the time and location in which the most severe damage would occur in the wellbore, we used field data of a Middle East crude oil and simulated gas injection process. The results showed that the injection of light gas composition can negatively affect the production facilities by intensifying asphaltene precipitation in the well, which eventually results in significant reduction in the wellbore production. The comprehensive thermal compositional wellbore model presented in this work can facilitate the design of work-over operation plans for asphaltic wells operating under gas lift.

4.1 BACKGROUND

It is clear that evaluation of operability and feasibility of gas lift from different aspects such as flow assurance is crucial. Addition of lighter hydrocarbons as lift-gas to the wellbore fluid results in composition changes that can negatively affect deposition of asphaltene in the tubing (Hudson et al. 2002; Jayawardena et al. 2007). This condition becomes more severe when the flow rate is low and the composition of the reservoir fluid is unstable. Higher water depth also results in cooler produced fluid which increases the chance of flow assurance issues. Accordingly, asphaltene deposition results in plugging the wellbore and surface facilities, reduction of the production rates, and adverse financial issues. In some severe cases, it becomes necessary to inject asphaltene inhibitors at the location of gas injection to prevent wellbore blockage. To mitigate the effect of asphaltene deposition on the well performance, it is necessary to have a comprehensive dynamic model to evaluate lift-gas composition and operating scenarios and predict the effect of asphaltene precipitation in the early life of the project.

Many researchers have studied asphaltene deposition in the production systems. Ramirez-Jaramillo et al. (2006) developed a model which couples multiphase flow, transport phenomena, and phase equilibrium of the fluid. Their model combined four-phase interacting system, rheological equation of state, and empirical correlation for multiphase flow to study asphaltene deposition in the wellbore. Vargas (2009) developed a single-phase simulator which can predict asphaltene precipitation and deposition in the wellbore. He showed fairly good agreement of simulation results with test tube experimental data. In addition, Kurup et al. (2011) developed a deposition tool to predict asphaltene deposition in wellbores and pipelines. Their model was compared to capillary pipe experiment and good agreement was observed. Moreover, Shirdel (2013) developed a compositional thermal wellbore model to simulate asphaltene precipitation and deposition in the wellbore. In this paper, additional capabilities are added to the Shirdel (2013) wellbore model to investigate asphaltene deposition in a Middle East producing wellbore under gas lift mechanism.

In the next section, the fluid characterization method and deposition model are presented. Furthermore, simulation case studies are presented for primary production and production under gas lift mechanism.

4.2 MODEL DEVELOPMENT

The development of the model consists of four parts: characterizing the experimental data, developing a thermal compositional wellbore model, incorporating gas lift module in the model, and integrating a deposition tool to accurately predict the asphaltene deposition on the tubing wall. In Chapter 2, a summary of the wellbore model

was given. Moreover, we presented a gas lift model in Chapter 3. In this chapter, fluid characterization and deposition models are described, respectively.

4.2.1 Fluid Characterization[2]

In this section, we present a guideline for characterization of non-asphaltic and asphaltic oil.

4.2.1.1 Non-asphaltic Fluid Characterization

Reservoir fluid characterization is one of the most important issues in compositional simulation. It is necessary to use a suitable Equation of State (EOS), an accurate fluid description, and a robust flash algorithm to accurately predict the phase behavior and match the experimental data.

Based on Pedersen et al. (2012), six to nine hydrocarbon components are often enough to characterize a reservoir fluid. The lumping scheme is as follows:

(1) Group non-hydrocarbons components separately

(2) Make separate groups of C_1-C_6 hydrocarbons

(3) Use a weight-based grouping for C_{7+} in a way that each pseudo component has approximately the same weight. In addition, the critical properties of each pseudo component are calculated using weight mean averages of the critical properties of each individual carbon number fraction

[2] Some parts of this section were presented in the following report:
Abouie, A., Darabi, H., and Sepehrnoori, K. April 2014. Progress Report on the Characterization of a Middle East Fluid During Gas Injection, The University of Texas at Austin

With the consideration of non-hydrocarbons components, this method usually leads to seven or eight pseudo components. This lumping scheme is very general. Khan (1992) presented more specific guidelines for fluid characterization as given below:

(1) Neglect non-hydrocarbons with small mole fraction, e.g. less than 0.005. The only exception to this assumption is when the non-hydrocarbon is injected.

(2) Usually, C_1 to C_6 are grouped as C_1, C_{2-3}, and C_{4-6}. Though, other combinations are also possible depending on the respective mole fractions.

(3) The number of pseudo components for splitting C_{7+} fraction is determined based on the procedure provided in Table 4.1.

4.2.1.2 Asphaltic Fluid Characterization

Asphaltic fluid characterization consists of tuning all the parameters of the phase behavior model to reproduce the experimental data. Normally, the experimental data includes bubble point pressure, separator test, liberations test, etc. In the case of asphaltic oil, SARA (Saturate, Aromatic, Resin, and Asphaltene) test usually will be performed to determine the asphaltene content of the fluid. In addition, asphaltene onset pressure at different conditions (pressure, temperature, and composition; in the case of gas injection) will be measured. Sometimes, the amount of precipitation at different conditions will also be measured. In this case, the precipitation model should be comprehensive enough to be able to predict the amount of precipitation at different conditions. Nevertheless, asphaltene precipitation data is not readily available for analysis. Darabi (2014a, b) provided a guideline for asphaltic fluid characterization for the precipitation model of UTCOMP, The University of Texas compositional simulator, as follows:

(1) Gather all the experimental data including bubble point pressure, asphaltene onset pressure, SARA analysis, etc.

(2) Split the heaviest component into the several heavier fractions. The fluid data are usually available up to C_{7+}. However, asphaltene molecular weight is usually larger than a typical C_{7+} molecular weight in a mixture. Asphaltene component usually can be represented by components between C_{30+} and C_{40+}.

(3) Split the heaviest component (e.g. C_{40}) into two components: a non-precipitating component (C_{40+A}) and a precipitating component (C_{40+B}). We refer to the precipitating component (C_{40+B}) as asphaltene. The properties of these two components are identical except for their binary interactions with the lighter components.

(4) Choose the tuning parameters. Tuning parameters provide a way to match the results of the phase behavior with the experimental data. For the asphaltic fluid, the tuning parameters include the number of lumping groups (n_L), binary interaction coefficients, volume shift parameters, and molar volume of asphaltene.

(5) Lump few of the middle components together to reduce the number of components in the simulation

(6) Perform phase behavior calculation.

(7) Compare the results of the phase behavior calculation with the experimental data.

(8) If the difference between the results of the phase behavior calculation and experimental data are less than the specified value, end this procedure. Otherwise, use trial and error or an optimization algorithm to update the tuning parameters values and go to step (5).

Accordingly, we used UTCOMP to characterize the fluid and tune the precipitation model (UTCOMP technical documentation 2011). The experimental data set available for the fluid includes bubble point pressure and onset pressure of the original fluid as well as the bubble point and onset point for the fluid after mixing. Table 4.2 shows the composition of the reservoir fluid and the associated gas used in gas lift process. Table 4.3 presents the tuned properties for the mixture fluid; Table 4.4 presents the binary interaction coefficients. As can be seen in Table 4.4, the binary interaction coefficients are larger between asphaltene and lighter components. The tuned phase behavior model predicts the bubble point and the onset pressure to be around 2100 psi and 5000 psi, respectively, which are in good agreement with the experimental data. In addition, the molar volume of asphaltene is set at 16.7 ft^3/lb-mol. To test the matched phase behavior model, the results of the phase behavior model are compared with the experimental data for the original fluid (no associated gas). Experimental data reports that both the bubble point and the onset pressure of the original fluid are 950 psi. The tuned phase behavior by UTCOMP suggests that the bubble point pressure of the original fluid to be around 950 psi, which matches the experimental bubble point. In addition, the asphaltene onset pressure is calculated to be 1000 psi, which is in good agreement with the experimental data.

Figure 4.1 shows the predicted asphaltene precipitation curves for the original fluid and the mixtures with 10%, 20% and 34.5% associated gas. As can be observed, the onset point, bubble point, and offset point pressures increase due to the gas injection. However, the rate of incline for the onset pressure is much higher than the offset point. Therefore, the asphaltene instability range expands due to gas injection. In addition, the maximum amount of asphaltene precipitation, which occurs around the bubble point,

increases because of introducing gas to the fluid. As shown, the maximum amounts of precipitation are about 0.5%, 2.5%, 5.5%, and 11.5% for the original fluid, 10%, 20%, and 34.5% associated gas, respectively.

Figure 4.2 shows the asphaltene precipitation envelope of the Middle East fluid, calculated using the tuned phase behavior model of UTCOMP. The purple line shows the onset pressures at different associated gas concentrations. In addition, the red and green lines correspond to the bubble point and offset point pressures. Asphaltene precipitation envelope indicates the asphaltene instability conditions. At any point between the purple and green lines, asphaltene precipitates from the oil. As can be seen, the experimental data points for the onset point and bubble point pressures are included in Figure 4.2. Therefore, it is obvious that the tuned phase behavior model is in agreement with the experimental data.

4.2.2 Deposition Model

Determining the solid particle deposition rate is very challenging and depends on several parameters, such as flow regime and distribution of the fluids. In this section, we present an inclusive model for particle deposition in the flow stream.

Several studies have been performed to develop solid deposition model on the flow lines wall. Lin et al. (1953) demonstrated a classical approach to model mass transfer between a turbulent flow stream and the walls. They introduced mass transfer equation considering the same eddy viscosity distribution found by Von Karman (1935). Their model addresses the diffusion mechanism for small particles (< 0.1m) to determine concentration profile in the wall layer and the buffer zone. Friedlander and Johnstone

(1957) proposed a different deposition model which considers the particle momentum effect and claimed the free flight velocity of the particles from stopping distance to the wall in the deposition process. Beal (1970) combined the last two approaches and came with a new model which considers flowing back the particles in the flow. Escobedo (1993) also proposed a new deposition mechanism to model asphaltene deposition in the tubing. Escobedo and Mansoori (1995) modified their previous model and added new assumptions to make their model more accurate and predictive.

In the developed wellbore model, deposition of the solid particles consists of two main steps. First, the solid particles move from the bulk fluid toward the tubing wall. Second, some of the particles adhere to the tubing surface. There are three mechanisms responsible for transferring solid particles from the bulk fluid to the tubing surface. These mechanisms are defined as diffusion, inertia, and impaction. To determine the dominant mechanism, it is necessary to define the particle relaxation time and particle stopping distance. Particle relaxation time is defined as

$$t_p = \frac{\rho_p {d_p}^2}{18\mu}, \tag{4.1}$$

where t_p is the particle relaxation time, ρ_p is the density of the solid particles, d_p is the diameter of the particles, and μ is the viscosity of the bulk fluid. Equation (4.2) is the dimensionless form of relaxation time:

$${t_p}^+ = \frac{\rho_p {d_p}^2}{18\mu} \times \frac{f/_2 {V_{avg}}^2}{\upsilon}, \tag{4.2}$$

where υ is the kinematic viscosity and f is the fanning friction factor. The value of ${t_p}^+$ determines the dominant mechanism of particle transportation from the bulk fluid to the wall surface. The diffusion mechanism becomes dominant for small particles (${t_p}^+ < 0.1$). As the particle size increases$(0.1 < {t_p}^+ < 10)$, the inertia effect becomes dominant

and particles move toward the surface of the wall by turbulent eddies. Finally, impaction mechanism becomes dominant for larger particles ($10 < {t_p}^+$).

In addition, particle stopping distance (S_p) is defined as the distance that a particle with initial velocity V_p travels and then stops due to the drag forces of the surrounding fluid and is given by

$$S_p = t_p V_p. \tag{4.3}$$

or

$$S_p = \frac{\rho_p {d_p}^2 V_p}{18\mu} = \frac{0.05 V_{avg} \rho_p {d_p}^2 \sqrt{f/2}}{\mu} + \frac{d_p}{2}. \tag{4.4}$$

Equation (4.5) is the dimensionless form of particle stopping distance:

$${S_p}^+ = \frac{S_p V_{avg} \sqrt{f/2}}{v}. \tag{4.5}$$

Considering particle transportation and adhesion, Equation (4.6) is used to illustrate particle deposition flux:

$$\dot{m}_d = SP\ K_t\ (C_b - C_s), \tag{4.6}$$

where *SP* is the sticking probability factor, K_t is the mass transport coefficient, C_b is the bulk fluid concentration, and C_s is the solid concentration at the wall interface.

The mass transport coefficient, K_t, is a term that indicates particle velocity toward the tubing wall and can be calculated by Equations (4.7) through (4.12).

If the stopping distance is located in the sub-laminar layer, $0 < S_p^+ \leq 5$, then

$$K_t = \frac{V_{avg}\sqrt{f/2}}{\left\{\begin{array}{l} \frac{11.15Sc^{2/3}}{3}F_1\left(Sc,S_p^+\right)-\frac{11.15^2 Sc^{1/3}}{1.5D_{pipe}^+}F_2\left(Sc,S_p^+\right) \\ +11.4\left[\frac{Sc}{(0.049774\cdot Sc-1)}\right]^{1/2}F_3(Sc)-\frac{11.4^2}{D_{pipe}^+}ln\left[\frac{1-0.049774\cdot Sc+\left(\frac{30}{11.4}\right)^2 Sc}{1-0.049774\cdot Sc+\left(\frac{5}{11.4}\right)^2 Sc}\right] \\ +\left(2.5+\frac{12.5}{D_{pipe}^+Sc}\right)ln\left(\frac{1+0.4r^+_{avg}Sc}{1+12Sc}\right)-\frac{5r^+_{avg}}{D_{pipe}^+}+\frac{150}{D_{pipe}^+} \end{array}\right\}}, \quad (4.7)$$

In the above equation, $F_1\left(Sc,S_p^+\right)$, $F_2\left(Sc,S_p^+\right)$ and $F_3(Sc)$ can be calculated by the following relations:

$$F_1\left(Sc,S_p^+\right) = \left\{\begin{array}{l} \frac{1}{2}ln\left[\frac{\left(1+\frac{5}{11.15}Sc^{1/3}\right)^2}{1-\frac{5}{11.15}Sc^{1/3}+\left(\frac{5}{11.15}\right)^2 Sc^{2/3}}\right]-\frac{1}{2}ln\left[\frac{\left(1+\frac{S_p^+}{11.15}Sc^{1/3}\right)^2}{1-\frac{S_p^+}{11.15}Sc^{1/3}+\left(\frac{S_p^+}{11.15}\right)^2 Sc^{2/3}}\right] \\ +\sqrt{3}tan^{-1}\left(\frac{\frac{10}{11.15}Sc^{1/3}-1}{\sqrt{3}}\right)-\sqrt{3}tan^{-1}\left(\frac{\frac{2S_p^+}{11.15}Sc^{1/3}-1}{\sqrt{3}}\right) \end{array}\right\}, \quad (4.8)$$

$$F_2\left(Sc,S_p^+\right)=\left\{\begin{array}{l}\frac{1}{2}ln\left[\frac{1-\frac{5}{11.15}Sc^{1/3}+\left(\frac{5}{11.15}\right)^2Sc^{2/3}}{\left(1+\frac{5}{11.15}Sc^{1/3}\right)^2}\right]-\frac{1}{2}ln\left[\frac{1-\frac{S_p^+}{11.15}Sc^{1/3}+\left(\frac{S_p^+}{11.15}\right)^2Sc^{2/3}}{\left(1+\frac{S_p^+}{11.15}Sc^{1/3}\right)^2}\right]\\ +\sqrt{3}tan^{-1}\left(\frac{\frac{10}{11.15}Sc^{1/3}-1}{\sqrt{3}}\right)-\sqrt{3}tan^{-1}\left(\frac{\frac{2S_p^+}{11.15}Sc^{1/3}-1}{\sqrt{3}}\right)\end{array}\right\},$$

(4.9)

$$F_3\left(Sc\right)=\frac{1}{2}ln\left[\frac{\sqrt{0.049774\,Sc-1}-\frac{30}{11.4}Sc^{1/2}}{\frac{30}{11.4}Sc^{1/2}+\sqrt{0.049774\,Sc-1}}\right]-\frac{1}{2}ln\left[\frac{\sqrt{0.049774\,Sc-1}-\frac{5}{11.4}Sc^{1/2}}{\frac{5}{11.4}Sc^{1/2}+\sqrt{0.049774\,Sc-1}}\right],$$

(4.10)

If the stopping distance is located in the buffer zone, $5 < S_p^+ \leq 30$, then

$$K_t=\frac{V_{avg}\sqrt{f/2}}{\left\{\begin{array}{l}11.4\left[\frac{Sc}{\left(0.049774\cdot Sc-1\right)}\right]^{1/2}F_3\left(Sc\right)-\frac{11.4^2}{D_{pipe}^+}ln\left[\frac{1-0.049774\cdot Sc+\left(\frac{30}{11.4}\right)^2Sc}{1-0.049774\cdot Sc+\left(\frac{S_p^+}{11.4}\right)^2Sc}\right]\\ +\left(2.5+\frac{12.5}{D_{pipe}^+Sc}\right)\ln\left(\frac{1+0.4r_{avg}^+Sc}{1+12Sc}\right)-\frac{5r_{avg}^+}{D_{pipe}^+}+\frac{150}{D_{pipe}^+}\end{array}\right\}},$$

(4.11)

If the stopping distance is located in the turbulent core, $30 < S_p^+$, then

$$K_t = \frac{V_{avg}\sqrt{f/2}}{\left[\left(2.5+\frac{12.5}{D_{pipe}^+ Sc}\right) ln\left(\frac{1+0.4r_{avg}^+ Sc}{1+0.4S_p^+ Sc}\right) - \frac{5r_{avg}^+}{D_{pipe}^+} + \frac{5S_p^+}{D_{pipe}^+}\right]}. \quad (4.12)$$

In the above equations, Sc is the Schmidt number determined by the following equation:

$$Sc = \frac{3\pi\mu^2 d_p}{\rho K_B T}, \quad (4.13)$$

where K_B is the Boltzman constant.

Watkinson and Epstein (1970) proposed the following definition for sticking probability factor:

$$SP \propto \frac{Adhesion\ forces\ between\ particles\ and\ the\ tubing\ surface}{Drag\ forces\ \ on\ the\ particles\ on\ the\ tubing\ wall}$$

By using Arrhenius type expression, we have the following equation for the sticking probability factor:

$$SP = K_d \frac{e^{\left(-\frac{E_a}{RT_S}\right)}}{{V_{avg}}^2}, \quad (4.14)$$

where K_d and E_a are related to the tubing material and come from experimental data, T_s is the surface temperature, and V_{avg} is the bulk average velocity.

Additionally, due to loose structure of the deposited asphaltene, the deposited asphaltene can be partially removed by shear forces at the wall. The following equation describes particle removal from the tubing surface:

$$\frac{d\delta}{dt} = k_r \delta \tau^a, \quad (4.15)$$

where δ is the thickness of asphaltene, K_r is the shear removal factor, τ is the shear stress, and a is the shear coefficient. Therefore, the removed mass of the deposited solids can be described by the following equation:

$$\dot{m}_r = \pi D \frac{d\delta}{dt} dz \rho_s, \quad (4.16)$$

where ρ_s is the density of the deposited solid particles and dz is the length of the gridblock.

4.3 SIMULATION STUDIES

In this section, three case studies are presented to investigate the effect of composition variation on asphaltene deposition in the wellbore. In our simulation case studies, we assume that sufficient injection pressure is available and the valve size is suitable to fully inject a constant composition of gas into the tubing. Therefore, we neglect composition variation happening at the beginning of gas lift process during transient stage.

4.3.1 Case Study 1

This case investigates asphaltene deposition in the wellbore for initial oil composition during primary production of the reservoir. The simulation input data is presented in Table 4.5. The initial reservoir pressure is assumed to be 2,500 psi and the well is producing under constant bottom-hole pressure of 2,400 psi. This case illustrates a well with low bottom-hole pressure, low oil production, and high water cut which makes it a good candidate for gas lift process. The initial wellbore diameter is 2.748 inch and wellbore length is 5,000 ft.

Figures 4.3 through 4.7 show the pressure, temperature, tubing diameter, asphaltene thickness, and oil superficial velocity along the wellbore after 0, 45, 90, 135, and 180 days of simulation, respectively. As Figure 4.3 shows, the pressure changes linearly from the bottom to the top of the wellbore. Due to small deposition of asphaltene in the wellbore, the wellhead pressure only drops 5 psi after 180 days of production. Figure 4.4 shows the temperature profile along the wellbore. As can be seen, the temperature does not change significantly over time. Figures 4.5 and 4.6 show tubing diameter and asphaltene thickness in the tubing, respectively. As shown, there is no asphaltene deposition from the bottom of the well up to the depth of 1,000 ft. Asphaltene starts to flash out from the crude oil as the pressure and temperature decline at the upper part of the wellbore. Pressure decline from the onset pressure to the bubble point pressure occurs at the top of the wellbore which results in asphaltene deposition at this section. Figure 4.7 shows oil superficial velocity after 0, 45, 90, 135, and 180 days of simulation. As can be seen, at the beginning of the production, the oil superficial velocity at the upper part of the wellbore is 6.3ft/s. As time progresses, the oil superficial velocity increases at the wellhead due to the constant production rate and reduction in the tubing size and eventually reaches 9ft/s after 180 days. In summary, the effect of asphaltene deposition on the dynamics of this well is negligible during the primary production under the stated conditions.

4.3.2 Case Study 2

In this case, we investigate gas lift operation for a wellbore similar to the previous case with lower reservoir pressure. Gas lift valve is used at the depth of 4,200ft and the injection gas temperature at the surface is 60°F. Moreover, the well is producing under

gas lift mechanism with wellhead pressure of 100 psi and reservoir pressure of 1,900 psi. Simulation study was performed on this well and it is found that this well would encounter flow assurance issue under gas lift process. Variable gas injection rate is employed in a way that gas lift mole fraction contains 10% of the mixture all the time. Figure 4.8 depicts the bottom-hole pressure versus time. As we observe, asphaltene deposition caused bottom-hole pressure to increase 12 psi after 180 days of simulation. Therefore, the amount of influx from the reservoir to the wellbore is not seriously reduced. As Figure 4.9 shows, temperature profile does not change significantly over time. Moreover, since temperature does not change significantly from the bottom to the top of the wellbore, we expect smaller amount of asphaltene precipitation above the gas lift valve. In fact, the most obvious drop occurs at the depth of 4,200ft, where the lift-gas is introduced to the wellbore fluid. Figure 4.10 depicts tubing diameter as time progresses. Tubing diameter is narrowed down by the factor of 10% after 180 days. As can be seen, most of the deposition occurs at the depth of 2,600ft around the bubble point pressure, where asphaltene solubility is minimum. As we go toward the wellhead, more gas comes out of the crude oil and asphaltene particles become more stable. From Figure 4.11, it is observed that as time proceeds, location of the maximum deposition slightly moves upward due to asphaltene removal by shear stresses. Figure 4.12 reveals that oil velocity slightly changes around the largest deposited area and surface velocity decreases over time as the fluid influx into the wellbore decreases.

4.3.3 Case Study 3

In this case, lift-gas is injected with the ratio of 0.53 to the fluid influx from the reservoir. The other parameters are the same as in case study 2. As shown in Figure 4.1,

we expect that by adding light hydrocarbon components to the unstable oil, asphaltene deposition becomes more severe due to increases in onset point and bubble point pressures. Figure 4.13 presents bottom-hole pressure at different simulation times. As can be seen, asphaltene deposition in the wellbore increases the bottom-hole pressure over the time resulting in smaller influx from the reservoir to the wellbore. Figure 4.14 shows temperature profile at various times. Since colder fluid is introduced to the reservoir fluid, the mixture's temperature decreases and as time progresses, the fluid temperature drops. This reduction in temperature is caused by dynamic effect of pressure, oil superficial velocity and asphaltene deposition. Figure 4.15 shows the pipe diameter at different time steps. As can be seen, there is no asphaltene deposition between 4,150ft and 5,000ft and around the perforation zone. Since the wellbore fluid is the initial reservoir fluid below the gas lift valve, no asphaltene deposition occurs as it was shown in case 1. The wellbore radius starts to decrease from the depth of 4,150ft all the way to the surface. As shown, most of the deposition occurs above the gas lift valve around the depth of 3,200ft and after 180 days, the tubing diameter decreased to 45% of the initial state. Figure 4.16 shows asphaltene thickness along the wellbore at different simulation times. Again, it is obvious that partial plugging occurs around the depth of 3,200ft. Figure 4.17 illustrates superficial oil velocity at 0, 45, 90, 135, and 180 days of simulation. At the beginning of the production, oil velocity is about 6ft/s at the wellhead with no plugging in the tubing. As time progresses, the bottom-hole pressure increases which results in less fluid influx from the reservoir into the wellbore and consequently less production rate. After 180 days of simulation, superficial oil velocity reduced to about 2ft/s at the wellhead. However, large deposition of asphaltene in the tubing causes the velocity field to increase significantly at the middle of the wellbore. The largest velocity is observed at the depth of 3,200ft where we have most of the deposition.

As shown in the presented case studies, a small amount of asphaltene deposition was observed at the top of the wellbore in the primary production case. In the second case, ratio of the lift-gas to the reservoir influx was 11.1%. We observed 15% reduction in tubing diameter and 8% reduction in oil production due to asphaltene deposition. In the third case, the well was producing under gas lift mechanism and the ratio of lift-gas to the reservoir influx was changed to about 52.7%. After 180 days, more than 50% of the tubing was blocked and the wellbore performance was severely damaged.

Table 4.1: Splitting of the C_{7+} fraction is determined based on the number of pseudo components (Khan, 1992)

C_{7+} mole fraction	**Number of pseudo components**
<0.05	1
0.05-0.4	2
0.4-0.6	3
0.6-0.8	4
>0.8	5

Table 4.2: Composition of the reservoir fluid and the associated gas

Component	**Reservoir Fluid Composition**	**Associated Gas Composition**
CO_2	0.0115	0.03
C_1	0.161	0.61
C_2	0.0582	0.18
C_3	0.0698	0.12
C_4	0.0611	0.04
C_5-C_8	0.0506	0.02
C_9-C_{20}	0.3127	0
C_{21}-C_{46}	0.209	0
C_{47+}	0.0613	0
Asphaltene	0.0048	0

Table 4.3: Mixture properties

Component	P_C psi	T_C °R	V_C ft3/lbmol	MW	OM	PARACHOR	VSP
CO_2	1070.16	547.56	1.50682	44.0095	0.2251	78	-0.00252
C_1	667.38	343.08	1.58697	16.0425	0.008	77	-0.00412
C_2	708.54	549.72	2.37244	30.069	0.098	108	-0.00413
C_3	615.93	532.512	3.25409	44.0956	0.152	150.3	-0.00413
C_4	545.664	758.1168	4.08077	58.122	0.1972	191	-0.00413
C_5-C_8	487.2756	838.944	4.98058	72.149	0.2414	231	-0.00309
C_9-C_{20}	383.4495	1129.99	8.17214	125.512	0.3677	327.5341	0.010382
C_{21}-C_{46}	206.0352	1330.454	15.346	287.88	0.87714	761.4413	0.05
C_{47+}	90.59904	1671.734	39.8162	660.294	1.2381	1174.0076	0.05
Asphaltene	90.59904	1671.734	39.8162	660.294	1.2381	1174.0076	0.05

Table 4.4: Binary interaction coefficients

	CO_2	C_1	C_2	C_3	C_4	C_5-C_8	C_9-C_{20}	C_{21}-C_{46}	C_{47+}	Asphaltene
CO_2	0									
C_1	0.12	0								
C_2	0.13	0	0							
C_3	0.135	0	0	0						
C_4	0.13	0	0	0	0					
C_5-C_8	0.125	0.0236	0.0075	0.0029	0	0				
C_9-C_{20}	0.105	0.2	0.0136	0.0066	0	0	0			
C_{21}-C_{46}	0.1352	0	0.0354	0.0196	0	0	0	0		
C_{47+}	0.1876	0.00008	0.0732	0.0423	0	0	0	0	0	
Asphaltene	0.21	0.29	0.17	0.13	0.12	0	0	0	0	0

Table 4.5: Simulation input data

Parameter	Value
Wellbore length	5000 ft
Gridblock size	200 ft
Tubing radius	0.1145 ft
Roughness	0.0008
Oil productivity index	0.2 ft^3/psi.ft
Water productivity index	1 ft3/psi.ft
Reservoir top	4800 ft
Reservoir bottom	5000 ft
Reservoir temperature	212 °F
Surface temperature	60 °F

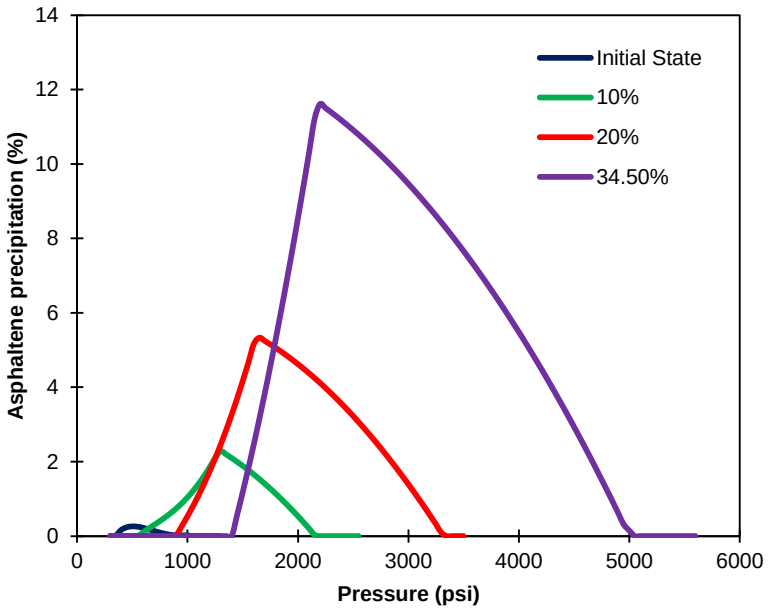

Figure 4.1: Asphaltene precipitation curve at the reservoir temperature (212°F) for different mixture composition generated by UTCOMP

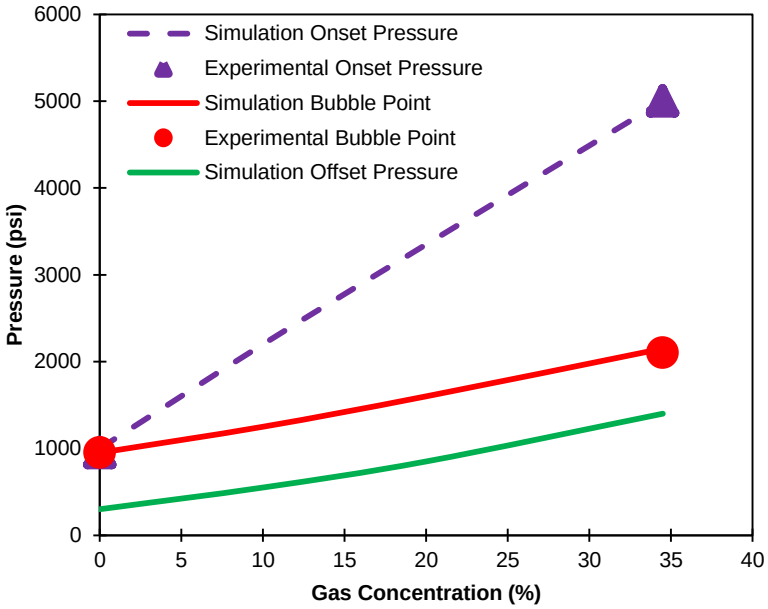

Figure 4.2: Onset points, bubble points, and offset points at different fraction of the associated gas at the reservoir temperature (212°F)

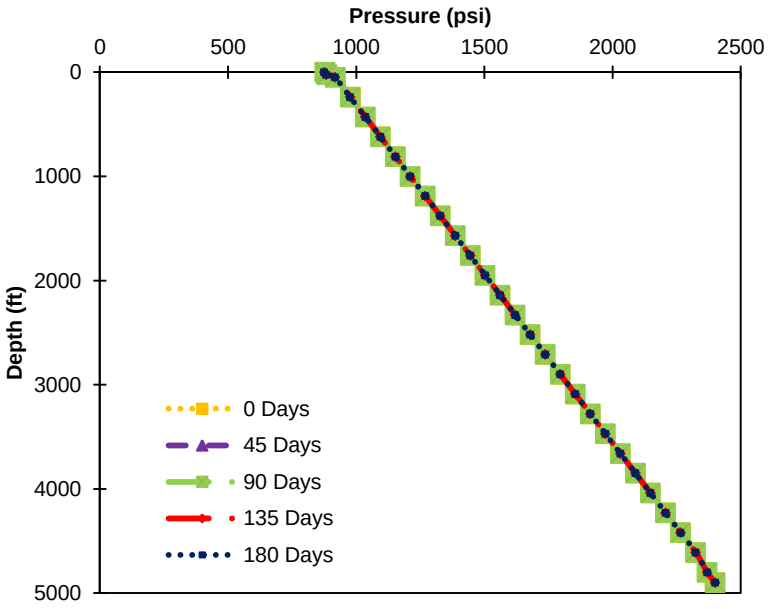

Figure 4.3: Pressure profile in the wellbore during primary production after 0, 45, 90, 135, and 180 days

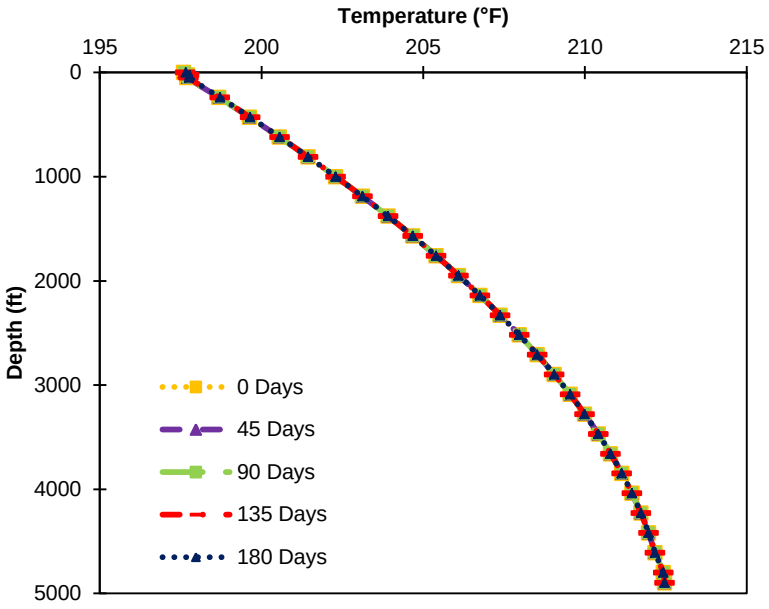

Figure 4.4: Temperature profile in the wellbore during primary production after 0, 45, 90, 135, and 180 days

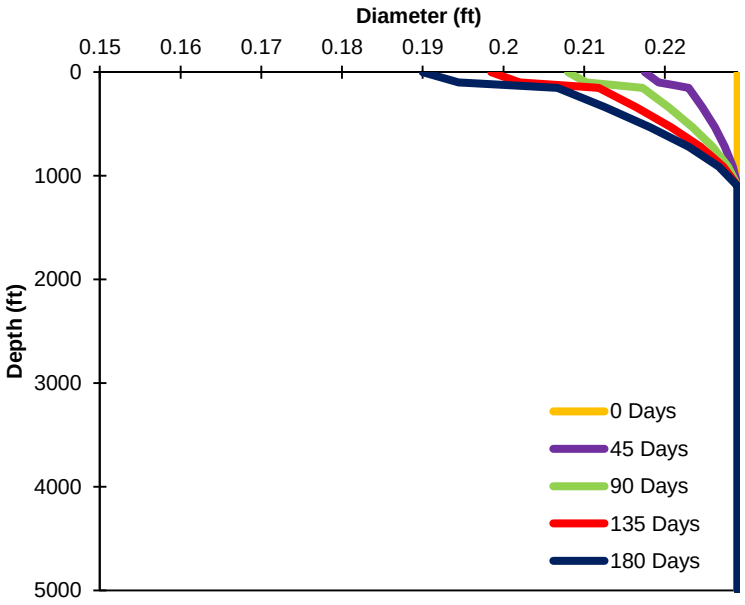

Figure 4.5: Tubing diameter during primary production after 0, 45, 90, 135, and 180 days

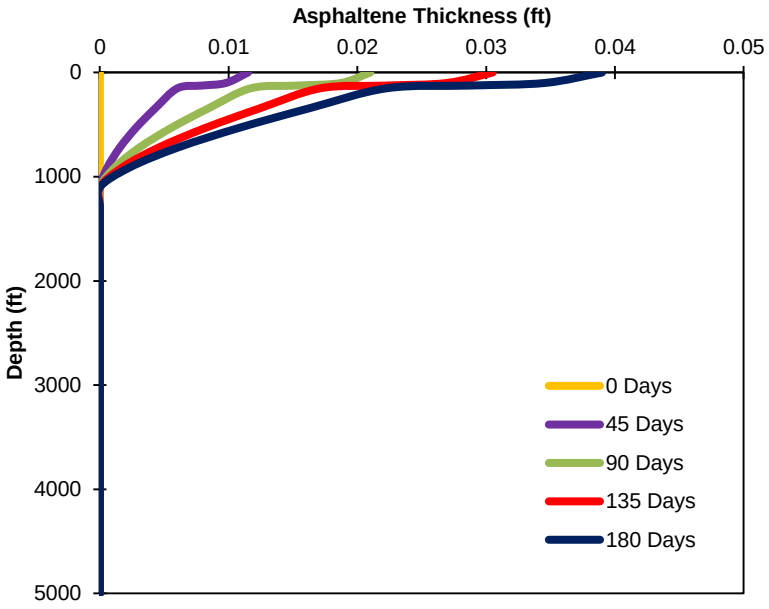

Figure 4.6: Asphaltene thickness in the wellbore during primary production after 0, 45, 90, 135, and 180 days

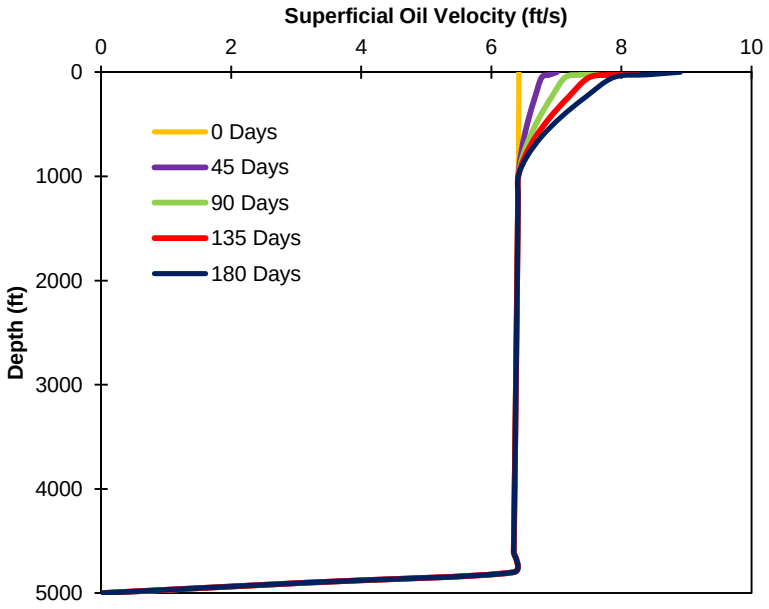

Figure 4.7: Oil superficial velocity during primary production after 0, 45, 90, 135, and 180 days

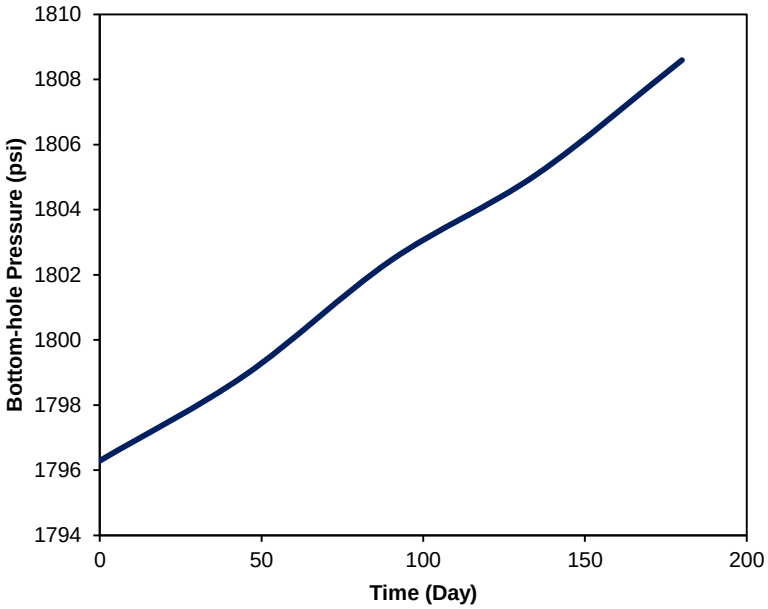

Figure 4.8: Increase in bottom-hole pressure versus time

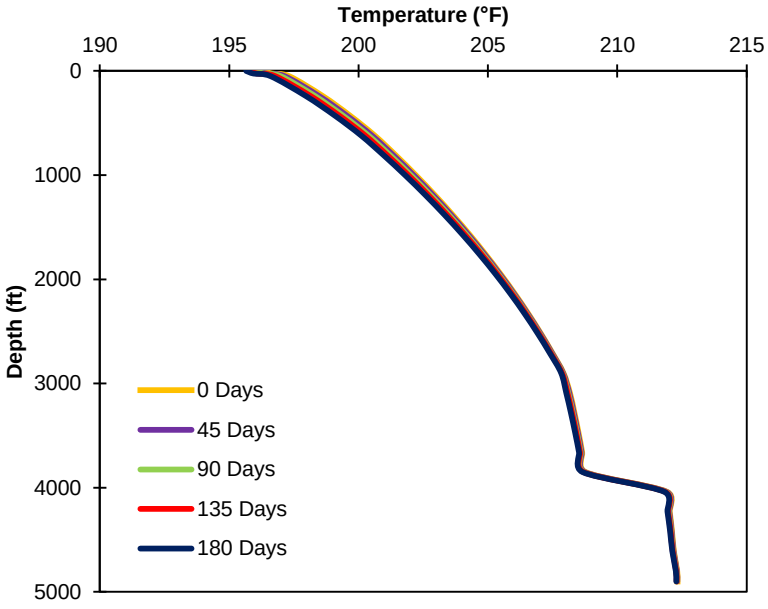

Figure 4.9: Temperature profile in the wellbore during 10% gas injection after 0, 45, 90, 135, and 180 days

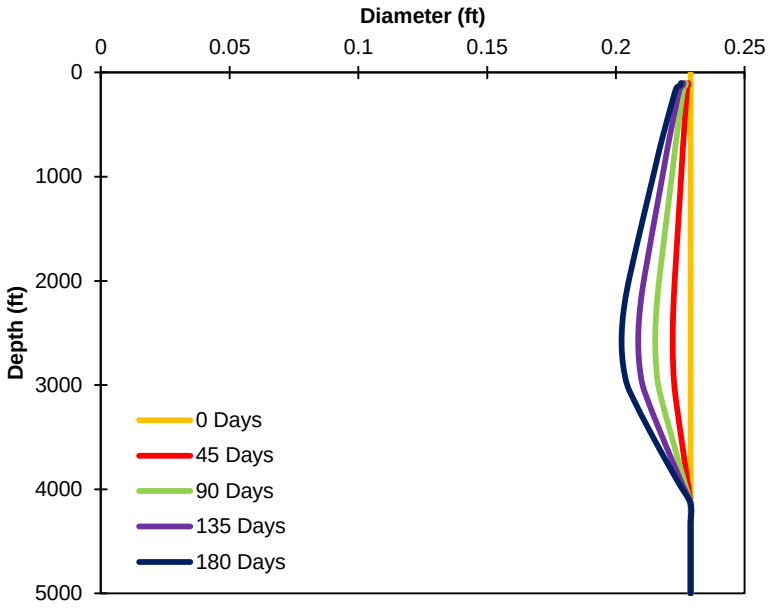

Figure 4.10: Tubing diameter during 10% gas injection after 0, 45, 90, 135, and 180 days

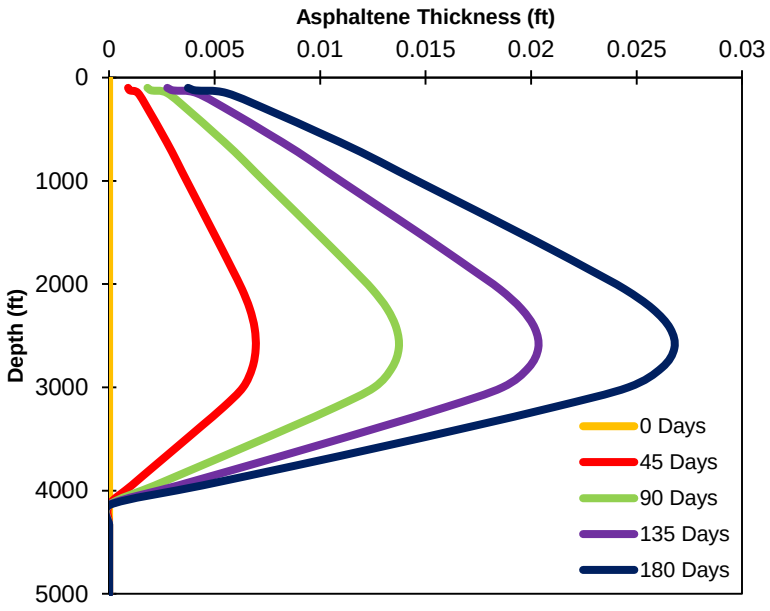

Figure 4.11: Asphaltene thickness in the wellbore during 10% gas injection after 0, 45, 90, 135, and 180 days

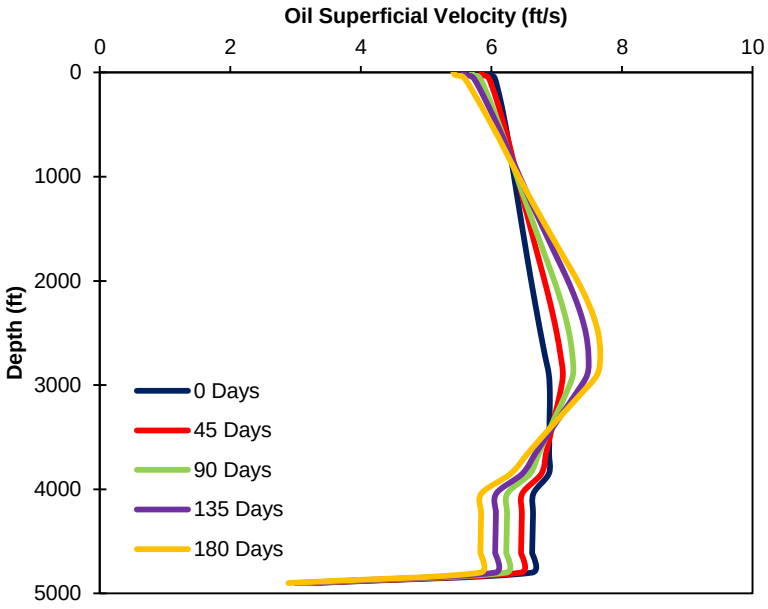

Figure 4.12: Oil superficial velocity during 10% gas injection after 0, 45, 90, 135, and 180 days

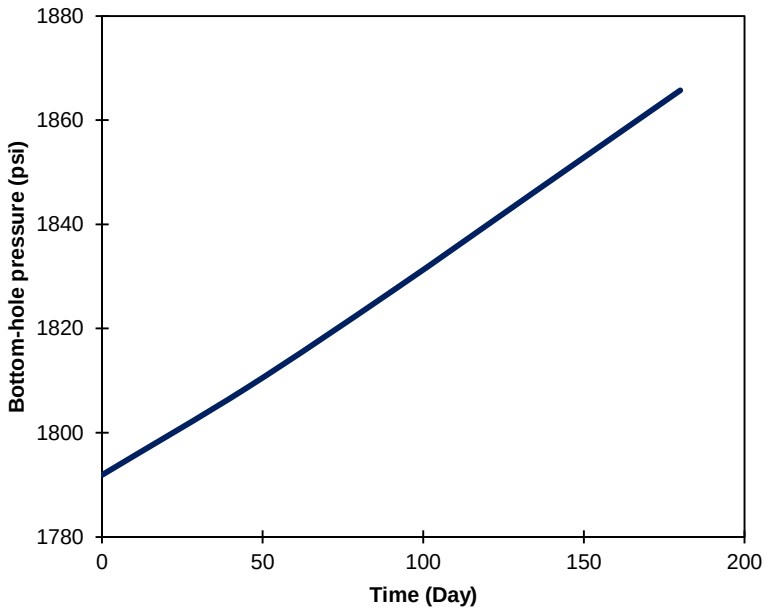

Figure 4.13: Increases in bottom-hole pressure versus time

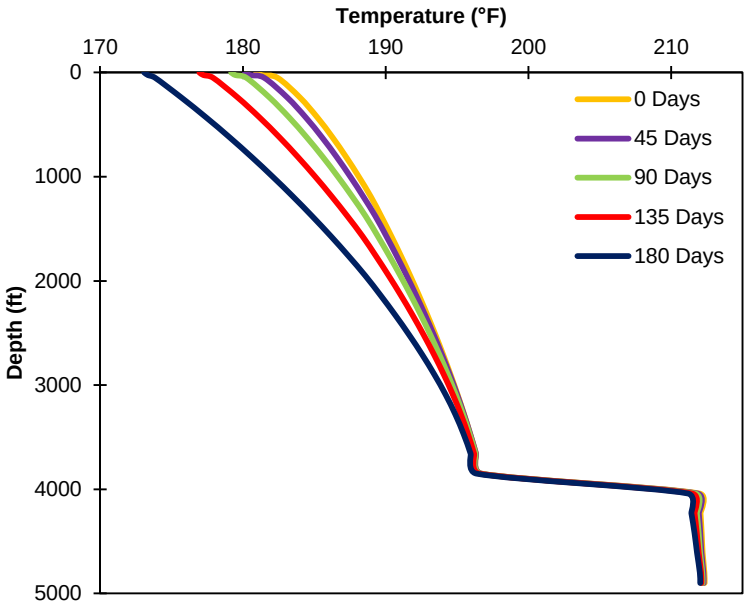

Figure 4.14: Temperature profile in the wellbore during 34.5% gas injection after 0, 45, 90, 135, and 180 days

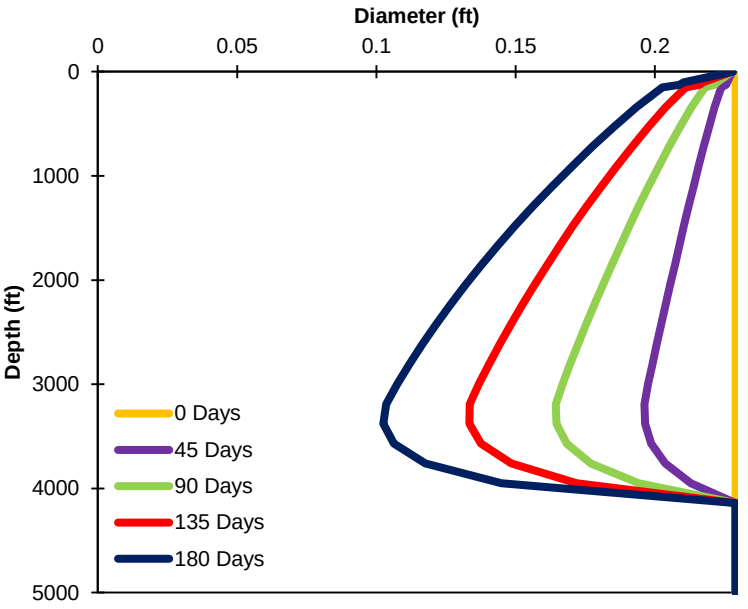

Figure 4.15: Tubing diameter during 34.5% gas injection after 0, 45, 90, 135, and 180 days

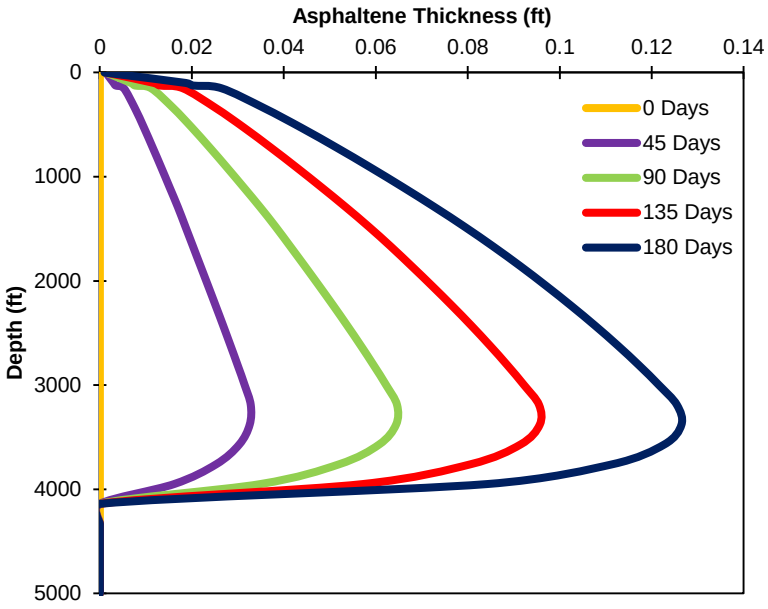

Figure 4.16: Asphaltene thickness in the wellbore during 34.5% gas injection after 0, 45, 90, 135, and 180 days

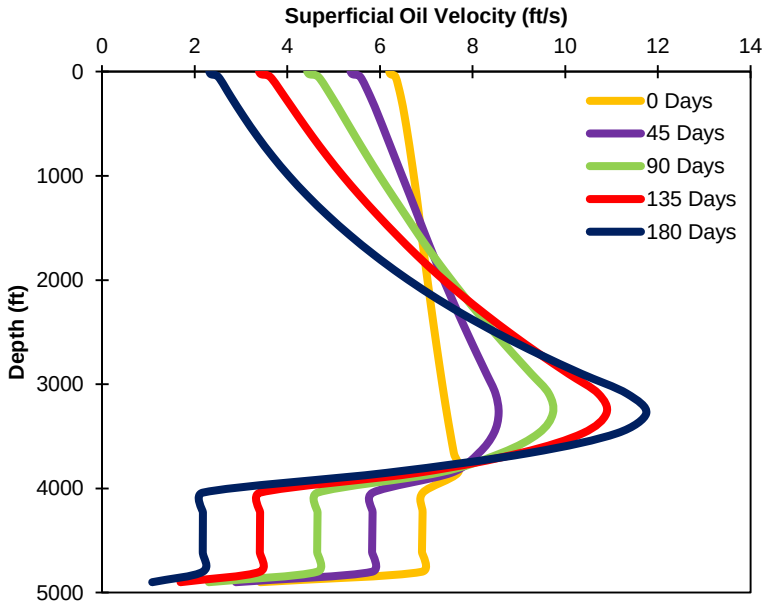

Figure 4.17: Oil superficial velocity during 34.5% gas injection after 0, 45, 90, 135, and 180 days

Chapter 5: Scale Deposition in the Wellbore

The deposition of carbonate and sulfate scales in the reservoir and wellbore is a challenging problem in the oil industry. Several explanations, such as incompatible water flooding and significant pressure/temperature changes cause scale precipitation which results in porosity and permeability reduction, wellbore plugging, equipment failure, equipment corrosion, and decrease in oil production rate. In the oil industry, substantial funds are spent each year for treatment of the deposited scale. In addition to the chemical inhibitors, mechanical workover is required to remove scale deposits from the wellbore and surface facilities. To plan for the best workover method, it is necessary to know the extent and location of scale deposition in the wellbore.

In this chapter, we present a robust algorithm which couples UTWELL with the geochemical package, IPhreeqc, which was developed by the United States Geological Survey. Then, we investigate the transportation, entrainment, and deposition of scales in the wellbore. Afterward, the developed tool is utilized to predict carbonate and sulfate deposition profile along the wellbore.

5.1 BACKGROUND

Prediction and prevention of scale precipitation become more significant as water production occurs throughout the production life of the reservoir. Scale results in equipment wear and corrosion, and decline in oil/gas production rate. In the literature, several authors have reported scale formation in the reservoir and wellbore and attempted

to predict mineral precipitation (Vetter and Phillips 1970; Read and Ringen 1982; Katsanis et al. 1983; Ganjdanesh et al. 2015).

Langelier (1936) proposed Stability Index (*SI*) as the reference for scale formation. They suggested Equation (5.1) for Stability Index:

$$SI = pH - pCA - pAlk - K, \quad (5.1)$$

where *SI* is the stability index, *pH* is the pH of the water sample, *pCa* is the negative logarithm of the calcium concentration, *pAlk* is the negative logarithm of the total alkalinity, and *K* is a function of total salt concentration and temperature. He showed that a positive value for *SI* indicates probable precipitation of the minerals and a negative value indicates the tendency of an existing scale for dissolution.

Stiff and Davis (1952) determined experimental *K* values for Langelier (1936) equation. By having the *K* value, they determined the stability index of the oil field water and applied this method to production systems.

Scale precipitation also became a main problem when North Sea fields, such as Forties, started to produce water (Mitchell et al., 1980). They attributed scale problems in the Forties field to two major factors: mixing of Forties formation water with the injected seawater, and variation of pressure/temperature in the production system. In fact, mixing of formation water and seawater caused precipitation of both barium and strontium sulfates. The production and injection wells were in the regions having a great fluid mixing. Since chemical inhibitor was initially added to the injected water, small deposition occurs near the injection well. Therefore, scale precipitation became the major problem mostly in the production system. To prevent scale deposition in this field,

development of barium sulfate solubilizers and suitable scale-inhibitor test methods were proposed.

Vetter and Kandarpa (1980) developed a model to predict calcium carbonate scale formation as a function of pressure, temperature, and water composition based on thermodynamic equilibrium. They used a database to determine solubility of $CaCO_3$ as a function of pressure, temperature, and the molarity of the sodium chloride. During multiphase flow, carbon dioxide may go/come to oil and gas phases and change the $CaCO_3$ precipitation and equilibrium conditions. Therefore, they considered solubility of CO_2 in the water by using solubility data for CO_2 reported in the literature.

Valone and Skillern (1982) developed a computer model to determine the amount of scale deposition. They improved Stiff and Davis (1952) calculation methods by introducing excess concentration of relatively insoluble salt (Q-value). Table 5.1 presents different scenarios that may happen based on the Q-value calculated by this model. They suggested that produced oil field water may have the possibility of a specific amount of scale deposition; however, in practice, the determined deposition does not happen. Therefore, Q-value helps in estimating the extent of scale precipitation and consequently, calculating the amount of scale-control chemicals.

Waterflooding of the Gulf of Suez oil fields using the seawater caused scale deposition in surface and subsurface equipment (El-Hattab, 1985). Studies showed that sulfate scale was the main mineral that precipitated in the oil wells and surface facilities causing equipment failure and production decline.

Shuler and Jenkins (1991) reported the Ninian field in North Sea having scale problem. Incompatibility between the formation water, which had a high concentration of barium and strontium, with the injected sea water, which had a high sulfate concentration,

was the main source of scale precipitation. The problem of scale precipitation became more severe when injected sea water broke through the production wells and caused barium sulfate and calcium carbonate precipitations. They proposed treatment program such as adsorption or equilibrium squeezes in the production wells.

Wright et al. (1994) reported scaling tendencies of carbonate and sulfate minerals in the Glamis field. Prior to seawater breakthrough, calcium carbonate deposition from formation water was the main problem observed within the tubing. After breakthrough, sulfate scaling became the main type of scale that mainly deposited at the perforations. They proposed both downhole injection and squeezing as the best way to control the scale deposition without damaging the formation.

Shuler et al. (2000) reported significant scaling problem of minerals such as calcium carbonate, sodium chloride, calcium fluoride, and lead and zinc sulfides in the gas wells of Nophlet in Mobil Bay. These gas wells produced salt-saturated formation brine that contained a large amount of heavy metals; due to significant changes in pressure/temperature along the wellbore scaling occurred. Hence, they developed a model to predict scaling conditions of the wells and determine the effective scale control mechanisms to prevent scale deposition. They considered pressure, temperature, water rate, and water chemistry as the main parameters necessary to determine the scaling tendencies of minerals along the wellbore. Based on the predicted values, time and location for injection of fresh water or chemicals were determined in the wells.

Rocha et al. (2001) developed a salt precipitation model. By coupling their model with an ion transport equation, they were able to predict ion movements and reactions through the porous media by considering the effect of pressure, temperature, and salinity on the salt precipitation.

Qing et al. (2002) observed silicate scale deposition in the production wells during ASP flooding in the Daqing oil field in China which made frequent workover jobs necessary. The reaction between NaOH and reservoir rock caused the dissolution of rock materials. The dissolved materials were taken into the production wells and deposited on the surface of the tubing. Moreover, mixing of the produced fluid from different layers, decrease in pressure/temperature, and loss of the dissolved gas result in more silicate precipitation on the tubing surface.

Deposition of calcium carbonate and barium sulfate was also observed in Veslefrikk field in North Sea (Tjomsland et al., 2003). Calcium carbonate precipitated due to significant pressure drops in the produced fluid when flowing into the well. On the other hand, barium sulfate deposition occurred as a result of mixing of seawater and formation water from different layers of the reservoir. As the injected sea water breakthroughs into the production well, barium sulfate scale becomes the major type of scale in this field.

Moghadasi et al. (2003) reported the most common types of scales in the oil field with the parameters that directly affect scale solubility (Table 5.2).

Delshad and Pope (2003) investigated barium sulfate deposition in an oil field using UTCHEM, The University of Texas at Austin three-dimensional chemical flooding reservoir simulator, under various water salinity and longitudinal dispersivity conditions by using reaction equilibrium models. Barium sulfate scale was caused by injection of seawater with high sulfate concentration into a formation with excessive amount of barium cations. Since chemical treatments did not work for severe barium sulfate precipitation, they suggested desulfurization of the sea water to prevent precipitation.

Their simulation results showed that in one of the severe cases without sulfate removal, 2500 tons of barium sulfate could precipitate in the wellbore and reservoir.

Deposition of scales such as calcium sulfate on surface and subsurface production equipment also occurred due to incompatibility of injected water with the formation water in Gemsa oil field (Elmorsey, 2013). Mechanical removal was suggested to remove the deposited scale, since calcium sulfate is very hard and cannot be dissolved with the common chemicals.

Shirdel (2013) investigated flow assurance issues such as scale deposition in the wellbore. By developing a wellbore model coupled with a geochemistry package, PHREEQC, he predicted the scale precipitation, deposition, and transportation along the well.

Kazemi Nia Korrani (2014b) developed a geochemical-based reservoir simulator by integrating IPhreeqc with UTCHEM to study reactive-transport phenomena. He investigated the effect of ion activities, temperature, and pressure on reactive transport phenomena. In addition, Kazemi Nia Korrani et al. (2014a) used permeability-porosity models such as Fair-Hatch, Kozeny-Carman, and Verma-Pruess to investigate the effect of scale deposition on reservoir permeability reduction.

In our study, we coupled a powerful geochemical tool, IPhreeqc, with the wellbore model to calculate scale equilibrium condition and transportation. In the next sections, we will describe PHREEQC, IPhreeqc, scale precipitation model, and coupling approach.

5.2 DESCRIPTION OF PHREEQC

PHREEQC that comes from the acronym (pH-Redox-Equilibrium) is a geochemical modeling program developed by the United States Geological Survey and written in C and C++ to model variety of geochemical reactions and transport calculations (Parkhurst and Appelo, 2013). This program models equilibrium condition of the aqueous solutions with minerals, gases, solid solutions, exchangers, and sorption surfaces. In addition, this program is capable of modeling kinetic reactions and one-dimensional transport including multi-component diffusion and transport of surface-complexing species. PHREEQC has the capability to model different types of aqueous models, such as two ion-association aqueous model, a Pitzer specific-ion-interaction aqueous model, and the SIT (Specific ion Interaction Theory) aqueous model. In addition, PHREEQC is able to calculate the solubility of the gases at high pressure using Peng-Robinson equation of state. Therefore, by coupling PHREEQC with a thermal compositional wellbore simulator, a comprehensive geochemical wellbore model is evolved which can accurately model geochemical reactions, such as scale precipitation in the wellbore.

Two types of coupling have been suggested in the literature: soft coupling and hard coupling methods. In the soft coupling approach, the wellbore creates an input file with PHREEQC format. In the created input file, data such as pressure, temperature, concentration of the elements, and the equilibrium phases are written. Then, the PHREEQC is called to perform the equilibrium calculations and it creates an output file of the results. Subsequently, the wellbore reads the output file and uses the calculated parameters in the transport module. Due to the frequent reading and writing of files, soft coupling is expected to be slow. Loading the database and redefining the solution

composition at each time step are the other reasons for higher CPU time of the soft coupling approach. In the hard coupling approach, the source code needs to be modified to transfer the data between PHREEQC and the wellbore. Hence, there is no need to write the input and output files. Although hard coupling is more desirable in the terms of CPU time, it is more difficult to be implemented due to the complicated structure of the PHREEQC. To make the coupling of other software with PHREEQC easier, a C++ class, IPhreeqc, was developed by USGS. In the next section, we discuss the characteristics and capabilities of IPhreeqc.

5.3 DESCRIPTION OF IPHREEQC

As mentioned in the previous section, PHREEQC was generalized into a computer object program, IPhreeqc, which makes it easier to integrate with the other programs and software that are needed to simulate geochemical reactions. In fact, IPhreeqc helps the user to easily transfer the data with the PHREEQC through a pre-defined framework. IPhreeqc like PHREEQC is capable of handling homogenous and heterogeneous, reversible and irreversible and ion-exchange reactions under either local equilibrium assumptions or kinetic conditions. IPhreeqc libraries are programmed in a way to be used by C, C++, and Fortran languages. Appendixes (A.3) and (A.4) show examples of a simplified input file and corresponding results, respectively. In the next section, the coupling approach of UTWELL with IPhreeqc is described.

5.4 SCALE PRECIPITATION MODEL

This section briefly presents the equations that are used in PHREEQC/IPhreeqc to define thermodynamic activities of aqueous species, gas phase components, solid solutions, and pure phases. Initially, IPhreeqc uses thermodynamic activities and mass equations for the aqueous phase. Then, a set of functions is solved simultaneously to determine equilibrium for a given condition. These functions are derived from mole balance equations for each element or from mass action equations for pure phases and solid solutions. The other functions are derived from alkalinity, activity of water, aqueous charge balance, gas phase equilibrium, and ionic strength. Finally, IPhreeqc uses a modified Newton-Raphson method to solve the simultaneous nonlinear equations to determine the equilibrium state (Parkhurst and Appelo, 1999).

5.4.1 Aqueous Species

Generally, the mass-action equations for the aqueous phase can be written as

$$K_i = a_i \prod_m^{M_{aq}} {a_m}^{-c_{m,i}}, \tag{5.2}$$

where $K_i$is a temperature-dependent equilibrium constant, $c_{m,i}$ is the stoichiometric coefficient of master species *m* in species *i* and M_{aq} is the total number of aqueous master species. PHREEQC assumes that the stoichiometric constants on the left side of the reaction are positive and the constants on the right side of the reaction are negative.

For example, for the following reaction, the mass-action equation is described as follows:

$$Ba^{+2} + {SO_4}^{-2} \rightarrow BaSO_4, \qquad Log\ K = 2.7\ at\ 25°C$$

$K = 10^{2.7} = \frac{a_{BaSO_4}}{a_{Ba^{+2}} \cdot a_{SO_4{}^{-2}}}$,

In addition, the following equations are used to determine the activity of the components.

For solid and liquid solutions:

$$a_i = X_i \gamma_{R_i}. \tag{5.3}$$

For gaseous solutions:

$$a_i = P_i \gamma_{f_i}. \tag{5.4}$$

For aqueous solutions:

$$a_i = m_i \gamma_{H_i}. \tag{5.5}$$

where a_i is the activity of substance *i*, X_i is the mole fraction, m_i is the molality, and P_i is the partial pressure of the gas component. The parameters γ_{R_i}, γ_{f_i}, and γ_{H_i} are the activity coefficients that indicate deviation from the ideal behavior of substance *i* from Raoult's law, Henry's law, and the ideal gas law, respectively.

Davies equation is used in IPhreeqc to determine the activity coefficient of aqueous species:

$$\log \gamma_i = -A z_i{}^2 \left(\frac{\sqrt{\mu}}{1+\sqrt{\mu}} - 0.3\mu \right), \tag{5.6}$$

Or WATEQ Debye-Huckel model can be used as follows:

$$log \gamma_i = -\frac{A z_i{}^2 \sqrt{\mu}}{1+B a_i{}^o} + b_i \mu, \tag{5.7}$$

In Equation (5.7), z_i is the ionic charge of aqueous species *i*, *A* and *B* are constants dependent only on temperature, *a* and *b* are Debye-Huckel coefficients, γ is the activity

coefficient, and μ is the ionic strength. Equation (5.7) is the extended Debye-Huckel equation, if b_i is zero, or the WATEQ Debye-Huckel equation, if b_i is not equal to zero. The ionic strength μ is defined as

$$\mu = \frac{1}{2}\sum m_i {z_i}^2, \tag{5.8}$$

where m_i is the molality of ionic species i, and Z_i is its charge.

5.4.2 Gas-Phase Components

PHREEQC models equilibrium between the gas phase and the aqueous phase with heterogeneous mass action equations and an equation for total pressure. It is assumed that the gas phase components behave ideally and the gas phase is an ideal mixture of the gas components. Ideal behavior of the gas phase assumes that the gas component's fugacity is equal to its partial pressure. As mentioned in the previous section, PHREEQC uses Henry's law constant to relate the partial pressure of the gas component, which is the same as the fugacity of the gas component, to the activity coefficient of the aqueous phase. For example, the dissolution reaction for hydrogen sulfide can be written as

$$H_2S_{(g)} = H_2S_{(aq)}, \qquad Log\ K = 7.9759$$

Therefore, the mass-action equation for this equilibrium reaction is written as

$$P_{H_2S} = 10^{7.9759}\ a_{H_2S(aq)},$$

Therefore, partial pressure of the gas component can be calculated using the activity of that component in the aqueous phase. In general, the partial pressure of the gas component can be written in the following form:

$$P_g = \frac{1}{K_g} \prod_m^{M_{aq}} {a_m}^{C_{m,g}}. \quad (5.9)$$

In Equation (5.9), P_g is the partial pressure of the gas component, K_g is the Henry's law constant for the gas component, and $C_{m,g}$ is the stoichiometric coefficient of aqueous species *m* in the dissolution equation.

5.4.3 Equilibrium with Pure Phases

PHREEQC models the equilibrium state between pure phases and the aqueous phase through heterogeneous mass action equations. For each pure phase, the activity is assumed to be equal to 1 and mole number is specified for the reaction calculation. Then, the mole balance equation for each element is used to determine the changes in the amount of each pure phase. To produce equilibrium between the pure phase and the aqueous phase, PHREEQC determines the mole transfer of the reactants necessary to produce equilibrium with the pure phase.

Dissolution reaction is used to determine the equilibrium state with the pure phases. Therefore, the pure phase equilibrium is estimated by the following equation:

$$K_p = \prod_m^{M_{aq}} {a_m}^{C_{m,p}}, \quad (5.10)$$

where $C_{m,p}$ is the stoichiometric coefficient of species *m* in the dissolution reaction.

In addition, the saturation index (*SI*) is defined for each mineral to determine the tendency of the mineral for dissolution or precipitation. Positive, zero, and negative values for *SI* indicates mineral precipitation, equilibrium state, and mineral dissolution, respectively. Saturation index for each phase can be determined by the following equation:

$$SI_p = \log \prod_m^{M_{aq}} {a_m}^{C_{m,p}}. \quad (5.11)$$

It should be noted that saturation index is equal to the log of the partial pressure of the gas component for fixed partial pressure gas component.

5.4.4 Charge Balance

The charge balance equation sums up the total equivalent of aqueous cations and anions. In real solutions, the total charge balance is zero. However, electrical imbalance may occur due to analytical errors and unanalyzed constituents in chemical analysis. In these cases, the PH or the activity of species can be adjusted to neutralize the charge balance in the solution. The charge imbalance for a solution is calculated by

$$T_{z,q} = \sum_i^{N_{aq}} Z_i n_i \,, \quad (5.12)$$

where $T_{z,q}$ is the charge imbalance for aqueous phase q, Z_i is the charge on aqueous species *I*, and q indicates the aqueous phase.

5.5 COUPLING UTWELL WITH IPHREEQC

In this study, IPhreeqc is explicitly coupled to the wellbore. The effects of hydrocarbon solution in the water and kinetic reactions are neglected in our model. Figure 5.1 presents the coupling scheme of IPhreeqc with UTWELL. As shown, once the flow variables, such as pressure, temperature, and velocities, are calculated in the wellbore, IPhreeqc input file is created in the computer memory to calculate the equilibrium conditions in the aqueous phase. Next, the amount of solid particles is calculated and transferred to the transport and deposition module to determine the amount

of deposition on the tubing surface. Then, the fluid properties are updated and the simulation is started for the next time step.

In UTWELL-IPhreeqc, transport-related parameters are defined in "GEOCHEMINPUT.DAT" which is an additional input file for UTWELL. To model reactive-transport problems, the flag for scale should be true in the main input file of UTWELL ("INPUT.CFG"). UTWELL-IPhreeqc input files can be described as follows:

- INPUT.CFG: Using this input file, the user can model scale deposition by turning on the "ISCALE" flag. The name of solid phases that may be precipitated, molecular weights, and molar densities are defined in this input file as well. In addition, all the wellbore parameters such as depth, diameter, productivity indices, etc. are defined in "INPUT.CFG".
- GEOCHEMINPUT.DAT: This file provides the initial wellbore gridblocks condition. In other words, initial aqueous solution should be defined for each wellbore gridblock in this file. In addition, the aqueous solution of the reservoir fluid that goes into the wellbore is defined with a specified unique number. Therefore, there should be a unique number for each solution that goes into the wellbore.
- IPhreeqc_Database.DAT: This is the main geochemistry database used by IPhreeqc to calculate the equilibrium condition. Details of the several reactions are defined in this file. Based on the purpose of simulation, one of the geochemistry databases can be used (phreeqc.dat, pitzer.dat, iso.dat, etc.). This database can be modified by the user under certain condition, such as matching the experimental core flood data.

In addition to mass balance for the $N_{element}$ geochemical elements existing in the aqueous and solid phases, total mass of hydrogen, oxygen, and charge balance should be transported to consider accurate solution composition and the effect of charge imbalance in IPhreeqc. Therefore, total $N_{element} + 3$ mass balance equations are solved to determine the concentration of the elements in each gridblock. To get the total moles of hydrogen, oxygen, and charge balance ***TOTMOLE("H")***, ***TOTMOLE("O")***, and ***CHARGE_BALANCE*** keywords are used. Therefore, charge balance should be maintained by doing mass balance similar to other elements.

The first step in coupling IPhreeqc with UTWELL is defining a module in the computer memory. Keyword ***CreateIPhreeqc*** is used for this purpose. Next, IPhreeqc is loaded in the generated module through ***LoadDataBase*** command. Then, the geochemistry input file is loaded into the computer memory through ***Include$*** keyword. ***GetComponentCount*** and ***GetComponent*** commands are used to determine the number of components in the geochemistry input file ($N_{element}$) and specified components name, respectively. It is worth to mention that to append one or more lines into the computer memory, ***AccumulateLine*** is used. For example, to define the GEOCHEMINPUT.DAT as the geochemistry input file, the following expression is used:

Ierr = AccumulateLine (IPhreeqc_ID, ' Include$ GEOCHEMINPUT.DAT ')

In the above expression, IPhreeqc_ID is the number which was assigned to the created and initialized module.

In the developed model, ***Solution*** keyword is used to define pressure, temperature, pH, equilibrium condition, and composition of the initial solution. To

modify the previously defined solution composition at the later time step, ***Solution_Modify*** keyword is used. Using this keyword, equilibrium conditions, and number of moles of the components can be changed or even new elements may be introduced to the aqueous solution.

To define a pure phase that can react with the aqueous phase, ***Equilibrium_Phases*** keyword is used to define phase name, saturation index, chemical formula, and number of moles of that phase. Since the defined phase is in contact with the aqueous phase, it may dissolve or precipitate to reach the equilibrium state. To modify the previously defined phase in equilibrium, ***Equilibrium_Phases_Modify*** is used. This keyword enables adding new phases or making changes in the phase properties, such as number of moles.

In the developed model, IPhreeqc input file is created using the described keywords and transferred to the computer memory. Finally, ***RunAccumulated*** is utilized to run IPhreeqc based on the existing input file. Then, the calculated concentrations of the elements are transferred to the wellbore simulator through ***GetSelectedOutputColumnCount***, ***GetSelectedOutputRowCount***, ***GetSelectedOutputValue*** keywords. Table 5.3 presents the useful keywords used in coupling IPhreeqc with UTWELL.

5.6 SCALE DEPOSITION

In terms of particle structure, it is assumed that scale is similar to asphaltene. In fact, both scale and asphaltene consist of solid spheres. Therefore, similar to asphaltene

particles, Eddy and Brownian diffusion are the dominant mechanisms of scale deposition. The detailed mechanism and model of particle deposition was discussed in Chapter4.

5.7 SIMULATION RESULTS

In this section, we performed the simulation using the coupled UTWELL-IPhreeqc version to study scale deposition of different scenarios.

5.7.1 Case 1: Comparing Different Coupling Methods

This case shows hard coupling and soft coupling models and compares the results and CPU time of these methods. We used the test case of Shirdel (2013) as the reference for soft coupling approach. In this case, scale deposition was investigated in a 5000ft wellbore that only produces water and oil. Table 5.4 presents the main input parameters for this simulation. In addition, we assume that the aqueous phase have sodium, calcium, sulfate, and anhydrite with concentration of 0.1, 0.001, 0.003, and 0.1 mole/kg, respectively. We performed the simulation for 90 days to depict the scale profile in the tubing.

Figure 5.2 compares the CPU time of hard coupling and soft coupling approaches. As shown, hard coupling is much faster than the soft coupling and reduces the simulation time by a factor of 22. Figure 5.3 illustrates the inner diameter of tubing after 90 days. As can be seen, most of the deposition occurred at the bottom of the well and as we move toward the wellhead, a small amount of scale is observed. In addition, it is observed that the result of hard coupling method is in agreement with soft coupling approach. Figure 5.4 illustrates a slight difference in the solid concentration in these two models. This

difference is attributed to the limited database Shirdel (2013) used for modeling geochemical reactions in his predictions. In addition, pressure and temperature affect the equilibrium condition which was neglected in his model. Therefore, the new approach is more accurate and faster compared to the Shirdel's model (2013). Figure 5.5 also illustrates the transport coefficient along the wellbore. This case clarifies that more scale deposition is observed in the tubing where solid concentration and transport coefficient have higher values. In other word, the combined effect of transport coefficient and solid concentration determines the deposition rate in the tubing.

5.7.2 Case 2: Scale Deposition in a Vertical Well

In this section, we designed a more complicated case to study scale deposition in the wellbore. All of the wellbore and fluid data are presented in Table 5.5. We use a 3000ft vertical well with initial pressure of 2000psi that operates with 840psi at the wellhead in this case study. In addition, concentrations of ions in the aqueous phase are presented in Table 5.6. We expect that six minerals can form and deposit on the surface of tubing that can be named as anhydrite, aragonite, calcite, dolomite, hausmannite, and hematit. The properties of these solids are presented in Table 5.7. In addition, it is assumed that no solid exists in the tubing at the beginning of simulation.

We performed multiphase simulation for this well for 300 days to determine the amount and risk of scale deposition in the wellbore. Figure 5.6 shows the trend of scale deposition in the wellbore through time. As can be seen, the scale thickness increases along the wellbore as time progresses. Most of the deposition is observed above the perforation zone at the depth of 2900ft where the transport coefficient and solid concentrations are high. As we go toward the wellhead, the thickness of deposited scale

decreases. In addition, since the velocity of the reservoir fluid that comes into the wellbore is high around the perforation zone, the thickness of scale is relatively small at that point. It can be seen that the cross section of the pipe at the depth of 2900ft is reduced to 30% of the initial value after 300 days, which suggests that the wellbore performance was severely damaged. Figures 5.7and 5.8 show scale concentration and transport coefficient along the wellbore, respectively. As mentioned in the previous case study, these parameters directly affect the scale deposition. Figure 5.9 also presents the bottom-hole pressure versus production time. As illustrated, scale deposition in the wellbore increases the bottom-hole pressure as time progresses and eventually results in smaller influx from the reservoir into the wellbore. In fact, blocking the area for fluid flow and subsequent increase in the friction factor between the deposited solid and the flowing fluid are two main reasons to increase the bottom-hole pressure.

Figure 5.10 shows the results after 100, 200, and 300 days of simulation for (a) temperature, (b) oil superficial velocity, (c) gas superficial velocity, and (d) water superficial velocity. It can be seen that scale deposition changed the profiles of temperature and velocities along the wellbore through time. As shown, the temperature of the fluid in the wellbore decreases with progression of time. In fact, reduction in temperature is attributed to the lower velocity of the fluid which allows for more heat transfer between the fluid and formation. Initially, the oil velocity was around 3.8ft/s at the wellhead. As the bottom-hole pressure increases over time, less fluid comes into the wellbore and reduces the production rate and consequently, fluid velocities at the wellhead. The sudden jump in the velocity profile near the bottom-hole is the result of enormous amount of deposited scale. As mentioned before, we expect that the velocity decreases at the wellhead as time proceeds. However, we do not see this trend for the

simulation results of 100 and 200 days. This trend can be explained by the parameters that affect fluid velocity. We expect that after 200 days, less fluid comes into the wellbore due to the higher bottom-hole pressure. On the other hand, the cross section of the pipeline is decreasing at the same time. Therefore, the amounts of fluid influx into the wellbore and deposited scale simultaneously affect the velocity field. In this case, effect of smaller cross section is more dominant than the smaller influx and results in greater velocity at the wellhead. This trend can be observed for all the other velocity profiles.

5.7.3 Case 3: Incompatible Water Production

In this section, we investigate scale deposition mainly due to the mixing of incompatible water. We designed a case where fluid is produced from two oil layers. These layers have completely different ion compositions as demonstrated in Table 5.8. A schematic view and the location of these oil layers and the wellbore are shown in Figure 5.11. The expected minerals that can form and deposit in the tubing are listed in Table 5.9 with their properties. All the wellbore and fluid properties are identical to Case 1. We assumed that the first layer has the initial pressure of 3000 psi and is located between the depth of 4950 and 5000ft. In addition, Layer 2 with the initial pressure of 2250 psi is extended from 3000 to 3100ft.

We performed multiphase flow simulations for 90 days to study the effect of mixing incompatible water on scale formation and deposition in the wellbore. Figure 5.12 presents the scale thickness along the wellbore after 30, 60, and 90 days. It can be seen that a small amount of scale is deposited at the bottom of the producer and as we go upward to the depth of 3100ft, the amount of deposited solid is decreasing. However, a sudden change in the profile of scale is observed at 3050ft where two different formation

waters are mixed together. In fact, most of the deposition occurs at this point in a way that inner diameter is reduced 10% after 90 days. As we continue moving toward the wellhead, the scale thickness starts to shrink till the depth of 1100ft where no deposition has occurred. Figures 5.13 and 5.14 also illustrate the solid concentration and transport coefficient along the wellbore across time. It can be seen again that scale concentration is maximum at 3050ft (mixing point).

Figure 5.15 presents the bottom-hole pressure versus time. After 90 days, the bottom-hole pressure increased 5 psi which results in smaller production rate. Figure 5.16 shows the results of simulation after 30, 60, and 90 days of simulation for (a) temperature, (b) oil superficial velocity, (c) gas superficial velocity, and (d) water superficial velocity. Figure 5.16(a) illustrates that temperature slightly decreases along the wellbore over time. Moreover, a slight decrease in the field velocities is observed at the wellhead since scale deposition has not greatly affected the well performance yet.

The problem of mixing incompatible water in this case showed that neglecting the importance of flow assurance results in tubing blockage and production loss. Multilateral wells are the other candidates for which scale deposition might happen with the same scenario. For the mentioned case, one of the remedies is to produce the incompatible water from another flow path (e.g. annulus) or to use scale inhibitor.

Table 5.1: Different scenarios based on the Q-value calculated by Stiff and Davis model (The unit of Q is PTB, pound per thousand barrels)

$Q < 0$	No scaling
$0 < Q < 100$	Little scale deposition is possible
$100 < Q < 250$	Moderate scaling is possible
$Q > 250$	Severe scale deposition will definitely happen

Table 5.2: Common types of scales in oilfield (Moghadasi et al., 2003)

Name	**Chemical Formula**	**Primary Variables**
Calcium carbonate	$CaCO_3$	Partial pressure of CO_2, Temperature, Total dissolved salts, PH
Calcium Sulphate: Gypsum Hemihydrate Anhydrite	 $CaSO_4.2H_2O$ $CaSO_4.1/2H_2O$ $CaSO_4$	Temperature, Total dissolved salts, pressure
Barium Sulphate	$BaSO_4$	Temperature, Pressure
Stronium Sulphate	$SrSO_4$	Temperature, Pressure,Total Dissolved salts
Iron Compunds: Ferrous Carbonate Ferrous Sulphide Ferrous Hydroxide Ferrous Hydroxide	 $FeCO_3$ FeS $Fe(OH)_2$ $Fe(OH)_3$	Corrosion, dissolved gases, PH

Table 5.3: The main keywords used in coupling IPhreeqc with the developed wellbore model (Charlton and Parkhurst, 2011)

Method	**Usage**
CreateIPhreeqc( )	Create and initialize a module
LoadDatabase(ID, File Name)	Reads the Iphreeqc database file
AccumulateLine(ID, String)	Append lines and commands in the computer memory
GetComponent(ID, N, Comp)	Get the name of the geochemical elements
GetComponentCount(ID)	Get the total number of geochemical elements
GetSelectedOutputColumnCount(ID)	Get the total number of columns in the output file
GetSelectedOutputRowCount(ID)	Get the total number of rows in the output file
GetSelectedOutputValue(ID, Row, Col, Vtype, Dvalue, Svalue)	Get the output value from a specific column and row
GetOutputFileOn(ID, Logical)	Prints the output file
GetSelectedOutputFileOn(ID, Logical)	Print the selected output file
RunAccumulated(ID)	Run the input saved in computer memory
CHARGE_BALANCE	Charge balance of a solution
EQUI("mineral")	Moles of the mineral in equilibrium with the aqueous phase
EQUI_DELTA("mineral")	The reacted moles of the mineral in equilibrium
MOL("AQ/EX/SURF")	Molality of an aqueous, exchange, or surface species
PHASE_FORMULA("mineral")	Return the chemical formula of the mineral
PUNCH	Writes to the selected-output file
SI("Phase")	Determines the saturation index of a phase
TOT("Element")	The total molality of an element
TOTMOLE("Element")	Moles of an elemtn in the aqueous solution

Table 5.4: Input parameters for simulation of scale deposition in the wellbore (Case 1)

Well Data		Reservoir and Fluid Data	
Well MD	5000 ft	Net pay zone	150 ft
Well TVD	5000 ft	Reservoir pressure	2500 psi
Max Grid Size	50 ft	Reservoir Temperature	180 °F
Surface Temperature	60 °F	Oil API gravity	30
Bottom hole Temperature	180 °F	Oil bubble point pressure	500 psi
Total Heat Transfer Coefficient	20 Btu/Hr.°F.ft^2	Gas specific gravity	0.55
Tubing ID	0.229 ft	Water specific gravity	1
Oil Productivity Index	0.5 ft^3/psi.ft.day	Gas heat capacity	0.55 Btu/lbm.°F
Water Productivity Index	0.1 ft^3/psi.ft.day	Oil heat capacity	0.45 Btu/lbm.°F
Gas Productivity Index	0.0 ft^3/psi.ft.day	Water heat capacity	1 Btu/lbm.°F
Wellhead Pressure	500 psi	Geochemical scale type	Anhydrite

Table 5.5: Input parameters for simulation of scale deposition in the wellbore (Case 2)

Well and Reservoir Data		Fluid Data	
Well MD	3000 ft	**Component name**	**Mole Fraction**
Well TVD	3000 ft	CO_2	0.12837
Max Grid Size	50 ft	C1	0.42134
Surface Temperature	60 °F	C2	0.05557
Bottom hole Temperature	180 °F	C3	0.02662
Total Heat Transfer Coefficient	0.2 Btu/Hr.°F.ft^2	C4	0.01535
Tubing ID	0.229 ft	C5	0.00985
Oil Productivity Index	0.3 ft^3/psi.ft.day	C6	0.00835
Water Productivity Index	0.15 ft^3/psi.ft.day	C7-C10	0.06971
Gas Productivity Index	0.01 ft^3/psi.ft.day	C11-C13	0.03578
Wellhead Pressure	840 psi	C14-C19	0.07131
Net pay zone	100 ft	C20-CC29	0.07629
Reservoir pressure	2000 psi	C30+	0.08146

Table 5.6: Reservoir water composition used in simulation studies (Case 2)

Ions	Concentration of formation water(ppm)
Ba	70
Ca	2320
Fe	210
Mg	348
K	1110
Na	11850
Sr	24
HCO3-	2000
Cl	17275
S(6)	6300

Table 5.7: Possible solids that may deposit in the wellbore (Case 2)

Solid name	Density (lb_m/ft^3)	Molecular weight (lb_m/lb_{mol})
Anhydrite	185.328	136
Aragonite	182.83	100.09
Calcite	169.1	100.09
Dolomite	177.84	184.4
Hausmannite	302.016	228.81
Hematite	330.72	159.69

Table 5.8: Formation sea water analysis (Case 3)

Ions	Concentration of formation water (ppm)	
	Layer 1	**Layer 2**
Na	37400	11400
K	329	400
Ca	3067	435
Mg	1114	1370
HCO3-	1029	10200
Cl	623	63500
Li	3.4	0
Sr	153	0
Ba	151	0
Fe	1.7	0
Ba	41	0
Br	325	0
S(6)	0	28000

Table 5.9: Possible solids that may deposit in the wellbore (Case 3)

Solid name	Density (lb_m/ft^3)	Molecular weight (lb_m/lb_{mol})
Anhydrite	185.328	136
Aragonite	182.83	100.09
Calcite	169.1	100.09
Dolomite	177.84	184.4
Barite	279.552	233.39
Hematite	330.72	159.69

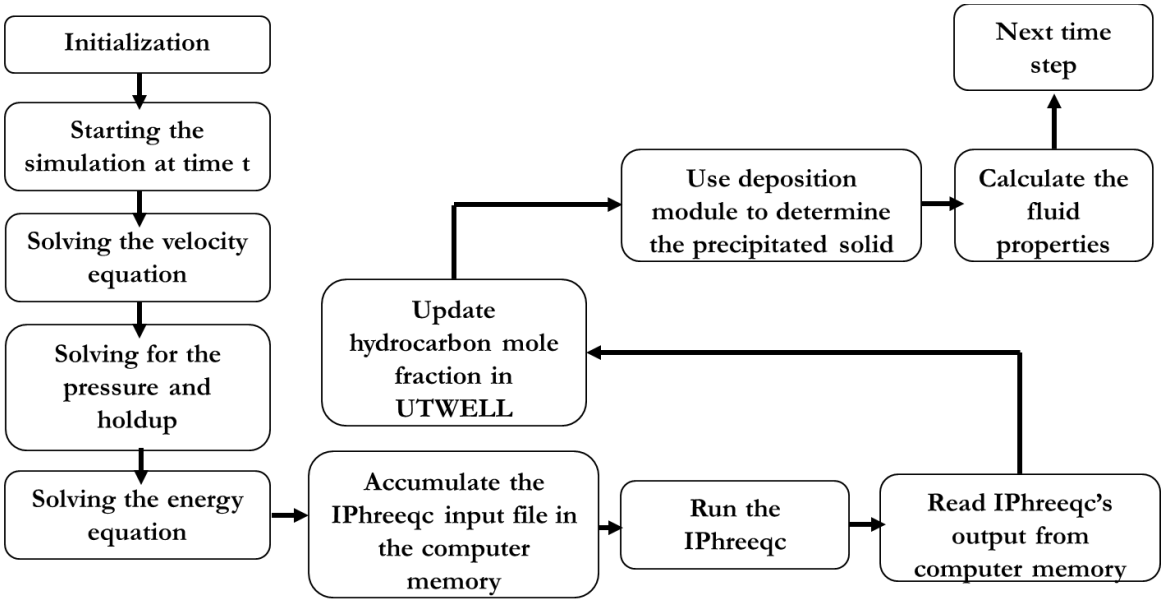

Figure 5.1: Schematic flowchart of coupled UTWELL-IPhreeqc

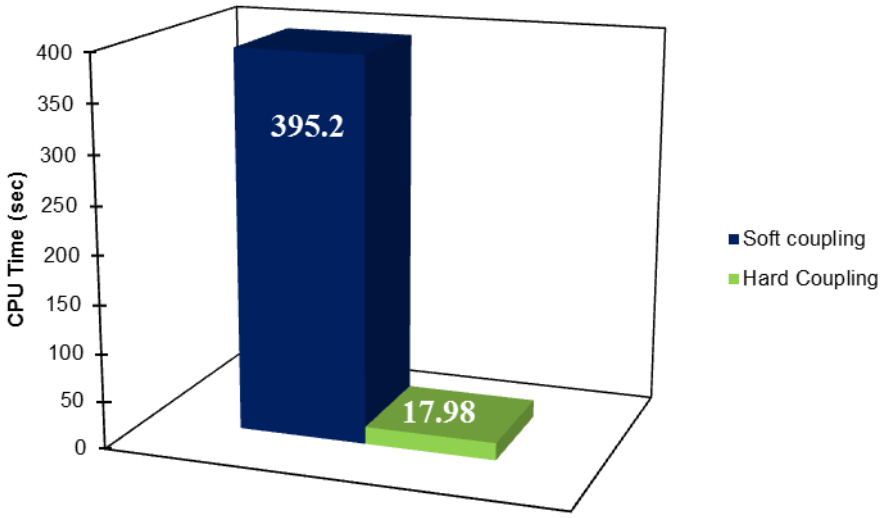

Figure 5.2: CPU time Comparison of Hard coupling and Soft coupling methods

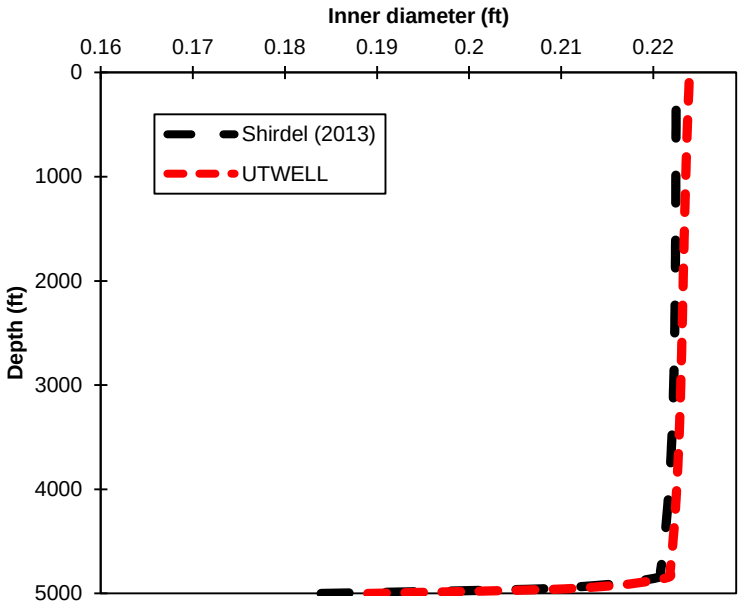

Figure 5.3: Comparing the inner diameter of tubing for Shirdel (2013) and IPhreeqc-UTWELL after 90 days

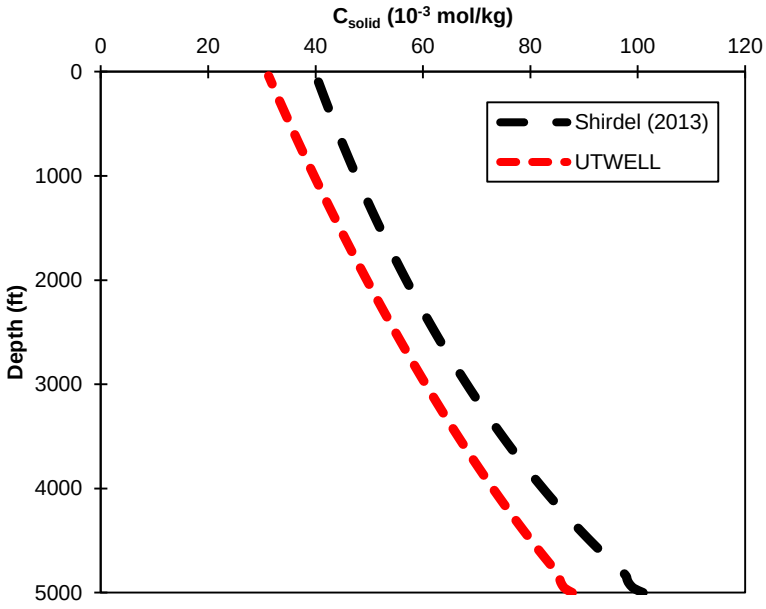

Figure 5.4: Comparing the concentration of anhydrite along the wellbore for Shirdel (2013) and IPhreeqc-UTWELL after 90 days

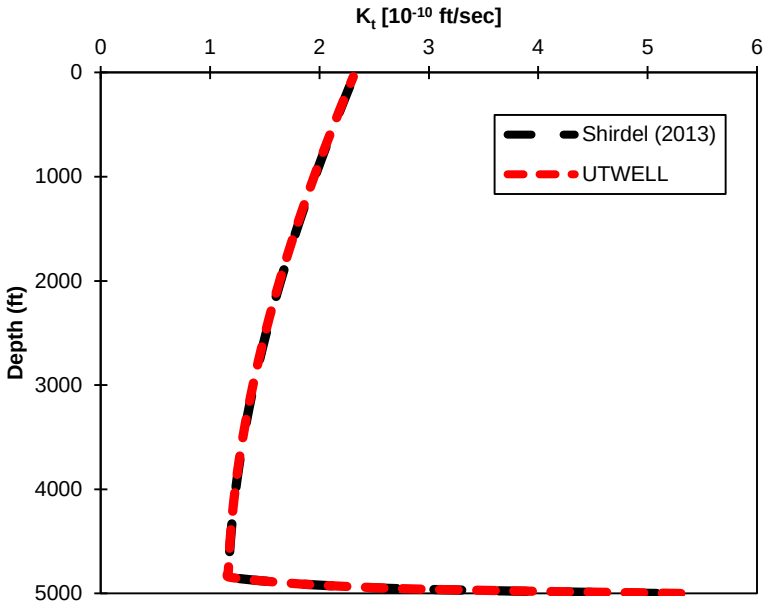

Figure 5.5: Comparing the transport coefficient for Shirdel (2013) and IPhreeqc-UTWELL after 90 days

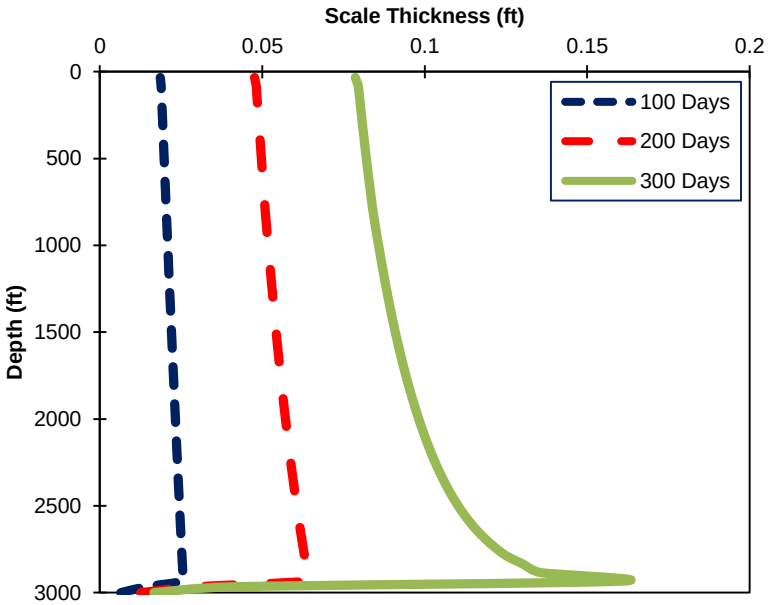

Figure 5.6: Scale thickness profile along the wellbore after 100, 200, and 300 days

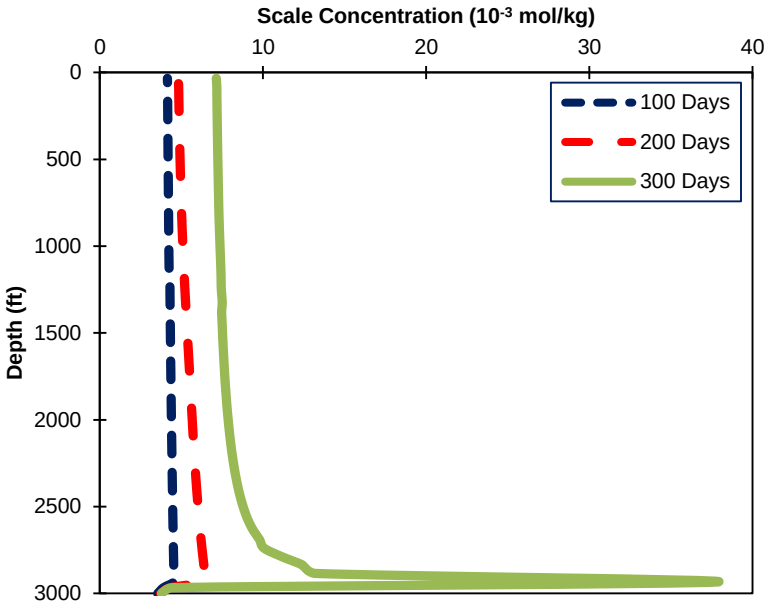

Figure 5.7: Scale concentration along the wellbore after 100, 200, and 300 days

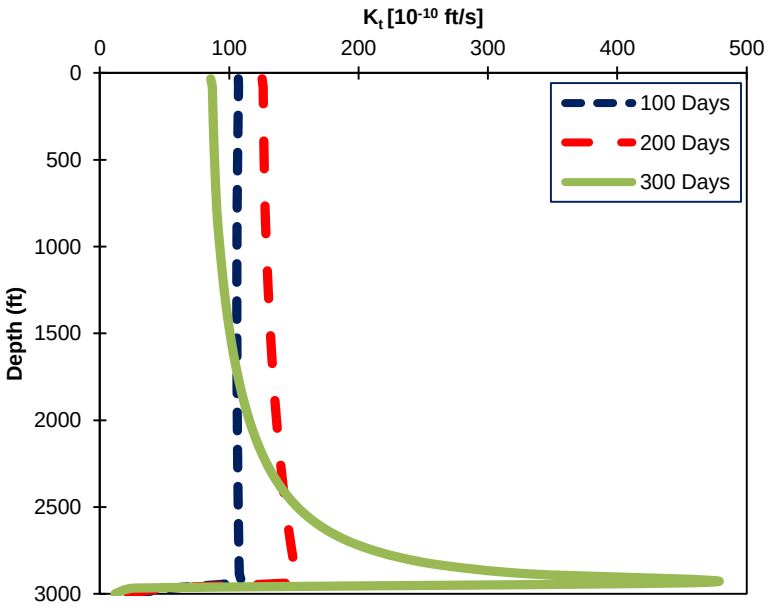

Figure 5.8: Transport coefficient along the wellbore after 100, 200, and 300 days

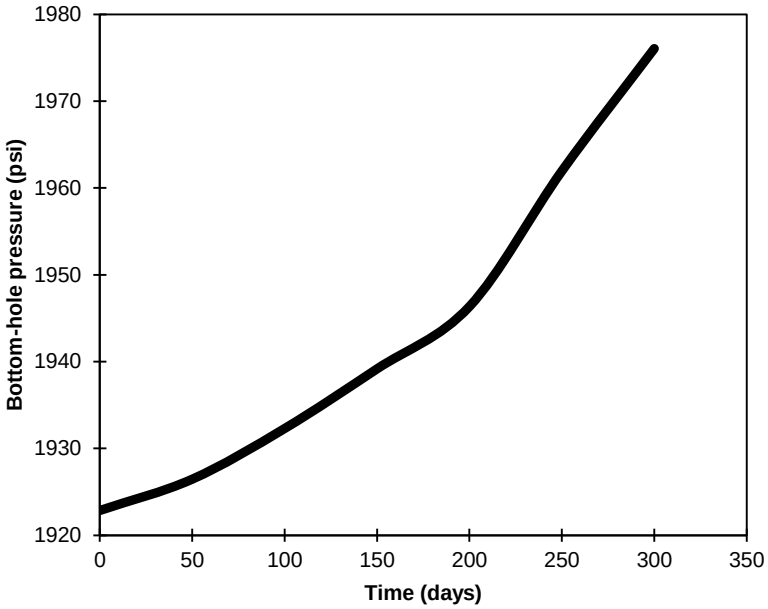

Figure 5.9: Bottom-hole pressure versus time

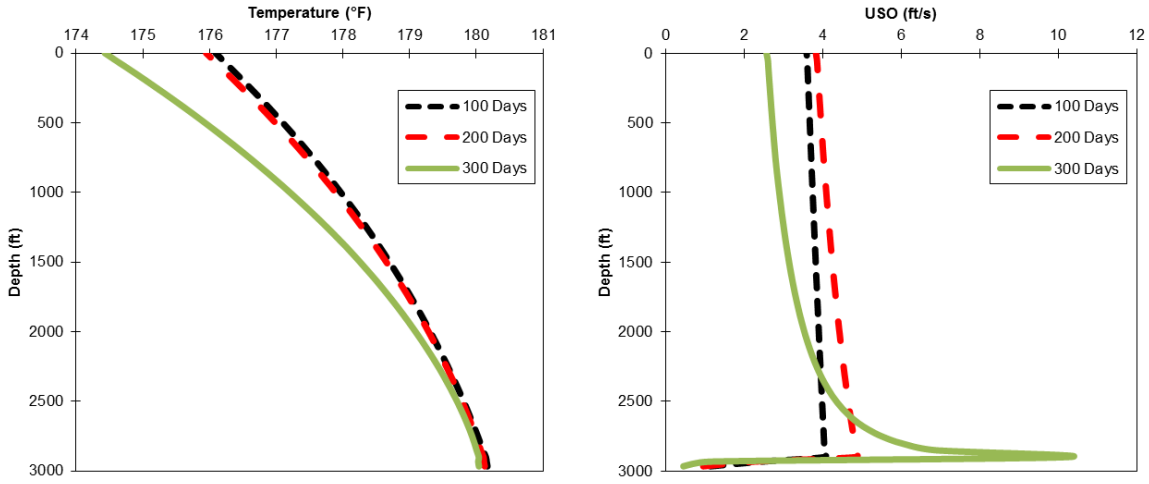

(a) (b)

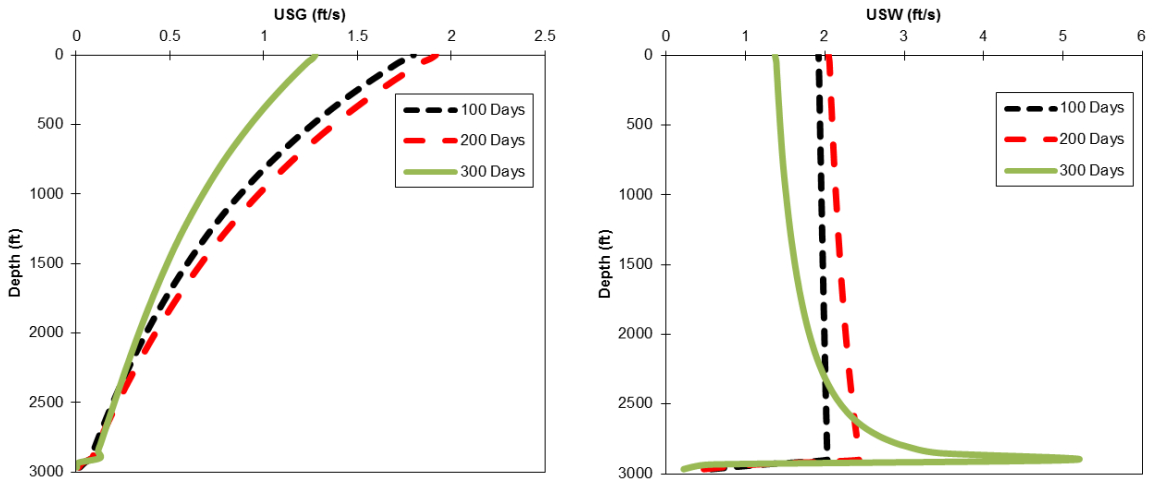

(c) (d)

Figure 5.10: (a) Temperature, (b) oil superficial velocity, (c) gas superficial velocity, (d) water superficial velocity profile along the wellbore after 100, 200, and 300 days

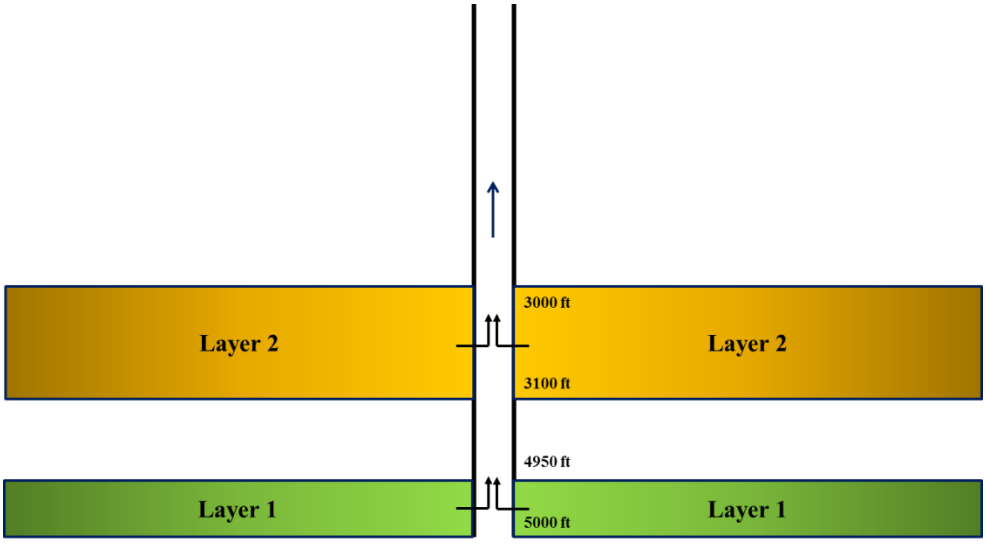

Figure 5.11: Schematic view of the wellbore and reservoir (Case 3)

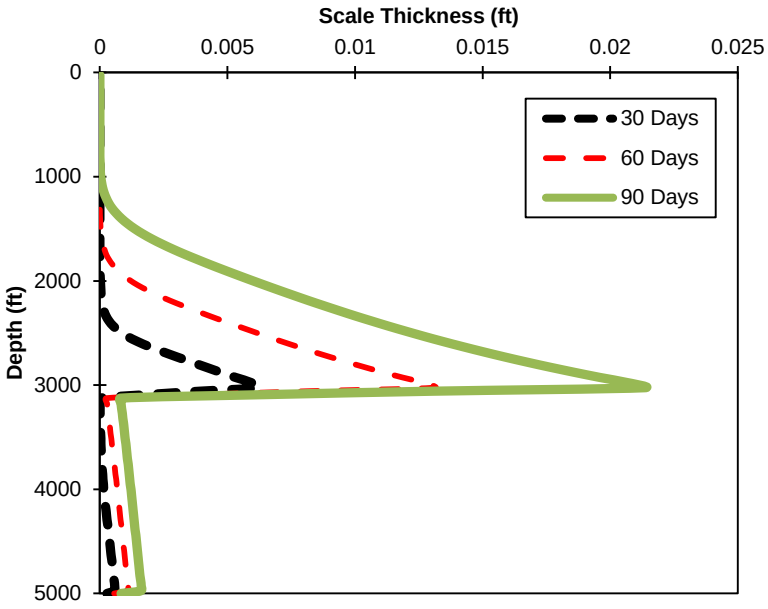

Figure 5.12: Scale thickness along the wellbore after 30, 60, and 90 days (Case 3)

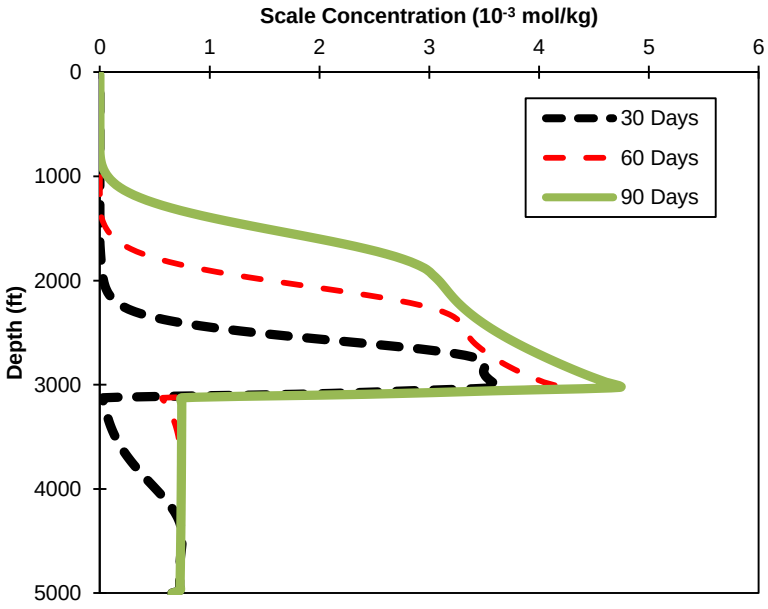

Figure 5.13: Scale concentration along the wellbore after 30, 60, and 90 days (Case 3)

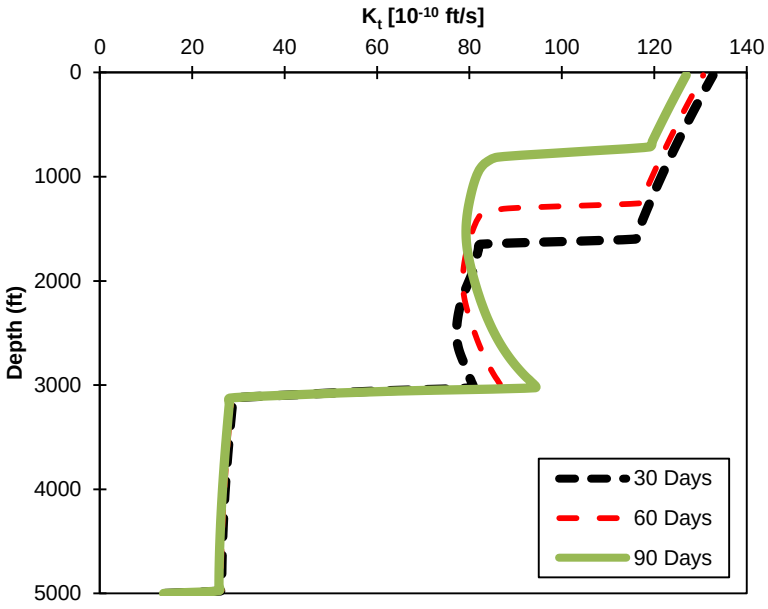

Figure 5.14: Transport coefficient along the wellbore after 30, 60, and 90 days (Case 3)

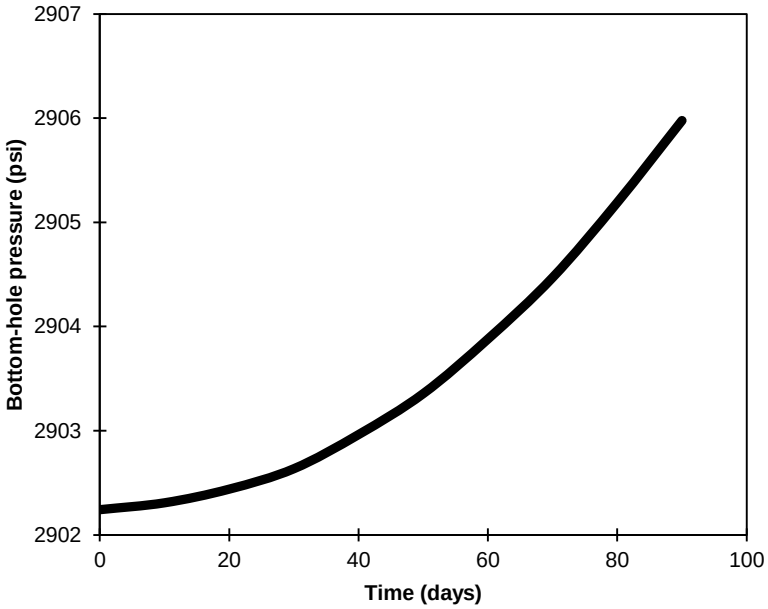

Figure 5.15: Bottom-hole pressure versus time (Case 3)

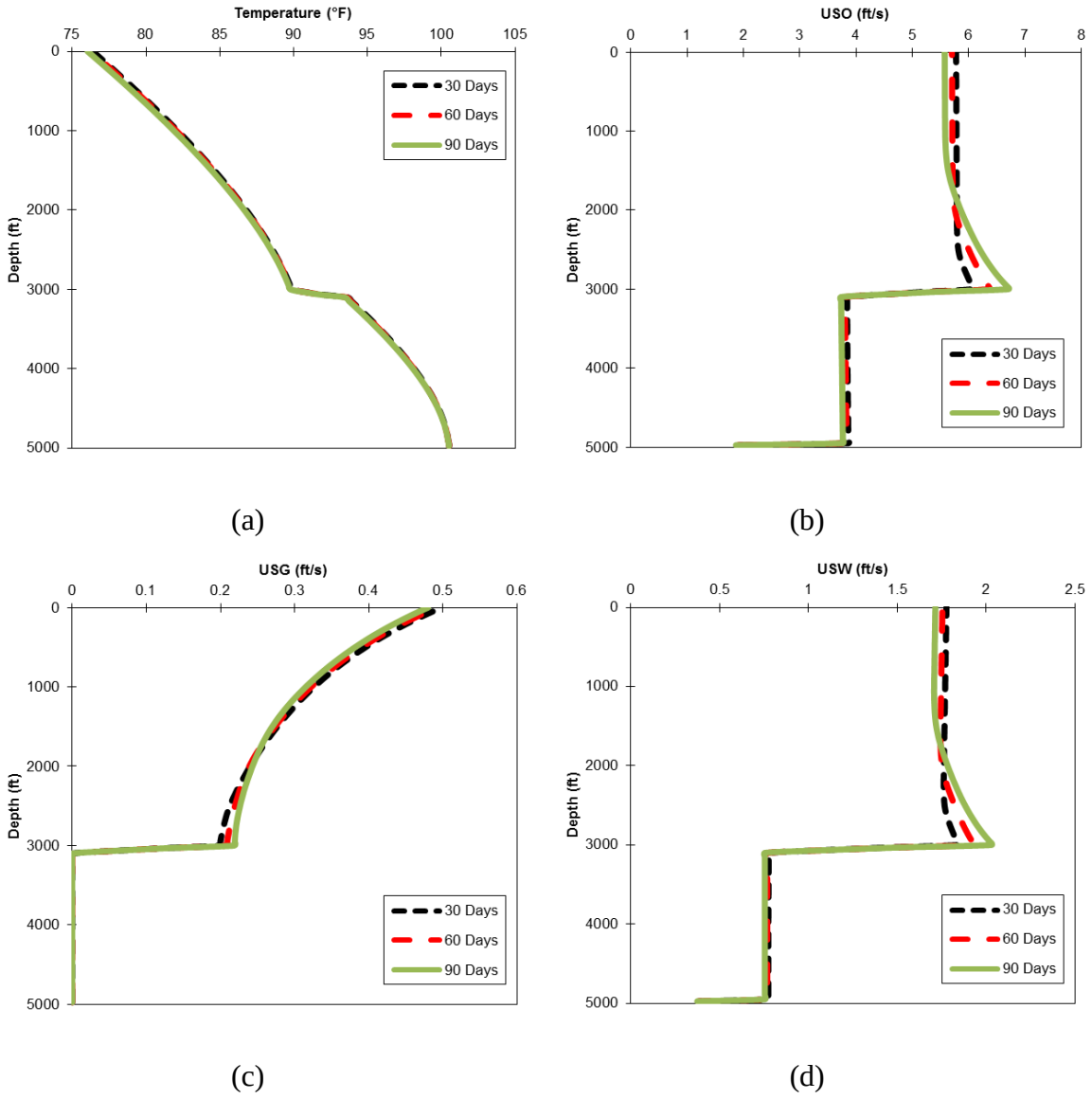

Figure 5.16: (a) Temperature, (b) oil superficial velocity, (c) gas superficial velocity, (d) water superficial velocity profile along the wellbore after 30, 60, and 90 days

Chapter 6: Summary, Conclusions, and Recommendations

This chapter presents the summary and conclusion of this work. In addition, recommendations for extension of this research are presented.

6.1 SUMMARY AND CONCLUSIONS

- A gas lift module was implemented in the University of Texas in-house wellbore simulator UTWELL to model gas lift mechanism in the wellbore. In the developed tool, both steady-state and transient models were incorporated for accurate modeling of single phase and multiphase flow in the annulus and tubing. Moreover, the formulation for mass, momentum, and energy equations were derived and discretized.
- In the implementation, thermodynamic equilibrium conditions during single phase and multiphase flow can be calculated using EOS compositional or black oil models. The mass transfer between the phases can also be determined by EOS or black oil models.
- The flow in the annulus was modeled using fully-implicit approach. This model can be used for gas injection or solvent injection. The mass flow rate between the annulus and tubing can be determined by the user or through the gas lift valve performance.
- The minimum time steps between tubing and annulus is selected as the time-step size of the system.

- The final wellbore model is able to calculate the pressure, temperature, and velocity fields in the tubing and annulus. The final version was successfully validated against a commercial simulator.
- Plot of oil production rate versus gas injection rate indicated that there is an optimum value for the gas injection flow rate. Increasing the injection flow rate above this optimum value results in more pressure drop, greater bottom-hole pressure, and consequently less liquid production.
- It is crucial to evaluate the operability and feasibility of gas lift process from different aspects, such as flow assurance issues (i.e. asphaltene deposition). Therefore, we investigated the effects of gas lift on asphaltene deposition of asphaltic oil.
- Characterizing the fluid and modeling the phase behavior is a crucial step for detecting the asphaltene problem. Thus, characterization procedure of asphaltic oil was discussed thoroughly. In addition, Peng-Robinson equation of state was tuned to mimic the experimental results of the Middle Eastern oil. Binary interaction coefficients, volume shift parameters, and molar volume of asphaltene are the parameters that were tuned.
- The tuned phase behavior was used to study the effect of lift gas composition on the dynamics of asphaltene precipitation, flocculation, and deposition for several scenarios.
- Asphaltene precipitation and deposition in the wellbore is a dynamic process. Many parameters, such as pressure, temperature, and velocity fields affect the trend of deposition. Injecting light hydrocarbons and CO_2 as lift gas into an

asphaltic oil increase the risk of asphaltene deposition in the tubing by extending the asphaltene deposition envelope. Therefore, a robust and compositional multiphase flow simulator is necessary for predicting the asphaltene phase behavior.

-
- The profile of asphaltene in the wellbore indicates that injection of lighter hydrocarbons can severely damage the wellbore performance. Moreover, most of the deposition occurs around the bubble point since asphaltene is unstable at that point. As we move from this point toward the wellhead, pressure decreases and smaller amount of deposition is observed in the tubing.
- The composition and percentage of the injection gas affect the amount of asphaltene deposition along the wellbore and the subsequent oil production rate. A lighter gas decreases the density of the reservoir fluid and results in a better lift and an increase in production. However, this composition may decrease the stability of asphaltene in the solution and reduce the production rate.
- Optimizing the flow rate of lift gas slows down the process of asphaltene precipitation.
- The new version of UTWELL is capable of tracking asphaltene deposition in the wellbore with and without gas lift process to diagnose the potential risk of asphaltene precipitation in the wellbore. Additionally, this model can suggest the optimum operating condition for the well to minimize the asphaltene problems.
- IPhreeqc, a geochemical package, was coupled to the wellbore model for simulation of geochemical reactions, transportation, and consequent deposition in

the wellbore. Using this tool, we are able to model geochemical reactions in the wellbore and determine the profile of scale deposition along the well.

- We presented hard coupling approach which is a more robust coupling algorithm and saves more computational time compared to the soft coupling method. For a specific study, we showed that the simulation time is reduced by the factor of 22 by utilizing hard coupling method.
- Several case studies were presented to indicate the profile of scale thickness, scale concentration, and transport coefficient along the wellbore.
- It was observed that combined effect of solid particle concentrations and transportation in the flow stream affects the deposition rate. The transport coefficient is also calculated as a function of particle diameter, viscosity, temperature, and bulk velocity.
- For the case of mixing an incompatible water, it was shown that severe scale deposition occurred at the mixing point and resulted in tubing blockage and loss of production. Therefore, inhibition and remediation work should be designed to prevent formation of scale.
- At the point where solid concentration and transport coefficient had high values in the wellbore, deposition was likely to occur which consequently increases the bottom-hole pressure and narrows down the pipe cross section.
- UTWELL simulation results indicate that most of the scale deposition occurred near the bottom of the well where the solid concentration is high. In addition, mixing of incompatible water results in scale deposition at the mixing point.

- The developed compositional wellbore model enables the operators to plan for asphaltene and scale inhibition and remediation strategies at the proper time and location.

6.2 RECOMMENDATIONS

The recommendations for further studies in the same area are presented as follows:

- As a future work, it is recommended to develop a gas lift optimization tool to determine the optimum gas injection rate based on the reservoir condition and the available amount of gas to maximize oil production rate.
- SAFT (Chapman et al., 1990) is an equation of state that has shown promise in modeling asphaltene phase behavior by considering the molecular interaction. Therefore, we recommend implementing SAFT equation of state in the wellbore model. In addition, this wellbore model can be coupled with a compositional reservoir simulator having PC-SAFT equation of state (Mohebbinia, 2013) for accurate modeling of asphaltene deposition in the coupled wellbore/reservoir system.
- The coupling of a compositional reservoir simulator with UTWELL enables the operators to monitor scale deposition in the wellbore/reservoir system. Using the geochemical feature of UTCOMP (Kazemi Nia, 2014), we can study various scenarios in the whole production system. In addition, coupling the wellbore with the thermal version of UTCHEM (Lashgari, 2014) allows for studying the possibility of scale deposition in the carbonate reservoir during steam injection.
- Solvent and chemical treatments are solutions to inhibit and remediate deposited asphaltene in the reservoir and wellbore. As a future work, it is recommended to

model the solvent phase behavior with the crude oil as an inhibition and remediation strategy. In addition, optimization of chemical treatment parameters, such as dispersant type, required amount of dispersant, soaking time, etc. should be performed.

Appendix A: Sample Input Data

A.1 SAMPLE INPUT DATA FOR COMPOSITIONAL GAS LIFT MODEL

```
CC ================================================================*
CC               WELLBORE MODEL INPUT DATA                        *
CC ================================================================ *
CC                                                                 *
CC CASE NAME:  4COMP FLUID PROD WELL                               *
CC             THIS CASE IS USED FOR TESTING THE CODE FOR GAS      *
CC             LIFT PROCESS FOR THE COMPOSITIONAL MODEL            *
CC                                                                 *
CC UNITS:      FIELD                                               *
CC             FT, DEGREE, BTU/HR.F.FT, BBL/PSI.FT.DAY             *
CC             LB/FT3, PSI, F, FT3/LBMOLE, LBM/LBMOLE, BTU/LB, DAY *
CC                                                                 *
CC CREATED BY: ALI ABOUIE 08/26/2014                               *
CC                                                                 *
CC ================================================================*
CC
CC MAXIMUM NUMBER OF WELLS IN CALCULATION AND FLOWPATH TYPE
* NWLBR  FLOWPATH
   1        WELL
CC*******************************************************************
CC WELL #01 DATA                                                   *
CC*******************************************************************
CC
CC CASE DEFINITION: {WELL ID}
* LW      WNAME
   1      ST.ST.COMP.GASLIFT
CC
CC MESH GRID SIZE [FT]
* MAXGRIDSIZE
     300.0
CC
CC WELL SURFACE [FT]
* WSURFACE
     0.0
CC
CC WELL PROFILE AND SURVEY
* TRAJINTVL  MD        TVD     INCLINATION     AZIMUTH
     1       7000.0    7000.0      90.0        0.0
CC
CC WELL CASING AND COMPLETION {Default RWB=RCO+0.041665}  (CODE:7")
* CASEINTVL HANGERDEPTH  SETTINGDEPTH  RCI         RCO        RWB    CEMENTOP
      1     0.0           7000.0       0.35        0.40       0.50   0.0

* EPSCI    EPSCO    KCASE           KCEM          HCFC    CASEANLSFLUID
  0.9      0.9      26.0            4.02          1.0     19
CC
CC WELL OPEN HOLE
* OPENHOLE_LENGTH  OPENHOLE_RWB  OPENHOLE_ROUGHNESS
       0.0           0.3333              0.0
CC
CC WELL TUBING COMPLETION (CODE:API 3 1/2" )(0.1 ft Black Aerogel)
* TUBINTVL  TUBETOP   TUBEBOTT     RTI          RTO          EPSTO    KTUB
      1       0.0       7000.0    0.23        0.28          0.0001    26.0
* INSTHICKNESS   KINS   HCFT  TUBANLSFLUID      ROUGHNESS
```

```
    0.0          0.002   1.0    19              0.0008
CC
CC FORMATION HEAT TRANSFER COEFFICIENTS
CC  {IUTO = 1 USES ONLY UTO AS THE TOTAL HEAT TRANSFER COEFFICIENT WUTO=Kavg/log(ro/ri)}
* FORMINTVL   FORMATIONTOP      FORMATIONBOTT  FORMATIONTVD   KEARTH  DENEARTH
    1             0               7000.0        7000.0    1.3      165.0

* CEARTH  TAMBTOP   TAMBOTT     IUTO   UTOTAL
  0.2       60       180.0       1      0.2

CC FLUID NUMBER OF PHASES TO HANDLE NP
CC {1:FLUID MIXTURE, 2:LIQ/GAS}, NUMBER OF COMPONENTS,PVTYPE{1:COMPOSITIONAL, 2:STEAM
3:BLACKOIL}
CC  PHASEID:{0:MIXTURE, 1:GAS 3:OIL 4:WATER }
* NPHASE  NCOMP NGLIFT PVTYPE  PHASEID
   2       4      1      1        0
CC
CC FLUID DATA FOR ONLY PVTYPE=1, {DEFINES COMPONENTS}
CC {ICOMPLIB: 0:OFF,1:ON- TAKES THE COMPNAMES AND READ FROM COMP LIB}
CC {EOSTYPE: 1:PR, 2:CUBIC_ASPH, 3:CUBIC_WAX} {IENTH: 1 H_COEFF 2:ACPI }
* ICOMPLIB     EOSTYPE    IENTH
    1             1         1
CC
CC FLUID DATA FOR ONLY PVTYPE=1,
CC {DEFINES COMPONENTS PROPERTIES, 0.0 VALUES MOEANS INTERNAL CORRELATION}
*  COMPNAME
   C1
   C2
   NC8
   NC10
CC
CC FLUID DATA FOR ONLY PVTYPE=1, {DEFINES COMPONENTS BIC}
* DELTA(1)  DELTA(2)  DELTA(3)  DELTA(4)
   0.0        0.0      0.0        0.0
   0.0        0.0      0.0        0.0
   0.0        0.0      0.0        0.0
   0.0        0.0      0.0        0.0
CC
CC FLUID DATA FOR WATER PARAMETERS
* GW    IFTWGCORR   ENTHCORR    CPWMETHOD    CPW  CPG
  1.0     1            1            1        1.0  0.25
CC
CC FLUID REFRENCE PRESSURE, TEMPERATURE
* REFPRESS     REFTEMP
     14.7         60.0
CC
CC FLUID FLOW ASSURANCE TYPE: {0:OFF, 1:ON}
* IASPH             IWAX              ISCALE
    0                0                 0
CC
CC RESERVOIR COUPLING:
CC {0: STATIC, 1:DYNAMIC} {RESINTVL: NUMBER OF RESERVOIR INTERVAL}{NTIME: NUMBER OF PI
VARIATION DATA}
* IRESERVOIR
   0
cc
cc GASLIFT PARAMETERS
cc
*  IGLIFT      GLVALVEMODEL          VALVEDEPTH     GLFRATE     CHP     CHT
    1             0                   4800.0        1          800.0   120.0
cc
cc COMPOSITION OF THE INJECTED GAS
*     ZG(1)    ZG(2)   ZG(3)   ZG(4)
      0.8      0.2     0.0     0.0
CC
CC RESERVOIR INTERVALS {VALUES ARE MD VALUES}
```

```
* RESINTVL  RESERVOIRTOP   RESERVOIRBOTT    PERFSHOT
   1          6950.0        7000.0           100

CC RESERVOIR PRODUCTIVITY INDEX: {FOR IRESERVOIR=0} {TIME INTERVAL SHOULD MATCH START/END
TIMES}
* RESTIME    PRESERVOIR     TRESERVOIR      PIO   PIW   PIG    Z(1)  Z(2)  Z(3)  Z(4)
    0.0      1500.0          180.0          1.0    0.0  0.0    0.05  0.05  0.1   0.8
CC
CC PROCESS CONDITIONS
CC IPROD {1:INJECTION, -1:PRODUCTION} IMODEL {0:no slip, 1:drift flux, 2:simp-two-fluid.
3:nimp-two_fluid}
* IPROD     ITHERMAL  ITRANSIENT    IMODEL    ISLIPOW  ISLIPGL
    -1        1          0            0          0         0
CC
CC INITIAL CONDITIONS {ZERO IS STATIONARY EQUILIBRIUM WITH RESERVOIR}
* TINIT   PINIT   HLDPHC   HLDPW   UGINIT   UOINIT  UWINIT
   0.0     0.0     0.0      0.0      0.0      0.0     0.0
CC
CC BOUNDARY CONDITIONS IN BOTTOM-HOLE {BHP: AUTOMATICALLY CLOSED INLET AND CONNECTS TO
RESERVOIR}
* IBCTIME    IBCTYPE
   1.0        CLOSE
CC
CC BOUNDARY CONDITIONS IN WELLHEAD {OPEN: AUTOMATIC COMBINED WITH BHP}
* OBCTIME    OBCTYPE    OBCP
   0.0       PRODWHP    100
CC
CC OUTPUT PRINT FREQUENCY
* TPRNT
    1
CC
CC OUTPUT PVT PLOTS {0: OFF, 1:ON}
* IPVT  PLOTTEMP1   PLOTTEMP2  PLOTPRES1   PLOTPRES2
   0     120.0       600.0      500.0      2500.0
CC
CC NUMERICAL CONVERGENCE TOLERRANCE
* WTOLP    WTOLT    WTOLQ    WMAXITER
  0.001     0.1      0.1     1000
CC
CC NUMERICAL SIMULATION TIME
CC {TIME STEP SIZE SHOUDL BE SETUP LESS THAN TIME INTERVALS FOR RESERVOIR CONDITION}
* STARTIME  ENDTIME     DTMIN   DTMAX
     6.0     6.0          1       1
CC
CC END OF INPUT.
```

A.2 SAMPLE INPUT DATA FOR ASPHALTENE DEPOSITION IN THE WELLBORE DURING GAS INJECTION

```
CC ================================================================*
CC               WELLBORE MODEL INPUT DATA                         *
CC ================================================================ *
CC                                                                 *
CC CASE NAME:  10COMP ASPH FLUID PROD WELL+GASLIFT                 *
CC             THIS CASE IS USED FOR ASPH                          *
CC             DEPOSITION SYSTEM DURING GAS LIFT INJECTION         *
CC                                                                 *
CC UNITS:      FIELD                                               *
CC             FT, DEGREE, BTU/HR.F.FT, BBL/PSI.FT.DAY             *
CC             LB/FT3, PSI, F, FT3/LBMOLE, LBM/LBMOLE, BTU/LB, DAY *
CC                                                                 *
CC CREATED BY: ALI ABOUIE 12/21/2014                               *
CC                                                                 *
CC ================================================================*

CC
CC MAXIMUM NUMBER OF WELLS IN CALCULATION AND FLOWPATH TYPE
* NWLBR  FLOWPATH
   1        WELL

CC*********************************************************************
CC WELL #01 DATA                                                      *
CC*********************************************************************

CC
CC CASE DEFINITION: {WELL ID}
* LW      WNAME
   1      ASPH.GASLIFT
CC
CC MESH GRID SIZE [FT]
* MAXGRIDSIZE
     200.0
CC
CC WELL SURFACE [FT]
* WSURFACE
          0.0

CC
CC WELL PROFILE AND SURVEY
* TRAJINTVL  MD        TVD     INCLINATION     AZIMUTH
     1       5000.0    5000.0      90.0        0.0

CC
CC WELL CASING AND COMPLETION {Default RWB=RCO+0.041665}  (CODE:7")
* CASEINTVL HANGERDEPTH  SETTINGDEPTH  RCI         RCO        RWB       CEMENTOP
      1     0.0              50.0        0.78       0.833      0.8749      0.0
      2     0.0              1000.0      0.51722    0.55725    0.59891     0.0
      3     0.0              5000.0      0.4010     0.4110     0.4427      0.0

* EPSCI    EPSCO    KCASE           KCEM          HCFC    CASEANLSFLUID
 0.9      0.9          26.0          4.02          1.0     19
 0.9      0.9          26.0          4.02          1.0     19
 0.9      0.9          26.0          4.02          1.0     19

CC
CC WELL OPEN HOLE
* OPENHOLE_LENGTH  OPENHOLE_RWB  OPENHOLE_ROUGHNESS
            0.0        0.3333             0.0
```

```
CC
CC WELL TUBING COMPLETION (CODE:API 3 1/2" )(0.1 ft Black Aerogel)
* TUBINTVL  TUBETOP   TUBEBOTT     RTI          RTO          EPSTO    KTUB
      1       0.0       5000.0    0.1145      0.2       0.0001     26.0

* INSTHICKNESS   KINS   HCFT  TUBANLSFLUID      ROUGHNESS
    0.0            0.002   1.0    19            0.0008

CC
CC FORMATION HEAT TRANSFER COEFFICIENTS
CC  {IUTO = 1 USES ONLY UTO AS THE TOTAL HEAT TRANSFER COEFFICIENT WUTO=Kavg/log(ro/ri)}
* FORMINTVL   FORMATIONTOP      FORMATIONBOTT  FORMATIONTVD   KEARTH  DENEARTH
    1             0.0              5000.0         5000.0        1.0      132.0

* CEARTH  TAMBTOP      TAMBOTT     IUTO   UTOTAL
  0.264     60.0         212.0       1     1.0

CC FLUID NUMBER OF PHASES TO HANDLE NP
CC {1:FLUID MIXTURE, 2:LIQ/GAS}, NUMBER OF COMPONENTS,PVTYPE{1:COMPOSITIONAL, 2:STEAM
3:BLACKOIL}
CC  PHASEID:{0:MIXTURE, 1:GAS 3:OIL 4:WATER }
* NPHASE  NCOMP PVTYPE  PHASEID
   2       10     1        0
CC
CC FLUID DATA FOR ONLY PVTYPE = 1, {DEFINES COMPONENTS}
CC {ICOMPLIB: 0:OFF,1:ON- TAKES THE COMPNAMES AND READ FROM COMP LIB}
CC {EOSTYPE: 1:PR, 2:CUBIC_ASPH, 3:CUBIC_WAX} {IENTH: 1 IDEAL GAS ENTHALPY 2:ACPI }
* ICOMPLIB     EOSTYPE    IENTH
    0             2         1
CC
CC FLUID DATA FOR ONLY PVTYPE=1,
CC {DEFINES COMPONENTS PROPERTIES, 0.0 VALUES MOEANS INTERNAL CORRELATION}
* COMPNAME   PC        TC        VC          WT           OM          PARACHOR   VSP
   CO2       1070.16   547.56   1.50682      44.0095     0.2251      78         -0.00252
   C1        667.38    343.08   1.58697      16.0425     0.008       77         -0.00412
   C2        708.54    549.72   2.37244      30.069      0.098       108        -0.00413
   C3        615.93    532.512  3.25409      44.0956     0.152       150.3      -0.00413
   C4F       545.664   758.1168 4.08077      58.122      0.1972      191        -0.00413
   C5F       487.2756  838.944  4.98058      72.149      0.2414      231        -0.00309
   C9F       383.4495  1129.99  8.17214      125.512     0.3677      327.5341    0.010382
   C21F      206.0352  1330.454 15.346       287.88      0.87714     761.4413    0.05
   C47F      90.59904  1671.734 39.8162      660.294     1.2381      1174.0076   0.05
   ASPH      90.59904  1671.734 39.8162      660.294     1.2381      1174.0076   0.05

*    HA             HB             HC                HD              HE           HF
   4.78E+00  1.14E-01       1.01E-04     -2.65E-08      3.47E-12      -1.31E-16
 -5.58E+00  5.65E-01      -2.83E-04      4.17E-07      -1.53E-10      1.96E-14
  -5.58E+00  5.65E-01      -2.83E-04      4.17E-07      -1.53E-10      1.96E-14
  -5.58E+00  5.65E-01      -2.83E-04      4.17E-07      -1.53E-10      1.96E-14
  -5.58E+00  5.65E-01      -2.83E-04      4.17E-07      -1.53E-10      1.96E-14
  0.00E+00 -2.780970E-02   4.091065E-04 -5.955861E-08   0.000000E+00  0.000000E+00
  0.00E+00 -2.780970E-02   4.091065E-04 -5.955861E-08   0.000000E+00  0.000000E+00
  0.00E+00 -2.780970E-02   4.091065E-04 -5.955861E-08   0.000000E+00  0.000000E+00
  0.00E+00 -2.780970E-02   4.091065E-04 -5.955861E-08   0.000000E+00  0.000000E+00
  0.00E+00 -2.780970E-02   4.091065E-04 -5.955861E-08   0.000000E+00  0.000000E+00

CC
CC FLUID DATA FOR ONLY PVTYPE=1, {DEFINES COMPONENTS BIC}
* DELTA(1)  DELTA(2)     DELTA(3)   DELTA(4)    DELTA(5)   DELTA(6)    DELTA(7)
DELTA(8)  DELTA(9)  DELTA(10)
0.000
0.120    0.000
0.130    0.000     0.000
0.135    0.000     0.000      0.000
0.130    0.000     0.000      0.000    0.000
0.125    0.0236    0.0075     0.0029   0.000    0.000
```

```
0.105    0.200     0.0136     0.0066   0.000    0.000       0.000
0.1352   0.000     0.0354     0.0196   0.000    0.000       0.000    0.000
0.1876   0.00008   0.0732     0.0423   0.000    0.000    0.000    0.000   0.000
0.2100   0.2900    0.1700     0.1300   0.1200   0.000    0.000    0.000   0.000     0.000

CC
CC FLUID DATA FOR WATER PARAMETERS
* GW    IFTWGCORR   ENTHCORR    CPWMETHOD    CPW
  1.0     1            1            1         1.0
CC
CC FLUID REFRENCE PRESSURE, TEMPERATURE
* REFPRESS      REFTEMP
     14.7         60.0
CC
CC FLUID FLOW ASSURANCE TYPE: {0:OFF, 1:ON}
* IASPH             IWAX              ISCALE
    1                0                 0

CC
CC FLUID FLOW ASSURANCE ASPHALTENE ONSET DATA
* VBS       KCONDASPH    KS1S2   IDEPOSIT    DPS1      DPS2
   16.8           1.0    1.0E5     4         5.0E-2    5.0E-6

* KDLMNAR    KDS1      KDS2       EAS1    EAS2
   5.0E6     1.0E8    1.0E8        65.3     65.3

CC
CC FLUID FLOW ASSURANCE ASPHALTENE ONSET DATA
*  NONSET    PSTAR      TSTAR
    1       1000      212
    2       1300      200
    3        1700     180
    4       2200      160
    5       2500      130
    6       3000      100

CC
CC RESERVOIR COUPLING:
CC {0: STATIC, 1:DYNAMIC} {RESINTVL: NUMBER OF RESERVOIR INTERVAL}{NTIME: NUMBER OF PI
VARIATION DATA}
* IRESERVOIR
   0
CC
CC RESERVOIR INTERVALS {VALUES ARE MD VALUES}
* RESINTVL  RESERVOIRTOP   RESERVOIRBOTT    PERFSHOT
   1           4800.0         5000.0            10

CC RESERVOIR PRODUCTIVITY INDEX: {FOR IRESERVOIR=0} {TIME INTERVAL SHOULD MATCH START/END
TIMES}
* RESTIME  PRESERVOIR   TRESERVOIR    PIO   PIW   PIG    Z(1)   Z(2)    Z(3)
Z(4)       Z(5)         Z(6)       Z(7)        Z(8)      Z(9)      Z(10)
   0.0      3500.0         212.0      0.2   0.0   0.0   0.0115  0.161   0.0582
0.0698     0.0611     0.0506   0.3127        0.209   0.0613 0.0048

CC
CC PROCESS CONDITIONS
CC IPROD {1:INJECTION, -1:PRODUCTION} IMODEL {0:no slip, 1:drift flux, 2:two-fluid}
* IPROD     ITHERMAL  ITRANSIENT    IMODEL    ISLIPOW  ISLIPGL
    -1        1          0            0          0         0
CC
CC INITIAL CONDITIONS {ZERO IS STATIONARY EQUILIBRIUM WITH RESERVOIR}
* TINIT   PINIT   HLDPHC   HLDPW   UGINIT   UOINIT  UWINIT
   0.0     0.0     0.0      0.0      0.0      0.0     0.0
CC
CC BOUNDARY CONDITIONS IN BOTTOM-HOLE {BHP: AUTOMATICALLY CLOSED INLET AND CONNECTS TO
RESERVOIR}
```

```
* IBCTIME    IBCTYPE        IBCP
   0.0        BHP            4200
CC
CC BOUNDARY CONDITIONS IN WELLHEAD {OPEN: AUTOMATIC COMBINED WITH BHP}
* OBCTIME    OBCTYPE
  0.0         OPEN
CC
CC OUTPUT PRINT FREQUENCY
* TPRNT
    1
CC
CC OUTPUT PVT PLOTS {0: OFF, 1:ON}
* IPVT  PLOTTEMP1   PLOTTEMP2  PLOTPRES1   PLOTPRES2
   0     120.0       600.0      500.0     2500.0
CC
CC NUMERICAL CONVERGENCE TOLERRANCE
* WTOLP    WTOLT    WTOLQ    WMAXITER
    1.0     0.1      0.1       20
CC
CC NUMERICAL SIMULATION TIME
CC {TIME STEP SIZE SHOUDL BE SETUP LESS THAN TIME INTERVALS FOR RESERVOIR CONDITION}
* STARTIME  ENDTIME     DTMIN   DTMAX
      0.0    180.0      0.1     0.1
CC
CC END OF INPUT.
```

A.3 SAMPLE INPUT DATA FOR IPHREEQC

```
SOLUTION 1
    temp      25
    pH        7
   -water    1 # kg
    units     mol/kgw

    Na        1
    Ca        1
    Ba        1
    K         1
    C(4)      1
    S(6)      1

EQUILIBRIUM_PHASES 1
    Anhydrite 0 0
    Calcite   0 0
END
```

A.4 SAMPLE RESULTS FOR IPHREEQC CALCULATION

```
-------------------------------------------
Beginning of initial solution calculations.
-------------------------------------------

Initial solution 1.

-----------------------------Solution composition------------------------------

        Elements           Molality       Moles

        Ba                1.000e+00   1.000e+00
        C(4)              1.000e+00   1.000e+00
        Ca                1.000e+00   1.000e+00
        K                 1.000e+00   1.000e+00
        Na                1.000e+00   1.000e+00
        S(6)              1.000e+00   1.000e+00

----------------------------Description of solution----------------------------

                                       pH  =   7.000
                                       pe  =   4.000
       Specific Conductance (µS/cm, 25°C)  = 119683
                            Density (g/cm³)  =   1.35186
                                 Volume (L)  =   1.03282
                        Activity of water  =   0.923
                           Ionic strength  =   3.339e+00
                       Mass of water (kg)  =   1.000e+00
                 Total alkalinity (eq/kg)  =   9.922e-01
                       Total CO2 (mol/kg)  =   1.000e+00
                         Temperature (°C)  =  25.00
                  Electrical balance (eq)  =   3.008e+00
 Percent error, 100*(Cat-|An|)/(Cat+|An|)  =  62.90
                                Iterations  =   8
                                   Total H  = 1.119792e+02
                                   Total O  = 6.248569e+01

----------------------------Distribution of species----------------------------

                                                 Log       Log       Log    mole V
   Species          Molality    Activity  Molality  Activity     Gamma   cm³/mol

   OH-             1.867e-07   9.346e-08    -6.729    -7.029    -0.301      1.23
   H+              1.398e-07   1.000e-07    -6.854    -7.000    -0.146      0.00
   H2O             5.551e+01   9.233e-01     1.744    -0.035     0.000     18.07
Ba            1.000e+00
   Ba+2            4.396e-01   1.142e-01    -0.357    -0.942    -0.585     -8.39
   BaSO4           4.269e-01   9.209e-01    -0.370    -0.036     0.334     (0)
   BaHCO3+         1.312e-01   1.991e-01    -0.882    -0.701     0.181     (0)
   BaCO3           2.333e-03   5.033e-03    -2.632    -2.298     0.334    -10.70
   BaOH+           6.109e-08   3.573e-08    -7.214    -7.447    -0.233     (0)
C(4)          1.000e+00
   CaHCO3+         4.935e-01   3.096e-01    -0.307    -0.509    -0.203     10.05
   HCO3-           3.016e-01   1.819e-01    -0.521    -0.740    -0.220     34.06
   BaHCO3+         1.312e-01   1.991e-01    -0.882    -0.701     0.181     (0)
   NaHCO3          4.038e-02   8.711e-02    -1.394    -1.060     0.334      1.80
   CO2             2.053e-02   4.429e-02    -1.688    -1.354     0.334     29.09
   CaCO3           8.863e-03   1.912e-02    -2.052    -1.719     0.334    -14.60
   BaCO3           2.333e-03   5.033e-03    -2.632    -2.298     0.334    -10.70
   NaCO3-          8.913e-04   1.353e-03    -3.050    -2.869     0.181     16.36
   CO3-2           6.454e-04   8.529e-05    -3.190    -4.069    -0.879      3.09
Ca            1.000e+00
```

```
   CaHCO3+         4.935e-01   3.096e-01    -0.307    -0.509    -0.203     10.05
   Ca+2            3.207e-01   1.334e-01    -0.494    -0.875    -0.381    -15.34
   CaSO4           1.770e-01   3.817e-01    -0.752    -0.418     0.334      7.50
   CaCO3           8.863e-03   1.912e-02    -2.052    -1.719     0.334    -14.60
   CaHSO4+         1.653e-07   2.509e-07    -6.782    -6.601     0.181      (0)
   CaOH+           1.347e-07   2.045e-07    -6.871    -6.689     0.181      (0)
H(0)          6.564e-26
   H2              3.282e-26   7.079e-26   -25.484   -25.150     0.334     28.61
K             1.000e+00
   K+              9.047e-01   5.082e-01    -0.043    -0.294    -0.250     10.95
   KSO4-           9.528e-02   5.745e-02    -1.021    -1.241    -0.220     35.80
Na            1.000e+00
   Na+             8.448e-01   8.518e-01    -0.073    -0.070     0.004      0.58
   NaSO4-          1.139e-01   6.868e-02    -0.943    -1.163    -0.220     31.42
   NaHCO3          4.038e-02   8.711e-02    -1.394    -1.060     0.334      1.80
   NaCO3-          8.913e-04   1.353e-03    -3.050    -2.869     0.181     16.36
   NaOH            3.690e-18   7.960e-18   -17.433   -17.099     0.334      (0)
O(0)          0.000e+00
   O2              0.000e+00   0.000e+00   -42.483   -42.149     0.334     30.40
S(6)          1.000e+00
   BaSO4           4.269e-01   9.209e-01    -0.370    -0.036     0.334      (0)
   SO4-2           1.869e-01   1.609e-02    -0.728    -1.794    -1.065     21.29
   CaSO4           1.770e-01   3.817e-01    -0.752    -0.418     0.334      7.50
   NaSO4-          1.139e-01   6.868e-02    -0.943    -1.163    -0.220     31.42
   KSO4-           9.528e-02   5.745e-02    -1.021    -1.241    -0.220     35.80
   CaHSO4+         1.653e-07   2.509e-07    -6.782    -6.601     0.181      (0)
   HSO4-           1.031e-07   1.564e-07    -6.987    -6.806     0.181     41.68

------------------------------Saturation indices-------------------------------

  Phase               SI** log IAP   log K(298 K,   1 atm)

  Anhydrite          1.61     -2.67   -4.28  CaSO4
  Aragonite          3.39     -4.94   -8.34  CaCO3
  Barite             7.23     -2.74   -9.97  BaSO4
  Calcite            3.54     -4.94   -8.48  CaCO3
  CO2(g)             0.11     -1.35   -1.46  CO2
  Gypsum             1.84     -2.74   -4.58  CaSO4:2H2O
  H2(g)           -22.05    -25.15   -3.10  H2
  H2O(g)           -1.54     -0.03    1.50  H2O
  O2(g)           -39.26    -42.15   -2.89  O2
  Witherite          3.55     -5.01   -8.56  BaCO3

**For a gas, SI = log10(fugacity). Fugacity = pressure * phi / 1 atm.
  For ideal gases, phi = 1.

-----------------------------------------
Beginning of batch-reaction calculations.
-----------------------------------------

Reaction step 1.

Using solution 1.
Using pure phase assemblage 1.

-------------------------------Phase assemblage--------------------------------

                                                        Moles in assemblage
Phase               SI  log IAP  log K(T, P)   Initial       Final       Delta

Anhydrite         0.00    -4.28     -4.28    0.000e+00   5.542e-01   5.542e-01
Calcite           0.00    -8.48     -8.48    0.000e+00   4.095e-01   4.095e-01

------------------------------Solution composition------------------------------

       Elements           Molality       Moles
```

Ba	9.929e-01	1.000e+00
C	5.864e-01	5.905e-01
Ca	3.612e-02	3.637e-02
K	9.929e-01	1.000e+00
Na	9.929e-01	1.000e+00
S	4.427e-01	4.458e-01

A.5 SAMPLE INPUT DATA FOR GEOCHEMICAL REACTIONS IN THE WELLBORE

```
CC ================================================================*
CC               WELLBORE MODEL INPUT DATA                        *
CC ================================================================ *
CC                                                                 *
CC CASE NAME:  12COMP FLUID PROD WELL                              *
CC             THIS CASE IS USED FOR FOR SCALE                     *
CC             DEPOSITION SYSTEM.                                  *
CC                                                                 *
CC UNITS:      FIELD                                               *
CC             FT, DEGREE, BTU/HR.F.FT, BBL/PSI.FT.DAY             *
CC             LB/FT3, PSI, F, FT3/LBMOLE, LBM/LBMOLE, BTU/LB, DAY *
CC                                                                 *
CC CREATED BY: ALI ABOUIE 04/17/2015                               *
CC                                                                 *
CC ================================================================*
CC
CC MAXIMUM NUMBER OF WELLS IN CALCULATION AND FLOWPATH TYPE
* NWLBR  FLOWPATH
   1        WELL
CC*********************************************************************
CC WELL #01 DATA                                                     *
CC*********************************************************************

CC
CC CASE DEFINITION: {WELL ID}
* LW      WNAME
   1      SCALE_DEPOSITION
CC
CC MESH GRID SIZE [FT]
* MAXGRIDSIZE
     50.0
CC
CC WELL SURFACE [FT]
* WSURFACE
     0.0

CC
CC WELL PROFILE AND SURVEY
* TRAJINTVL  MD        TVD     INCLINATION     AZIMUTH
     1       3000.0    3000.0      90.0        0.0

CC
CC WELL CASING AND COMPLETION {Default RWB=RCO+0.041665}  (CODE:7")
* CASEINTVL HANGERDEPTH  SETTINGDEPTH  RCI         RCO        RWB    CEMENTOP
      1     0.0              50.0      0.78       0.833      0.8749      0.0
      2     0.0              1000.0    0.51722    0.55725    0.59891     0.0
      3     0.0              3000.0    0.3648     0.4010     0.4427      0.0

* EPSCI    EPSCO    KCASE           KCEM          HCFC    CASEANLSFLUID
 0.9       0.9       26.0           4.02          1.0         19
 0.9       0.9       26.0           4.02          1.0         19
 0.9       0.9       26.0           4.02          1.0         19

CC
CC WELL OPEN HOLE
* OPENHOLE_LENGTH  OPENHOLE_RWB  OPENHOLE_ROUGHNESS
       0.0            0.3333             0.0
CC
CC WELL TUBING COMPLETION (CODE:API 3 1/2" )(0.1 ft Black Aerogel)
* TUBINTVL  TUBETOP   TUBEBOTT     RTI          RTO          EPSTO    KTUB
      1       0.0       3000.0    0.1145      0.14583       0.0001     26.0
```

```
* INSTHICKNESS   KINS   HCFT  TUBANLSFLUID      ROUGHNESS
    0.0          0.002   1.0       19            0.0008

CC
CC FORMATION HEAT TRANSFER COEFFICIENTS
CC  {IUTO = 1 USES ONLY UTO AS THE TOTAL HEAT TRANSFER COEFFICIENT WUTO=Kavg/log(ro/ri)}
* FORMINTVL   FORMATIONTOP      FORMATIONBOTT  FORMATIONTVD   KEARTH  DENEARTH
    1             0.0               3000.0        3000.0        1.0      132.0

* CEARTH  TAMBTOP   TAMBOTT     IUTO   UTOTAL
  0.264   60.0        180.0       1     0.2

CC FLUID NUMBER OF PHASES TO HANDLE NP
CC {1:FLUID MIXTURE, 2:LIQ/GAS}, NUMBER OF COMPONENTS,PVTYPE{1:COMPOSITIONAL, 2:STEAM
3:BLACKOIL}
CC  PHASEID:{0:MIXTURE, 1:GAS 3:OIL 4:WATER }
* NPHASE  NCOMP PVTYPE  PHASEID
   2       12     1        0
CC
CC FLUID DATA FOR ONLY PVTYPE=1, {DEFINES COMPONENTS}
CC {ICOMPLIB: 0:OFF,1:ON- TAKES THE COMPNAMES AND READ FROM COMP LIB}
CC {EOSTYPE: 1:PR, 2:CUBIC_ASPH, 3:CUBIC_WAX} {IENTH: 1 H_COEFF 2:ACPI }
* ICOMPLIB     EOSTYPE    IENTH
    0            1        1
CC
CC FLUID DATA FOR ONLY PVTYPE=1,
CC {DEFINES COMPONENTS PROPERTIES, 0.0 VALUES MOEANS INTERNAL CORRELATION}
*  COMPNAME      PC    TC      VC       WT      OM      PARACHOR              VSP
CO2(g)  1070.535624    547.5  2.243201575    44     0.2276         49             0
C1N2    666.972984     342.5  1.442237287    16.1   0.0109         71             0
C2      707.6591358    549.6  2.371294757    30.1   0.099          134.825        0
C3      616.2902348    665.6  3.252343124    44.1   0.1518         233.048        0
C4      544.3147329    756.4  4.122115282    58.1   0.1885         394.499        0
C5      489.3334468    838.4  4.883768876    72.1   0.24           707.76         0
C6      476.1379381    913.8  5.423128436    84     0.2711         1035.85        0
C710    412.859476     1048.7 6.959539271    113.3  0.3683         1035.85        0
C1113   318.1916979    1196.4 10.20105981    161.9  0.5239         1035.85        0
C1419   249.6150391    1328.9 14.31231704    226    0.6932         1035.85        0
C2029   192.4345015    1475.9 21.23608053    331.5  0.9            1035.85        0
C30P    133.6545083    1574.9 37.15367911    588    1.2            1035.85        0
CC
CC
*      HA              HB             HC              HD             HE            HF
  0.000000E+00 -2.780970E-02  4.091065E-04   -5.955861E-08  0.000000E+00   0.000000E+00
  0.000000E+00 -2.780970E-02  4.091065E-04   -5.955861E-08  0.000000E+00   0.000000E+00
  0.000000E+00 -2.780970E-02  4.091065E-04   -5.955861E-08  0.000000E+00   0.000000E+00
  0.000000E+00 -2.780970E-02  4.091065E-04   -5.955861E-08  0.000000E+00   0.000000E+00
  0.000000E+00 -2.780970E-02  4.091065E-04   -5.955861E-08  0.000000E+00   0.000000E+00
  0.000000E+00 -2.780970E-02  4.091065E-04   -5.955861E-08  0.000000E+00   0.000000E+00
  0.000000E+00 -2.780970E-02  4.091065E-04   -5.955861E-08  0.000000E+00   0.000000E+00
  0.000000E+00 -2.780970E-02  4.091065E-04   -5.955861E-08  0.000000E+00   0.000000E+00
  0.000000E+00 -2.780970E-02  4.091065E-04   -5.955861E-08  0.000000E+00   0.000000E+00
  0.000000E+00 -2.780970E-02  4.091065E-04   -5.955861E-08  0.000000E+00   0.000000E+00
  0.000000E+00 -2.780970E-02  4.091065E-04   -5.955861E-08  0.000000E+00   0.000000E+00
  0.000000E+00 -2.780970E-02  4.091065E-04   -5.955861E-08  0.000000E+00   0.000000E+00
CC
CC FLUID DATA FOR ONLY PVTYPE=1, {DEFINES COMPONENTS BIC}
* DELTA(1)  DELTA(2)  DELTA(3)   DELTA(4)   DELTA(5)  DELTA(6)  DELTA(7)   DELTA(8)
DELTA(9)  DELTA(10)  DELTA(11)   DELTA(12)
  0            0.105  0.125     0.12       0.12      0.12     0.12       0.12       0.13
       0.13        0.13       0.13
    0.105      0       0.0028    0.0089     0.0156    0.0216   0.0257     0.0369     0.0575
       0.0789      0.1072     0.1523
    0.125      0.0028 0          0.0017     0.0053    0.009    0.0118     0.0198     0.0359
       0.0538      0.0784     0.1193
```

```
    0.12       0.0089  0.0017    0          0.001     0.0029   0.0045     0.01       0.0223
       0.037       0.0584     0.0954
    0.12       0.0156  0.0053    0.001      0          0.0005   0.0013     0.0047     0.0141
       0.0263      0.045      0.0788
    0.12       0.0216  0.009     0.0029     0.0005    0        0.0002     0.0022     0.0093
       0.0198      0.0365     0.0677
    0.12       0.0257  0.0118    0.0045     0.0013    0.0002   0          0.0011     0.0069
       0.0161      0.0316     0.0612
    0.12       0.0369  0.0198    0.01       0.0047    0.0022   0.0011     0          0.0025
       0.009       0.0213     0.0469
    0.13       0.0575  0.0359    0.0223     0.0141    0.0093   0.0069     0.0025     0
       0.002       0.0093     0.0284
    0.13       0.0789  0.0538    0.037      0.0263    0.0198   0.0161     0.009      0.002
       0           0.0027     0.0156
    0.13       0.1072  0.0784    0.0584     0.045     0.0365   0.0316     0.0213     0.0093
       0.0027      0          0.0054
    0.13       0.1523  0.1193    0.0954     0.0788    0.0677   0.0612     0.0469     0.0284
       0.0156      0.0054     0

CC
CC FLUID DATA FOR WATER PARAMETERS
* GW    IFTWGCORR   ENTHCORR    CPWMETHOD     CPW
  1.0     1           1           1         1.0
CC
CC FLUID REFRENCE PRESSURE, TEMPERATURE
* REFPRESS     REFTEMP
     14.7         60.0
CC
CC FLUID FLOW ASSURANCE TYPE: {0:OFF, 1:ON}
* IASPH             IWAX              ISCALE
    0                 0                 1

CC
CC FLUID AQUEOUS PHASE SOLIDS
* AQSOLID      DENAQSOLID     MWAQSOLID
  Anhydrite    185.328        136.0
  Aragonite    182.83         100.09
  Calcite      169.10         100.09
  Dolomite     177.84         184.40
  Hausmannite  302.016        228.81
  Hematite     330.72         159.69

CC
CC FLUID SCALE DEPOSITION PARAMETERS
*  KCONDSCALE    IDEPOSITAQ    DPSAQ    KDLMNRAQ    KDAQ    EAQ
       1.0         4          1.0E-3    1.0E-4    8.0E-6   0.0

CC
CC NUMBER OF THE COMPONENTS SOLUBLE IN THE HYDROCARBON
*  NSOLUBLE
      0

CC
CC RESERVOIR COUPLING:
CC {0: STATIC, 1:DYNAMIC} {RESINTVL: NUMBER OF RESERVOIR INTERVAL}{NTIME: NUMBER OF PI
VARIATION DATA}
* IRESERVOIR
   0

CC
CC RESERVOIR INTERVALS {VALUES ARE MD VALUES}
* RESINTVL  RESERVOIRTOP   RESERVOIRBOTT    PERFSHOT
   1          2900.0         3000.0           10

CC RESERVOIR PRODUCTIVITY INDEX: {FOR IRESERVOIR=0} {TIME INTERVAL SHOULD MATCH START/END
TIMES}
```

```
* RESTIME    PRESERVOIR     TRESERVOIR      PIO   PIW   PIG    Z(1)       Z(2)    Z(3)
Z(4)    Z(5)    Z(6)    Z(7)    Z(8)   Z(9)    Z(10)   Z(11)   Z(12)
    0.0      2000.0         180.0           0.3   0.15   0.01    0.12837   0.42134 0.05557
        0.02662 0.01535 0.00985 0.00835 0.06971 0.03578 0.07131 0.07629 0.08146

CC
CC PROCESS CONDITIONS
CC IPROD {1:INJECTION, -1:PRODUCTION} IMODEL {0:no slip, 1:drift flux, 2:two-fluid}
* IPROD     ITHERMAL  ITRANSIENT    IMODEL    ISLIPOW  ISLIPGL
    -1        1          0           0          0        0
CC
CC INITIAL CONDITIONS {ZERO IS STATIONARY EQUILIBRIUM WITH RESERVOIR}
* TINIT   PINIT   HLDPHC   HLDPW   UGINIT   UOINIT  UWINIT
   0.0     0.0     0.0      0.0      0.0      0.0     0.0
CC
CC BOUNDARY CONDITIONS IN BOTTOM-HOLE {BHP: AUTOMATICALLY CLOSED INLET AND CONNECTS TO
RESERVOIR}
* IBCTIME    IBCTYPE
   0.0        CLOSE
CC
CC BOUNDARY CONDITIONS IN WELLHEAD {OPEN: AUTOMATIC COMBINED WITH BHP}
* OBCTIME    OBCTYPE    OBCP
   0.0        PRODWHP    840
CC
CC OUTPUT PRINT FREQUENCY
* TPRNT
    1
CC
CC OUTPUT PVT PLOTS {0: OFF, 1:ON}
* IPVT  PLOTTEMP1   PLOTTEMP2  PLOTPRES1   PLOTPRES2
   0     120.0       600.0      500.0     2500.0
CC
CC NUMERICAL CONVERGENCE TOLERRANCE
* WTOLP    WTOLT    WTOLQ    WMAXITER
    0.01     0.1      0.1       200
CC
CC NUMERICAL SIMULATION TIME
CC {TIME STEP SIZE SHOUDL BE SETUP LESS THAN TIME INTERVALS FOR RESERVOIR CONDITION}
* STARTIME  ENDTIME     DTMIN   DTMAX
      0.0    300.0       0.5     2.0
CC
CC END OF INPUT.
```

A.6 SAMPLE GEOCHEMINPUT.DATA FILE

```
SOLUTION 1-100
-water 1
units mg/L
-temp 120.000

Ba      0.0
Ca      0.0
Fe      0.0
Li      0.0
Mg      0.0
Mn      0.0
P       0.0
K       0.0
Si      0.0
Na      0.0
Sr      0.0
Zn      0.0
C       0.0     AS      HCO3-
Br      0.0
Cl      0.0
F       0.0
S(6)    0.0
END

EQUILIBRIUM_PHASES 1-100

Anhydrite       0.0     0.0
Aragonite       0.0     0.0
Calcite         0.0     0.0
Dolomite        0.0     0.0
Hausmannite     0.0     0.0
Hematite        0.0     0.0
END

##INFLUX INTO THE WELLBORE
## CONNATE WATER

SOLUTION 0
units ppm
-temp 180
-water 1

Ba      7.0
Ca      2320.0
Fe      210.0
Li      0.0
Mg      348.0
Mn      0.0
P       0.0
K       1110.0
Si      0.0
Na      11850.0
Sr      24.0
Zn      0.0
C       2000    AS      HCO3-
Br      0.0
Cl      17275.0
F       0.0
S(6)    6300.0

END
```

Nomenclature

Wellbore parameters

A	Wellbore cross section area (ft^2)
C_d	Discharge coefficient
D	Wellbore diameter (ft)
g	Gravity acceleration (ft/sec^2)
$\bar{h}$	Fluid enthalpy (Btu/lb_m)
K	Temperature dependent equilibrium constant
K_B	Boltzman constant (1.38×10^{-23} J/K)
MD	Measured depth (ft)
P	Pressure (psi)
SI	Saturation index
T	Temperature (°F)
TVD	True Vertical Depth (ft)
u	Velocity (ft/sec)
U	Heat transfer coefficient ($Btu/ft^2.sec.°F$)

Greek Symbols

α	Fluid volume fraction
$\dot{\psi}$	Mass influx of the fluid per gridblock volume ($lb_m/sec.ft^3$)
$\dot{H}$	Enthalpy influx of the fluid per gridblock volume ($Btu/sec.ft^3$)
ρ	Fluid density (lb_m/ft^3)
μ	Viscosity (cp)
τ	Shear stress ($lb_m/sec^2.ft$)
Γ	Interphase mass transfer per bulk volume ($lb_m/sec.ft^3$)

γ	Specific gravity
θ	Well inclination angle (radian)

Subscripts

p	Particle
d	Drift
g	Gas
l	Liquid
m	Mixture
o	Oil
w	Water

References

Abouie, A., Darabi, H., and Sepehrnoori, K. April 2014. Progress Report on the Characterization of a Middle East Fluid During Gas Injection, The University of Texas at Austin, Austin, Texas.

Abouie, A., Shirdel, M., Darabi, H., and Sepehrnoori, K. 2015. Modeling Asphaltene Deposition in the Wellbore During Gas Lift Process. Presented in SPE Western Regional Meeting, Garden Grove, California.

Arreola, F. M. V. 2009. Modeling of Asphaltene Precipitation and Arterial Deposition .PhD dissertation, Rice University, Houston, Texas.

Beal, S. K. 1970. Deposition of Particles in Turbulent Flow on Channel or Pipe Walls. *Nuclear Science and Engineering*, *40*(1), 1-11.

Betancourt, S., Dahlberg, K., Hovde, Ø., and Jalali, Y. 2002. Natural gas-lift: Theory and Practice. Presented in SPE International Petroleum Conference and Exhibition in Mexico, Villahermosa, Mexico.

Blann, J. R., and Williams, J. D. 1984. Determining the Most Profitable Gas Injection Pressure for a Gas Lift Installation (includes associated papers 13539 and 13546). *Journal of petroleum technology*, *36*(08), 1-305.

Chapman, W. G., Gubbins, K. E., Jackson, G., and Radosz, M. 1990. New Reference Equation of State for Associating Liquids. *Industrial and Engineering Chemistry Research*, *29*(8), 1709-1721.

Charlton, S. R., and Parkhurst, D. L. 2011. Modules Based on the Geochemical Model PHREEQC for Use in Scripting and Programming Languages. *Computers and Geosciences*, *37*(10), 1653-1663.

Chia, Y. C., and Hussain, S. 1999. Gas Lift Optimization Efforts and Challenges. Presented in SPE Asia Pacific Improved Oil Recovery, Kuala Lumpur, Malaysia.

Clegg, M., Bucaram, S., J. D., and Hein, N. J. 1993. Recommendations and Comparisons for Selecting Artificial-Lift Methods.

Darabi, H. 2014a. Development of a Non-Isothermal Compositional Reservoir Simulator to Model Asphaltene Precipitation, Flocculation, and Deposition and Remediation. PhD dissertation, The University of Texas at Austin, Austin, Texas

Darabi, H., Shirdel, M., Kalaei, M. H., and Sepehrnoori, K. 2014b. Aspects of Modeling Asphaltene Deposition in a Compositional Coupled Wellbore/Reservoir Simulator. Presented in SPE Improved Oil Recovery Symposium, Tulsa, Oklahoma.

Decker, K. L. 1986. Computer Modeling of Gas-Lift Valve Performance. Presented in the 18th Annual OTC, Houston, Texas.

Delshad, M., and Pope, G. A. 2003. Effect of Dispersion on Transport and Precipitation of Barium and Sulfate in Oil Reservoirs. Presented in SPE International Symposium on Oilfield Chemistry, Houston, Texas.

El-Hattab, M. I. 1985. Scale Deposition in Surface and Subsurface Production Equipment in the Gulf of Suez. *Journal of Petroleum Technology*, *37*(9), 1640-1650.

Elmorsey, S. A. 2013, March. Challenge and Successful Application for Scale Removal Gemsa Oil Field, Egypt: Field Study, Presented in SPE Middle East Oil and Gas Show and Conference, Manama, Bahrain.

Escobedo, J. 1993. Mexican Crude Oils and the Asphaltene Deposition Problem, M.Sc. thesis, The University of Illinois at Chicago, Chicago, IL.

Escobedo, J., and Mansoori, G. A. 1995. Asphaltene and Other Heavy-Organic Particle Deposition during Transfer and Production Operations. Presented in SPE Annual Technical Conference and Exhibition, Oklahoma city, Oklahoma.

Faustinelli, J. G., and Doty, D. R. 2001. Dynamic Flow Performance Modeling of a Gas-lift Valve. Presented in SPE Latin American and Caribbean Petroleum Engineering, Buenos Aires, Argentina.

Friedlander, S. K., and Johnstone, H. F. 1957. Deposition of Suspended Particles from Turbulent Gas Streams. *Industrial and Engineering Chemistry*, *49*(7), 1151-1156.

Ganjdanesh, R., Pope, G. A., and Sepehrnoori, K. 2015. Production of Energy From Saline Aquifers: A Method to Offset the Energy Cost of Carbon Capture and Storage. *International Journal of Greenhouse Gas Control*, *34*, 97-105

Guet, S., Ooms, G., Oliemans, R. V. A., and Mudde, R. F. 2003. Bubble Injector Effect on the Gaslift Efficiency. *AIChE journal*, *49*(9), 2242-2252.

Hepguler, G., Schmidt, Z., Blais, R. N., and Doty, D. R. 1993. Dynamic Model of Gas-Lift Valve Performance. Society of Petroleum Engineers.

Hernandez, A., Gasbarri, S., Machado, M., Marcano, L., Manzanilla, R., and Guevara, J. 1999. Field-scale Research on Intermittent Gas Lift. Presented in SPE mid-continent operations Symposium, Oklahoma City, Oklahoma.

Hudson, J. D., Dutsch, D. B., Lang, P. P., Lorimer, S. L., and Stevens, K. A. 2002. An Overview of the Na Kika Flow Assurance Design. Presented in Offshore Technology Conference, Houston, Texas.

Jayawardena, S. S., Zabaras, G. J., and Dykhno, L. A. 2007. The Use of Subsea Gas-Lift in Deepwater Applications. Presented in Offshore Technology Conference, Houston, Texas.

Katsanis, E. P., Krumrine, P. H., and Falcone Jr, J. S. 1983. Chemistry of Precipitation and Scale Formation in Geological Systems. Presented in SPE international symposium on oilfield and Geothermal chemistry, Denver, Colorado.

Kaya, A.S, Sarica, C., and Brill J.P. 1999. Comprehensive Mechanistic Modeling of Two-phase Flow in Deviated Wells. Presented at Annual Technical Conference and Exhibition, Houston, Texas.

Kazemi Nia Korrani, A., Sepehrnoori, K., and Delshad, M. 2014a. A Comprehensive Geochemical-Based Approach to Quantify the Scale Problems. Presented in SPE International Symposium and Exhibition on Formation Damage Control, Lafayette, Louisiana.

Kazemi Nia Korrani, A. 2014b. Mechanistic Modeling of Low Salinity Water Injection, PhD Dissertation, The University of Texas at Austin, Austin, Texas.

Khan, S.A., 1992. An Expert System to Aid in Compositional Simulation of Miscible Gas Flooding. PhD dissertation, The University of Texas at Austin, Austin, Texas.

Kurup, A. S., Vargas, F. M., Wang, J., Buckley, J., Creek, J. L., Subramani, H. J., and Chapman, W. G. 2011. Development and Application of an Asphaltene Deposition Tool (ADEPT) for Well bores. *Energy and Fuels*, *25*(10), 4506-4516.

Langelier, W. F. 1936. The Analytical Control of Anti-corrosion Water Treatment. *Journal (American Water Works Association)*, 1500-1521.

Lashgari, H. 2014. Development of a Four-Phase Thermal-Chemical Reservoir Simulator for Heavy Oil, PhD Dissertation, The University of Texas at Austin, Austin, Texas.

Liao, T., Schmidt, Z., and Doty, D. R. 1995. Investigation of Intermittent Gas Lift by Using Mechanistic Modeling. Presented in Production Operations Symposium, Oklahoma City, OK.

Lin, C. S., Moulton, R. W., and Putnam, G. L. 1953. Mass Transfer between Solid Wall and Fluid Streams. Mechanism and Eddy Distribution Relationships in Turbulent Flow. *Industrial and Engineering Chemistry*, *45*(3), 636-640.

Mach, J., Proano, E., and Brown, K. E. 1979. A Nodal Approach for Applying Systems Analysis to the Flowing and Artificial Lift Oil or Gas Well.

Mitchell, R. W., Grist, D. M., and Boyle, M. J. 1980. Chemical Treatments Associated with North Sea Projects. *Journal of Petroleum Technology*, *32*(05), 904-912.

Moghadasi, J., Jamialahmadi, M., Müller-Steinhagen, H., Sharif, A., Ghalambor, A., Izadpanah, M. R., and Motaie, E. 2003. Scale Formation in Iranian Oil Reservoir and Production Equipment during Water Injection, Presented in International Symposium on Oilfield Scale, Aberdeen, United Kingdom.

Mohebbinia, S. 2013. Advanced Equation of State Modeling for Compositional Simulation of Gas Floods, PhD Dissertation, The University of Texas at Austin, Austin, Texas.

Parkhurst, D. L., and Appelo, C. A. J. 1999. User's guide to PHREEQC (Version 2): A Computer Program for Speciation, Batch-reaction, One-dimensional Transport, and Inverse Geochemical Calculations.

Parkhurst, D. L., and Appelo, C. A. J. 2013. Description of Input and Examples for PHREEQC Version 3: a Computer Program for Speciation, Batch-reaction, One-dimensional Transport, and Inverse Geochemical Calculations (No. 6-A43), US Geological Survey.

Pedersen, K. S., Christensen, P. L., and Shaikh, J. A. 2012. *Phase Behavior of Petroleum Reservoir Fluids*, CRC Press.

Peng, D. Y., and Robinson, D. B. 1976. A new two-constant equation of state. *Industrial and Engineering Chemistry Fundamentals, 15*(1), 59-64.

PIPESIM 2013. PIPESIM Online Help- Software User's Manual. Schlumberger, Version 2013.1.

Qing, J., Zhou, B., Zhang, R., Chen, Z., and Zhou, Y. 2002. Development and Application of a Silicate Scale Inhibitor for ASP Flooding Production Scale, Presented in International Symposium on Oilfield Scale, Aberdeen, United Kingdom.

Ramirez, M., Zdenkovic, N., and Medina, E. 2000. Technical/Economical Evaluation of Artificial Lift Systems for Eight Offshore Reservoirs. Presented in the SPE International Petroleum Conference and Exhibition in Mexico, Villahermosa, Mexico.

Ramirez-Jaramillo, E., Lira-Galeana, C., and Manero, O. 2006. Modeling asphaltene deposition in Production Pipelines. *Energy and fuels, 20*(3), 1184-1196.

Read, A. P., and Ringen, K. J. 1982. The Use of Laboratory Tests to Evaluate Scaling Problems during Water Injection. Presented in SPE international symposium on oilfield and geothermal chemistry, Dallas, Texas.

RELAP5-3D. 2012. Code Manual Volume IV: Models and Correlations. INEEL-EXT-98-00834, Revision 4.0.

Rocha, A. A., Frydman, M., da Fontoura, S. A. B., Rosario, F. F., and Bezerra, M. C. M. 2001. Numerical Modeling of Salt Precipitation during Produced Water Reinjection. Presented in SPE International Symposium on Oilfield Scale. Aberdeen,UK.

Santos, O. G., Bordalo, S. N., and Alhanati, F. J. 2001. Study of the Dynamics, Optimization and Selection of Intermittent Gas-lift Methods—a Comprehensive Model. *Journal of Petroleum Science and Engineering, 32*(2), 231-248.

Shirdel, M., and Sepehrnoori, K. 2009. Development of a coupled compositional wellbore/reservoir simulator for modeling pressure and temperature distribution in horizontal wells. Presented at Annual Technical Conference and Exhibition, New Orleans, Louisiana.

Shirdel, M. 2010. Development of a coupled wellbore-reservoir compositional simulator for horizontal wells, MSc Thesis, The University of Texas at Austin, Austin, Texas.

Shirdel, M., and Sepehrnoori, K. 2012a. Development of a transient mechanistic two-phase flow model for wellbores, *SPE Journal, 17(3),* pp. 942-955.

Shirdel, M., Paes, D., Ribeiro, P., and Sepehrnoori, K. 2012b. Evaluation and comparison of different models for asphaltene particle deposition in flow streams. *Journal of Petroleum Science and Engineering*, *84*, 57-71.

Shirdel, M. 2013. Development of a Coupled Wellbore-Reservoir Compositional Simulator for Damage Prediction and Remediation. PhD dissertation, The University of Texas at Austin, Austin, Texas.

Shoham, O. 2006. *Mechanistic Modeling of Gas-Liquid Two-phase Flow in Pipes*, Society of Petroleum Engineering.

Shuler, P. J., and Jenkins, W. H. 1991. Prevention of Downhole Scale Deposition in the Ninian Field. *SPE Production Engineering*, *6*(02), 221-226.

Shuler, P. J., Daniels, E. J., Burton, L., and Chen, H. J. 2000. Modeling of Scale Deposition in Gas Wells with Very Saline Produced Water. *CORROSION 2000*.

Stiff Jr, H. A., and Davis, L. E. 1952. A Method for Predicting the Tendency of Oil Field Waters to Deposit Calcium Carbonate. *Journal of Petroleum Technology*, *4*(09), 213-216.

Tjomsland, T., Grotle, M. N., and Vikane, O. 2003. Scale Control Strategy and Economical Consequences of Scale at Veslefrikk, Presented in SPE International Symposium on Oilfield Scale, Aberdeen, United Kingdom.

"*UTCOMP: Technical Documentation for UTCOMP 3.8*." Reservoir Engineering Research Program, Center for Petroleum and Geosystems Engineering. The University of Texas at Austin, 2011.

Valone, F. W., and Skillern, K. R. 1982. An Improved Technique for Predicting the Severity of Calcium Carbonate. Presented in SPE Oilfield and Geothermal Chemistry Symposium, Dallas, Texas.

Vazquez-Roman, R., and Palafox-Hernández, P. 2005. A New Approach for Continuous Gas Lift Simulation and Optimization. Presented in SPE Annual Technical Conference and Exhibition, Dallas, Texas.

Vetter, O. J. G., and Phillips, R. C. 1970. Prediction of Deposition of Calcium Sulfate Scale Under Down-hole Conditions. *Journal of Petroleum Technology*, *22*(10), 1299-1308.

Vetter, O. J., and Kandarpa, V. 1980. Prediction of CaCO3 Scale Under Downhole Conditions. Presented in SPE Oilfield and Geothermal Chemistry Symposium, Stanford, California.

Von Karman, T. 1935. Transaction. In *Am. Soc. Mech. Eng* (Vol. 61, p. 705).

Wang, P., Litvak, M., and Aziz, K. 2002. Optimization of Production Operations in Petroleum Fields. Presented in SPE Annual Technical Conference and Exhibition, San Antonio, Texas.

Wright, R. J., Hall, and J. R. F. 1994. Scale Prediction Measurement and Control in a Subsea Satellite Field, Presented in European Production Operations Conference and Exhibition, Aberdeen, United Kingdom.